Spring 1996

Measurement of the electroencephalogram (EEG) coherence, atmospheric noise, and Schumann resonances in group meditation

Douglas A. Newandee
New Jersey Institute of Technology

Copyright Warning & Restrictions

The copyright law of the United States (Title 17, United States Code) governs the making of photocopies or other reproductions of copyrighted material.

Under certain conditions specified in the law, libraries and archives are authorized to furnish a photocopy or other reproduction. One of these specified conditions is that the photocopy or reproduction is not to be "used for any purpose other than private study, scholarship, or research." If a, user makes a request for, or later uses, a photocopy or reproduction for purposes in excess of "fair use" that user may be liable for copyright infringement,

This institution reserves the right to refuse to accept a copying order if, in its judgment, fulfillment of the order would involve violation of copyright law.

Please Note: The author retains the copyright while the New Jersey Institute of Technology reserves the right to distribute this thesis or dissertation

Printing note: If you do not wish to print this page, then select "Pages from: first page # to: last page #" on the print dialog screen

ABSTRACT

MEASUREMENT OF THE ELECTROENCEPHALOGRAM (EEG) COHERENCE, ATMOSPHERIC NOISE, AND SCHUMANN RESONANCES IN GROUP MEDITATION

by
Douglas A. Newandee

Electrical activity in the human body was investigated using EEG and ECG measurements while subjects remained with eyes open, eyes closed and in a meditation state. During these measurements, additional antennas were attached to the equipment to record atmospheric noise and signal activity simultaneously. The obtained data was analyzed and various observations were made.

Processed data based on antenna signals clearly showed the presence of man-made signals, having narrow spectral widths that could be treated as atmospheric noise in the frequency range up to 50 Hz. In addition, signals clustered around 7.8, 14.1, 20.3, 26.4, and 32.5 Hz were observed as Schumann resonances of the earth-ionosphere waveguide.

Careful analysis of the noise in the EEG and ECG signals showed the noise activity to be identical to the signals detected by the antennas. Hence, it was possible to differentiate the physiological brain and heart activity from the noise, which is now clearly identified as man-made signals and Schumann resonances up to 50 Hz. The presence of coherence in dual EEG channels is a good measure to quantify the meditation state. The performed measurements showed high coherence around 10 Hz in single subjects while meditating. When these measurements extended to two subjects, with the goal to study group meditation, it was observed that coherence spectra spread significantly to other frequencies.

MEASUREMENT OF THE ELECTROENCEPHALOGRAM (EEG) COHERENCE, ATMOSPHERIC NOISE, AND SCHUMANN RESONANCES IN GROUP MEDITATION

by
Douglas A. Newandee

A Thesis
Submitted to the Faculty of
New Jersey Institute of Technology
in Partial Fulfillment of the Requirements for the Degree of
Master of Science in Biomedical Engineering

Biomedical Engineering Committee

January 1996

APPROVAL PAGE

MEASUREMENT OF ELECTROENCEPHALOGRAM (EEG) COHERENCE, ATMOSPHERIC NOISE, AND SCHUMANN RESONANCES IN GROUP MEDITATION

Douglas A. Newandee

Dr. Stanley S. Reisman, Thesis Advisor — Date
Professor of Electrical Engineering and Associate
Chairperson for Graduate studies, NJIT

Dr. Edip Niver, Committee Member — Date
Associate Professor of Electrical Engineering Program, NJIT

Dr. David Kristol, Committee Member — Date
Professor of Chemistry and Director of Biomedical
Engineering Program, NJIT

BIOGRAPHICAL SKETCH

Author: Douglas A. Newandee

Degree: Master of Science in Biomedical Engineering

Date: January 1996

Undergraduate and Graduate Education:

- Master of Science in Biomedical Engineering
  New Jersey Institute of Technology, Newark, NJ, 1996
- Bachelor of Science in Biology / Pre-chiropractic
  Bloomfield College, Bloomfield, NJ, 1994
- Master of Science in Electrical Engineering
  Stevens Institute of Technology, Hoboken, NJ, 1987
- Bachelor of Science in Electrical Engineering
  Rochester Institute of Technology, Rochester, NY, 1981

Major: Biomedical Engineering

Presentations and Publications

Davis, B. A., Krivickas, L. S., Findley, T. W., Maniar, Newandee, D. A., R., Feinberg, J. H., "Evaluating the Reliability of Monopolar and Bipolar Fine Wire for Measuring Muscle Fatigue." *American Academy of Physical Medicine & Rehabilitation 57th Annual Assembly*, Orlando, FL, November 19, 1995.

Newandee, D. A., Reisman, S. S., "Measurement of EEG Coherence in Individual and Group Meditation: A Pilot Study." *22 nd Annual Northeast Bioengineering Conference*, New Brunswick, NJ, March, 1996.

Newandee, D. A., Niver, E., Reisman, S. S., "Measurement of Man-made and Natural Atmospheric Noise - Schumann Resonance During Meditation Session: A Pilot Study." *22 nd Annual Northeast Bioengineering Conference*, New Brunswick, NJ, March, 1996.

Science is not meant to be conformism and majoring rule. Innovation does not come from a majority in science. It always comes from someone considered an outsider.

Peter Duesberg

This thesis is dedicated to my parents, Andrew and Pamela Newandee,
for all their support and guidance throughout my education
and
Dr. Maria T. Vogt for believing in me and assisting me to enter medical
school.

ACKNOWLEDGMENT

The author wishes to express his sincere gratitude to his advisor, Dr. Stanley S. Reisman, for his patience, guidance, friendship, and moral support throughout this research.

Special thanks are extended to Dr. David Kristol and Dr. Edip Niver for serving as members of the committee. Dr. Niver has provided the idea, the articles on Schumann Resonances, and the use of the shielded room in the NJIT Microwave Laboratory as the research facility for this thesis.

Special gratitude and appreciation are extended to Dr. Thomas W. Findley and Miriam Daum, PT, MPH of the Kessler Institute for Rehabilitation, who provided expert assistance on clinical and regulatory questions. The author also appreciates the following NJIT students: Rindala Saliba, Melissa Leifer, Xiaorui Tang, Santiago Augeraud, Robert Okojie, Oksana Mazhura, M. Basi and others for volunteering their time being the subjects for this research.

Many thanks to John Andrews for his ideas and technical assistance.

And finally, much gratitude should go to Dr. Ronald Kane and Annette Damiano of the NJIT Graduate Studies Department for reviewing and providing correction recommendation for the final draft of this thesis.

TABLE OF CONTENTS

TABLE OF CONTENTS
(Continued)

Chapter **Page**

TABLE OF CONTENTS
(Continued)

Chapter **Page**

LIST OF TABLES

LIST OF FIGURES

Figure **Page**

LIST OF FIGURES

Figure **Page**

CHAPTER 1

INTRODUCTION

Recent studies have demonstrated that the practice of meditation has a measurable effect on the human body. These studies have also shown links between the clear relaxed subjective state a person experiences during meditation and such observed physiological phenomena as increased coherence of the electroencephalogram (EEG), changes in heart rate, etc. [1][2].

Other studies have suggested that mass meditation may influence population of a big city resulting in a decline in the city's crime rate [3]. It has been shown that many species are sensitive to stimuli not previously known to be within the receptive domain (e.g., Baker [4], Schmidt-Koenig & Keeton [5]). Humans, for example, have been shown to be responsive to weak electromagnetic fields on the order of 10 Hz with brain tissue gradient of 10^{-5} to 10^{-7} V/cm which are many order of magnitude less than the gradient needed to fire neuronal action potentials [6]. Such evidence has led Domash [7] and others [8] to suggest that in addition to its classical action potentials, the brain has quantum mechanical modes of functioning [9]. For many years studies on the effect of the Transcendental Meditation (TM) program on EEG spectra and coherence in the individual provided results which are interpreted as supporting a field theory of consciousness. Since the EEG is sensitive to changes in consciousness, it is hypothesized that field fluctuations might be detected by analyzing the EEG coherence between subjects. This work was initiated to quantify the relation between subjects in a group meditation state.

Measurements conducted on subjects were confined to EEG and ECG data and in addition, signals present in the environment were monitored by connecting antennas.

Antenna data analysis revealed the presence of man-made strong and weak signals in the atmosphere and the naturally occurring signal components due to Schumann resonances that were clustered around 7.8, 14.1, 20.3, 26.4, and 32.5 Hz The EEG and ECG signals detected through attached electrodes yielded physiological signals due to electrical activity in the brain and the body. The man-made signals of large amplitudes were strongly evident in the EEG and ECG electrode data. Relative comparison of the antenna dimensions (12 x 12 in^2) to the electrode dimensions (0.5 x 0.5 in^2) suggested that the electrode acting as an antenna would have a much smaller gain than the antenna. This would obviously affect the acquisition of the Schumann resonance signal. Hence, the remaining noise components of the electrode data having much lower amplitudes would be difficult to identify.

Data analysis methods in terms of time-frequency analysis, spectral analysis, and coherence analysis seem to complement each other. Each approach revealed more information that could not be observed otherwise. For example, wide band coherence confined to a relatively short time interval could not be identified from the power spectra alone which was a sign of a deep meditative state.

Data obtained in pre-meditation periods, including eyes open and eyes closed states differed significantly from the meditation period. Meditation data on the individual subject appeared to be very similar to what has been reported in the open literature [10]. However, measurements conducted on two subjects simultaneously, differed significantly than individual measurements. Additionally, simultaneous measurements of the EEG and

the ECG channels with atmospheric noise, might suggest that the possibility of physiological signals produced during mass meditation, being coupled to the earth-ionosphere wave guide which can lead to more pronounced effects.

CHAPTER 2

MEDITATION

Since the goal of this thesis is to investigate the nature of the relation between human subjects involved in a group meditation, a brief introduction and recent research on the subject are presented in this chapter.

2.1 Background

Meditation is a stylized mental technique repetitively practiced for the purpose of attaining a subjective experience that is frequently described as very restful, silent, and of heightened alertness, often characterized as blissful [1].

Most meditation techniques fall into three categories: concentration, contemplation and transcendental. Concentration techniques, nearly endless in variety, are all those which involve an effort to focus the mind on a particular thought, sensation, image, part of the body, or other object of experience [3]. Contemplative techniques such as Zen comprise the second principle category of meditation methods. Contemplation involves thinking about an important idea or question, (i.e., God, Love, Who am I?) in a free and unconstrained manner [3].

Transcendental meditation and Yoga form the last category of meditation techniques. In the late 1950's, Maharishi Mahesh Yogi introduced the technique of Transcendental Meditation (TM). The novelty of TM was that it required no special circumstances for practice, nor any diet or lifestyle changes. The TM technique is defined

as "turning the attention inwards towards the subtler levels of a thought until the mind that transcends the experience of a thought arrives at its source [11]. This source of thought termed "pure consciousness," is experienced as a state of least excitation of consciousness or consciousness without activity [12].

Using meditative "exercises" such as transcendental meditation, the human nervous system can get to what we may call the transcendental state. Certain physiological processes have been found to take place when the human nervous system is in this meditative state. Some of the physiological changes are:

- reduction of the metabolic rate by up to 25-30 per cent;
- reduction of the total oxygen consumption by up to 20 per cent;
- reduction of the breathing rate to 4-6 breaths per minute from 12-14 per minute;
- increase of the amount of alpha wave power (8-12 Hz) in the EEG;
- appearance of theta waves (5-8 Hz) in the EEG;
- reduction of the blood pressure by an average 20 per cent in hypertensive patients;
- significant increase (more than five times) of the skin resistance;
- changes in the pH and sodium bicarbonate concentration of blood;
- reduction of the uropepsin output;
- decrease of the cardiac output (heart blood flow) by about 25 per cent;
- marked decrease (up to 50 per cent) of the lactate ion in the blood;

Some of the additional positive results of the TM technique in particular are:

- increased energy and efficiency in performing a task;
- increased calmness and decreased physical and mental tension;

- increases in creativity, productivity, inventiveness, discrimination, intuitiveness and concentration;

- loss of a desire for or a complete elimination of hallucinogenic or depressant substances such as LSD, marijuana, amphetamines, tobacco, coffee or alcohol;

- attenuation of such symptoms as bad body posture, insomnia, high blood pressure;

- better mobilization of body resources to combat various strenuous circumstances such as in accidents, sensory monotony, confined places, cases of injury and others [1] [13].

Man, therefore can exist in at least four major states of consciousness: those of sleep, dreaming, wakefulness and transcendental. The time we spend in sleep is apparently used to rejuvenate the body by the emission of certain growth hormones, and to remove body fatigue so we can function physically during wakefulness. The time we spend during dreaming is apparently used to remove psychological strains and stresses from our minds so that we can function better mentally and physically during wakefulness. Many well-known sleep and dreaming deprivation experiments on human and animals support this view [13].

Similarly, the time spent during meditation is used to rejuvenate both the body and the mind at deeper and finer levels, i.e. to rejuvenate our machinery of experiencing the central nervous system itself. If a person is deprived of his daily meditation time, then he feels not as sharp, not as clear, not as fulfilled. He is not energetic and he strains more in whatever he does. TM, which takes the practitioner to the fourth major state of human existence, comes to fill this vital need of our time.

2.2 Meditation Research

Although meditation is centuries old, scientific study of meditation began only some 60 years ago. As early as 1935 a French cardiologist, Theresa Brosse, traveled to India to study the physiology of meditation. She reported that one of her subjects was apparently able to stop his heart [3].

Some 20 years latter, in an attempt to follow up and extend Brosse's original study, a team of American and Indian researchers investigated autonomic function of yoga practitioners [3]. They founded decreased respiratory frequency and increased skin resistance, but no consistent changes of heart rate, blood pressure, or ECG, during physical and mental yoga exercise [1].

In the area of EEG, early studies are more consistent and in general, show increased alpha and theta wave activity in Yoga and Zen meditation techniques. Other studies on Zen meditators showed such changes as significant decreases of respiration rate, oxygen consumption, and slight increase of pulse rate and blood pH during meditation [1].

Initial EEG studies of TM reported increased intensity (mean squared amplitude) of slow alpha activity (8-12 Hz) in central and frontal regions, occasionally interspersed with high voltage frontal theta activity. Beta (13-30 Hz) and delta (2-4 Hz) waves either decreased or remained constant during meditation [1].

Levine and Levine et al. [14] have shown that during the TM technique there is an increase in frontal and central alpha coherence and a spreading of coherence to other frequencies, particularly theta. The most common feature was the onset of strong alpha

coherence (above 0.95) during the TM technique relative to the eye-closed control period [15].

Other researchers have measured EEG coherence between pairs of three different subjects during a one-hour practice of the TM program. Orme-Johnson et al [9] evaluated the coherence between subjects for two sequential fifteen minute periods. On six experimental days, these periods preceded and then coincided with a fifteen minute period during which 2500 students participated in the TM - Sidhi program at a course 1000 miles away. After the course had ended coherence was evaluated on six control days. It was found that intersubject coherence was generally low, between 0.35 and 0.4, with coherence in the alpha (8 - 12 Hz) and beta (16 - 20 Hz) frequencies significantly higher than at other frequencies. Coherence increased significantly on experimental days compared with control days particularly in the alpha and theta frequencies. The results reinforce previous sociological studies showing decreased social disorder in the vicinity of TM - Sidhi participants and prove the hypothesis of a field theoretic view of consciousness [9].

CHAPTER 3

SCHUMANN RESONANCES

In this study, experimental investigation of human subjects in a meditation state was carried out. Measured EEG data were observed to have a significant noise component in the presence of the physiological signal. Detailed analysis revealed that the noise component included man-made signals in addition to naturally occurring signals due to Schumann resonances of the earth-ionosphere waveguide. More detailed explanation of Schumann resonances is given below and in Appendix A.

3.1 Background

The earth surrounded by an atmosphere can be considered as a medium where electromagnetic waves of various frequencies are being generated. The sources of these frequencies are either man-made or from natural events such as lightning, cosmic storms, etc. and are propagated in various directions. The earth surface's uneven geometry and chemical composition can be viewed as a layer with variable electrical parameters that may show seasonal, daily and hourly variations. The atmosphere, especially the ionosphere can also be viewed as a plasma medium inhomogeneous in all directions and a function of time. The idea that the surface of the earth and the lower edge of the ionosphere form a cavity whose resonant frequencies occur in the extremely low frequency (ELF) region of the radio spectrum was formulated mathematically by Schumann [16] in 1952. His initial work considered an idealized model of the earth surface and ionosphere as two concentric

spheres with infinite conducting walls. Later he calculated resonance frequencies and attenuation constants predicting a lowest order resonance of f ≈ 10 Hz and quality factor Q ≈ 12. Schumann and his student, König, further continued to work in this field and published the first experimental data indicating observation of these resonances [16]. Later Balser and Wagner [1] determined experimentally that resonances at 8, 14.1, 20.3, 26.4, and 32.5 Hz with the cavity quality factors of Q ≈ 4 (at the lowest resonant frequency) were measured for one particular day. Since then to the present day much more work has been done in improving the theoretical models and experimental techniques. Good literature surveys are found in books by Wait [17] and Galejs [18]. More recent developments are due to Bliokh [19], and others.

3.2 Outline

The frequencies of the earth-ionosphere cavity resonances, now commonly called "Schumann resonances," may be calculated for a uniform cavity with perfectly conducting walls according to W. O. Schumann [16] or J. R. Wait [17]. Refer to Appendix B for a brief derivation of the earth-ionosphere cavity resonances using Maxwell's equations. This gives:

$$f_n = \frac{\omega_n}{2\pi} \approx \frac{c}{2\pi a}\sqrt{n(n+1)} = 10.6\sqrt{\frac{n(n+1)}{2}} \tag{3.1}$$

Assuming the earth's radius to be 6370 Km, equation (3.1) yields the Schumann frequencies:

$$f_1 = 10.6Hz \quad f_2 = 18.3Hz \quad f_3 = 25.9Hz \quad f_4 = 33.5Hz \quad f_5 = 41.1Hz$$

for $n = 1, 2, 3, 4$, and 5, respectively.

Table 3.1 lists the comparison of these theoretical frequencies with the experimentally determined ones [19]

Table 3.1 Theoretical and Experimental Schumann Resonance Frequencies.

Studies	Resonance frequency					Reference
1	10.6	18.3	25.9	33.5	41.1	**Schumann [16] (calculated frequencies for perfectly conducting cavity; see equation (B.33).**
2	7.8	14.1	20.3	26.4	32.5	**Balser and Wagner [20]**
3	7.8	14.1	20.3	26.3	32.5	**Chapman and Jones [21]**
4	8.0	14.1	20.3	26.4	-	**Galejs [18]**
5	7.8	14.1	20.0	26.0	-	**Rycroft [22]**
6	7.8	14.0	20.3	26.1	32.1	**Egeland and Larsen [23]**
7	7.8	14.0	20.0	26.1	31.8	**Bliokh *et al.* [19]**

The agreement is much less satisfactory, however, when the calculated and experimental values of the Q - factor of the resonator are compared. We define the experimental value $\tilde{Q}_n$ of this factor for the nth resonance as the ratio of the central frequency $\tilde{f}_n$ of the resonance peak in the noise power spectrum to its width $\Delta\tilde{f}_n$ at the half-power points:

$$\tilde{Q}_n = \frac{\tilde{f}_n}{\Delta\tilde{f}_n} \tag{3.2}$$

The calculated result is obtained from the formula:

$$Q_n = \frac{\mathrm{Re}\, f_n}{2\,\mathrm{Im}\, f_n} \tag{3.3}$$

where f_n is the complex resonance frequency. Table 3.2 list the values of f_n, $\tilde{f}_n$, Q_n, and $\tilde{Q}_n$ for an ionospheric model in which parameters are adjusted so that the first two resonance frequencies agree ($b-a=75$ km, $\frac{\omega_0^2}{V}=8.1\times10^5/s$).

Table 3.2 Eigenfrequencies f_n and quality factor $\tilde{Q}_n$ of resonance modes in earth-ionosphere cavity.

Number	Experimental $\tilde{f}_n$ [Hz]	Calculated f_n [Hz]		Experimental $\tilde{Q}_n$	Calculated Q_n	
		perfect cavity	homogenous ionosphere		perfect cavity	homogenous ionosphere
1	7.8	10.6	7.8	4.63	-	1.39
2	13.8	18.3	14.0	5.96	-	1.90
3	19.7	25.9	21.6	6.56	-	2.25
4	25.7	33.5	28.5	6.83	-	2.58
5	31.7	41.1	35.5	6.95	-	2.88

CHAPTER 4

THE ELECTROENCEPHALOGRAM (EEG)

The gross electrical activity of different parts of the brain can be recorded electrographically. As early as 1875, evidence of spontaneous electrical activity was detected in the brain of animals. Observing that sensory stimulation transformed the characteristics of the ongoing electrical activity, the early pioneers of electrophysiology concluded that what they were recording was somehow related to the cerebral function. By 1920, sensitive string galvanometers were being used to record the electrical activity from the human brain through the intact skull [24]. Electroencephalography as a clinical tool was introduced by Hans Berger in 1929. The technique was crude and most physiologists thought Berger's records were artifactual. However, by the mid 1930's Electroencephalography began to play an important role in neurological diagnosis.

4.1 Types of Recordings

The recording of gross electrical activity from the brain through the intact skull provides an electroencephalogram (EEG). When the skull is trephined (opened with a circular saw) and the electrodes are placed either on the meninges covering the brain or within the cortex itself, the recordings constitute an electrocorticogram (ECoG). In a third recording procedure, the electrodes penetrate deep within the brain, and the readings obtained are called depth recordings [24].

4.2 Modes of Recordings

To record the voltage changes through the skin covering the skull, either from the surface of the cortex or from deep within the brain, the electrodes may be arranged for either bipolar or monopolar (a misnomer) recording. Typically, bipolar recordings are used to assess the fluctuations in potential between two electrodes deep within the brain, and the electrode tips are frequently less than 0.5 mm apart. The recording provides the algebraic resultant of the potentials under each electrode.

In contrast to bipolar recording, in which both leads are in proximity to the brain, the technique of monopolar recording attempts to provide a record of the potential differences between an active cortical or subcortical electrode and an indifferent electrode that is situated at a location relatively distant from the brain, such as the ear. For the most part, the active lead picks up the brain potentials that are immediately near it, but the interpretation of the results is sometimes difficult. This is particularly true of human EEG recordings, in which both electrodes are actually distant from the brain. For this reason, a common reference electrodes is sometimes affixed to the skull, and readings between this lead and various other placements are compared. Although the term "monopolar" is inexact and misleading, it continues to be widely used in both research and clinical practice [24].

4.3 Types of Brain Waves

It was not until after the turn of this century that observations were made indicating that the normal oscillation found in the recordings of the brain activity could be interrupted by the stimulation of an afferent nerve. By 1930, it was known that the EEG was dominated

by large-amplitude, slow-wave fluctuations during sleep, while the recordings showed considerably less amplitude and less obvious periodicity during wakefulness.

As mentioned briefly in the previous section, electrodes placed on the head measure continuing oscillations due to the electrical activity of the brain. These variations in potential are called brain waves, and when they are recorded, the record is termed an electroencephalogram. The amplitude of these waves when measured through the scalp is about 10-100 μV, and their frequency can vary from 0.5 up to 100 Hz. The character of the brain waves is highly dependent on the degree of activity in the cortex [25]. Much of the time, especially during alert activity, the brain waves are small in amplitude and quite asynchronous. However, at other times the brain will exhibit very rhythmic activity that is almost sinusoidal in nature. While the behavioral state of the subject remains so far as possible constant, the EEG changes continuously throughout life, rapidly during childhood and adolescence, and more gradually thereafter. Not only does the EEG of any individual change continuously, but there are also considerable differences between one subject and another. However, the EEG that is best described statistically (in terms of its amplitude, spectral properties etc.), retains some constant features and may, for most purposes, be regarded as a stationary random process [25]. These brain wave patterns are divided into four different types of waves: alpha, beta, theta, and delta waves. (see Figure 4.1) [26].

Alpha waves consist of high-amplitude, well-synchronized sinusoidal waves having frequency of between 8 and 12 Hz. They occur in almost all adults, particularly in the back of the head, when they are awake but in a quiet, resting state with the eyes closed. Alpha waves will disappear during sleep and when an awake person focuses attention on a specific mental activity [26]. Alpha waves are also prominent during

meditation, and tend to decrease in frequency as meditation progresses. In experienced meditators, lower frequency alpha waves sometimes persist even after the person stops meditating [27]. Alpha waves will not occur in the cortex without connections with the thalamus, so it is likely that a general thalamocortical origin of alpha waves exists, producing the periodicity and the ability to activate millions of neurons in the cortex [26].

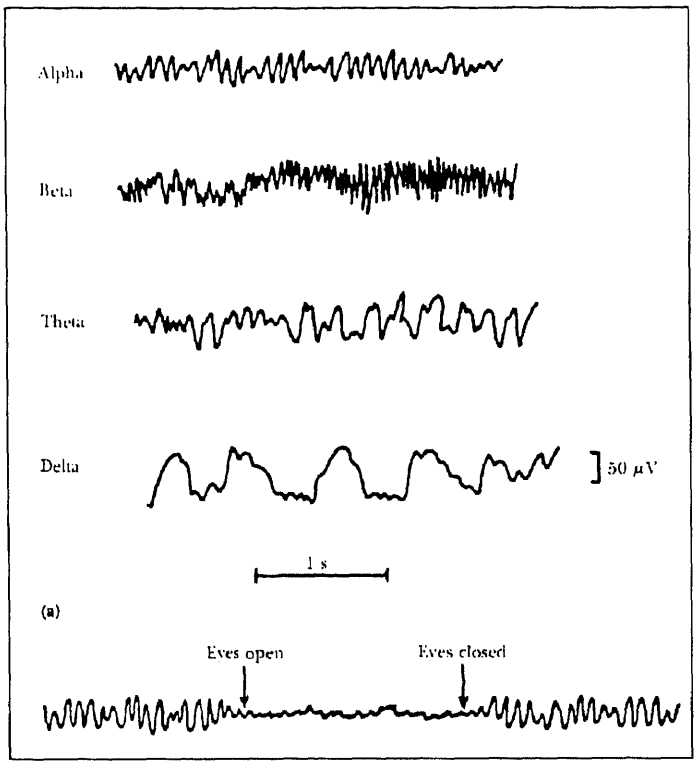

Figure 4.1 Examples of EEG (from Guyton, A. C., *Textbook of Medical Physiology,* 1991)

Beta waves are desynchronized, lower-amplitude than alpha waves. Desynchronization is not only characteristic of the transition between the closing and the opening of the eyes, but also of the most alert, attentive, or excited states. Beta waves normally occur at frequencies above 13 Hz, sometimes they can be as high as 50 Hz.

These mostly appear in the parietal and frontal lobes during intense mental activity [26].

Theta waves oscillate at frequencies between 4 and 7 Hz. These waves occur mainly in the parietal and temporal lobes of children, but they can also appear during emotional stress in adults, especially during disappointment and frustration [26]. Theta waves also appear during deep meditation, especially in experienced meditators [27].

Delta waves include all frequencies below 4 Hz. These occur in very deep sleep, in infants, and in serious organic brain disease. They also have occurred in animals whose cerebral cortex has been transected from the thalamus, indicating the waves can occur in the cortex independent of other brain areas [26].

The EEG is still a very crude measurement of the brain functioning. All that is being detected is the overall pattern of activity of millions of neurons. It is rather like hanging a microphone above a large city and recording the traffic noise. One might be able to tell whether the traffic lights are changing in synchrony, but that is about all. Nevertheless, crude as it is, the EEG is the most convenient technique available for assessing the general activity of the brain and relating it to different states of consciousness.

CHAPTER 5

SIGNAL PROCESSING

During the course of this thesis a significant amount of collected data was related to EEG activity of human subjects and the atmospheric noise surrounding them. Better appreciation of this collected data required signal processing techniques such as Fast Fourier Transform (FFT), frequency analysis and coherence. These techniques are summarized in the remainder of this chapter.

5.1 Fast Fourier Transform (FFT)

In order to use the FFT, it is necessary to digitize the EEG signal at an appropriate sampling rate. If one wants only to observe the basic frequency of beta waves and does not care whether they are spindle shaped, then the highest frequency of interest is about 30 Hz, and digitizing at the Nyquist rate, i.e. at 60 times per second should be adequate. On the other hand, if it is important to know whether a 16-Hz beta wave is spindle shaped, then probably even the fifth harmonic (that is, 80 Hz) is important. In this case the digitization rate should be near 160 or 200 samples per second. Thus the range of 160 to 200 would seem reasonable as a first approximation. In order to demonstrate that all necessary information is suitably preserved, it may be necessary to compare results using higher frequency components. The sampling rate used in this thesis is kept at 200 samples per second.

The FFT yields a series of terms describing the function in the frequency domain as a finite series of complex numbers [28]

$$\alpha_1,\ \alpha_2, \ldots,\ \alpha_{N/2} \tag{5.1}$$

where N = number of points in time that are included in the discrete time series. Recalling the Fourier transform definition as

$$F(\omega) = \int_{-\infty}^{+\infty} f(t) \cdot e^{-i \cdot \omega \cdot t} \cdot dt \tag{5.2}$$

or the discrete transform definition

$$\alpha_j = \frac{1}{N} \sum_{1}^{N} f_k \cdot e^{-i \cdot 2 \cdot \pi \cdot j \cdot \frac{k}{N}} \tag{5.3}$$

If one changes time zero by an amount t_0 the first of these two equation can be rewritten

$$\begin{aligned} F_{t_0}(\omega) &= \int_{-\infty}^{+\infty} f(t + t_0) \cdot e^{i \cdot \omega \cdot t} \cdot dt \\ &= e^{-i \cdot \omega \cdot t_0} \cdot \int_{-\infty}^{+\infty} f(\tau) \cdot e^{i \cdot \omega \cdot \tau} \cdot d\tau \\ &= e^{-i \cdot \omega \cdot t_0} \cdot F(\omega) \end{aligned} \tag{5.4}$$

In the second case it is equivalent to altering the subscript k by t_0/N and hence

$$\alpha_{j,t_0} = e^{-2 \cdot \pi \cdot i \cdot t_0 / N} \cdot \alpha_j \tag{5.5}$$

Comparing (5.4) and (5.5) it is seen that the phase of $F(\omega)$ and α_j are altered by a shift in the location of time zero, but their absolute values remain unchanged

$$\left|F_{t_0}(\omega)\right|^2 = \left|F(\omega)\right|^2$$
$$\left|\alpha_{j,t_0}\right|^2 = \left|\alpha_j\right|^2 \qquad (5.6)$$

Spectral analysis as used in the EEG literature almost always refers to the discrete power spectrum $\left|\alpha_j\right|^2$. (Strictly, the power spectrum is the expected value of $\left|\alpha_j\right|^2$, that is, the limiting value as the time interval T becomes very large.)

In this thesis, the FFT is used to compute all the power spectra. Another function called the cross-correlation, the integral of the product of two signals with one lagged relative to the other, is also used. For example, the two signals may come from two different locations on the scalp. If these two signals are *f(t)* and *g(t),* and their cross-correlation is x(t), then x(t) in the transform space is

$$X(\omega) = \overline{F}(\omega) \cdot G(\omega) \qquad (5.7)$$

In comparing the signals from two locations on the scalp, it is sometimes desirable to have a measure of the consistency of the phase differences, that is, the "coherence" of the two signals. Because the cross-correlation spectrum $X(\omega)$ is amplitude dependent, the average of its absolute values must be normalized to yield a coherence spectrum $Y(\omega)$. To compute this new function time is divided into suitable intervals, and the discrete Fourier Transform, $F(\omega)$ and $G(\omega)$, as well as cross-correlation spectra, $X(\omega)$, are computed for each interval. The coherence spectrum, $Y(\omega)$, is usually calculated by the relationship:

$$Y^2(\omega) = \frac{AV \cdot |X(\omega)|^2}{AV \cdot |F(\omega)|^2 \cdot AV \cdot |G(\omega)|^2} \tag{5.8}$$

where the function AV represents the average over the transforms for the various time intervals. This expression is readily computed by multiple applications of the FFT algorithm. Coherence spectra are illustrated in Section 5.2. A more precise definition of the coherence spectrum (or function) replaces the averages in Equation (5.8) with expected values, that is, with the limit of these averages as the number of time intervals becomes very large [28].

5.2 Coherence Spectral Array (COSPAR)

The coherence spectral array, or cospar, is a graphical representation of the coherence between two signals. For the EEG, a high coherence (near 1) over time indicates range spatial ordering. This type of ordering increases in physical systems as they relax to lower states of excitation. Therefore, increased spatial ordering in the EEG indicates a lowering of the excitation level of the brain, which is the response obtained from relaxation. The cospar graph makes this order in the EEG much easier to visualize [14].

Coherence can be viewed as a correlation coefficient in the frequency domain, analogous to the autocorrelation function in the time domain [28]. Coherence is a measure of the linear dependence between a pair of signals, normalized to values between zero and one. The coherence is unity if two signals have the exact same frequency content, in other words if one signal is completely linearly dependent on the other; however for most pairs of real signals coherence is less than unity [29].

If the autocorrelation function of a random process $X(t)$ is defined as: [28]

$$R_X(\tau) = E[X(t+\tau), X(t)] \tag{5.9}$$

then the power spectrum of that process can be further defined as

$$S_X(j\omega) = \mathcal{F}[R_X(\tau)] = \int_{-\infty}^{\infty} R_X(\tau) e^{-j\omega\tau} d\tau \tag{5.10}$$

Similar expressions can be written for the autocorrelation and power spectral density of a second random process $Y(t)$. The cross correlation of the two signals $X(t)$ and $Y(t)$ can further be defined as:

$$R_{XY}(\tau) = E[X(t+\tau), Y(t)] \tag{5.11}$$

with the corresponding cross spectral density as

$$S_{XY}(j\omega) = \mathcal{F}[R_{XY}(\tau)] = \int_{-\infty}^{\infty} R_{XY}(\tau) e^{-j\omega\tau} d\tau \tag{5.12}$$

The coherence function is then defined as the ratio between the cross spectral density of $X(t)$ and $Y(t)$ to the product of the individual power spectral densities.

$$\gamma_{XY}^2 = \frac{|S_{XY}(j\omega)|^2}{S_X(j\omega) S_Y(j\omega)} \tag{5.13}$$

Levine developed a method for calculating the coherence spectrum between pairs of EEG signals. In this technique, the two signals were first divided into short epochs of 256 samples, which for Levine's work corresponded to 5.12 seconds of EEG. The power spectra and cross spectrum of each epoch were computed using an ensemble average on overlapping data segments first discussed by Welch [30].

Welch first outlined this method of power spectrum estimation in 1967. One of its main advantages was that it involved the transformation of data sequences which were much shorter than the whole record, which was an advantage on machines with limited

memory space or for very long records. Welch stated that if $x(n)$, n=0, ... , N–1 was a stationary second order stochastic process, then the sequence could be divided into K sections of length L, that might overlap. To estimate the power spectrum, the sequence x(n) was multiplied by a window w(n), and then the Fourier transformed of the K sequences were calculated. From the Fourier transforms, K periodograms (magnitude squared function) were calculated, then averaged to produce the power spectrum estimate [30].

Once the power and cross spectra were computed, the squared coherence spectrum for each epoch was calculated. A threshold was applied to the coherence spectrum at a fixed level. Levine used 0.95 as the coherence threshold to reduce the likelihood of spurious coherence, or coherence events not representative of long range spatial ordering. The resulting coherence spectra for all epochs were assembled together in time, resulting in a three-dimensional looking graph of coherence level versus time and frequency [14].

For the present study, an algorithm based on the methods of Levine was written in MATLAB to compute the squared coherence function of two EEG channels (see Appendix B). The output of the program was a surface mesh plot of coherence above a 0.95 threshold versus time and frequency. Details of the data analysis technique are presented in section 6.1.5.2.

5.3 Time Frequency Analysis

One of the drawbacks of the spectral analysis of EEG signals is that it cannot track rapid changes over time. Often the level of neural activity can change in as rapidly as ten to fifteen seconds. [31] Time frequency analysis was performed on the EEG data using the Wigner distribution to show other brain-affected interference as a function of time.

The Wigner distribution was first introduced by Wigner (1932) and was subsequently incorporated into signal analysis by Ville (1948). The distribution is defined by the following equation.

$$P_w(t,f) = \int_{-\infty}^{\infty} e^{-j2\pi f\tau} s^*(t-\tfrac{1}{2}\tau)s(t+\tfrac{1}{2}\tau)d\tau \qquad (5.14)$$

The time signal is represented above by $s(t) = A(t)e^{j\varphi(t)}$, where $A(t)$ is the amplitude and $\varphi(t)$ the phase. The Wigner distribution decomposes a signal into time and frequency components, and it has been shown to be a good method for estimating a nonstationary time series [31].

CHAPTER 6

EXPERIMENTAL METHODS

This chapter describes the experimental setup, the EEG electrode placement, the procedure for acquiring data and signal processing tools used. This work is due to a combination of efforts in:

- EEG signals as a part of the on-going relaxation and meditation study at Kessler Institute for Rehabilitation, and
- antenna characterization inside the shielded room at New Jersey Institute of Technology.

The first part involves the study of the EEG coherence taken from volunteers in individual and in group meditation using frontal electrodes. This part will be referred to as experiment I.

The second part involves the developing of a data acquisition system including several simple antennas for studying the atmospheric electrical activity including man-made signals and naturally occurring events such as Schumann resonances in the frequency range below 50 Hz. This part will be referred to as experiment II.

6.1 Experiment I

6.1.1 Setup for Experiment I

Ten subjects participated in this experiment. Some had no previous meditation experience and some practiced various meditation techniques for several years. Table 6.1 shows the distribution of the tested subjects.

Table 6.1 Distribution of the tested subjects (with and without meditation experience)

	Ages	No Meditation	TM	Zen	Yoga
Female	**24 - 28**	**2**	**2**	**0**	**0**
Male	**21 - 47**	**3**	**1**	**1**	**1**

In this experiment, the objective was to compare the EEG coherence of the same subject between individual and group meditation. Hence, the experiment involved two parts: meditation alone and meditation in a group of two. In individual meditation the EEG coherence between F3 and F4 (frontal) electrodes from the individual subject was measured and calculated in order to reproduce the results of Levine, Dillbeck and Orme-Johnson, and others [14] [32] [33]. In group meditation the same EEG coherences between F3 and F4 electrodes from two meditating subjects were found in order to verify the results of Orme-Johnson in group meditation [9].

In experiment I, if the subject had no previous meditation experience, a list of intructions on how to meditate was given. When the subject was an experienced meditator, no instructions were given and he/she would have complete freedom to practice his/her own meditation technique.

In individual meditation, the subject meditated alone inside the shielded room. One channel of antenna, two channels of EEG and one channel of ECG data were collected. The data of the antenna channel were used later as part of experiment II and all details will be discuss in section 6.2. The EEG coherence of the subject was calculated from the two EEG channels and then compared with the coherence of the same subject in group meditation.

In group meditation, two subjects were arbitrarily selected to meditate together sitting side-by-side inside the shielded room. Two EEG channels were collected for each subject.

The EEG signals were recorded using silver electrodes affixed to the forehead of the volunteering subjects with EEG paste and silk adhesive tape. All four input signals of the Experiment I were fed through the wall of the shielded room into the Gould universal amplifiers (model 13-4615-58, Gould, Inc., Valley View, OH). The signals from the amplifier channels were fed into the data acquisition computer, which will be discussed in detail later in this chapter. All data acquisition equipment was placed outside the shielded room.

6.1.2 Electrode Placement

The placement of EEG electrodes on the scalp historically has been subject to much debate. In 1958, the International Federation of Societies for Electroencephalography and Clinical Neurophysiology presented the "10-20 electrode system" to standardize the placement of scalp electrodes. (see Figure 6.1) As its name implies, electrodes are placed in intervals of 10 or 20% of the distance from the nasion to the inion in the sagittal plane and between the preaurical points in the coronal plane [24]. Because of the need for standardization, many EEG laboratories now make use of the International 10-20 system for electrode placements.

Electrical potentials can only be measured with reference to a second point. Since this is the case, electrode placement is crucial, since the measured signal is the algebraic difference of the potentials measured between the two points. The resulting signal is by

definition bipolar. Much of the time in EEG study, a "monopolar" recording is desired so that the activity in one part of the brain can be studied independently of the rest. Monopolar recording (sometimes called common reference recording) assumes the existence of an electrically inactive site for the reference electrode. Strictly speaking, this is not true, since all the cells in the body can conduct electrical potentials. However, the ears have been found a good reference site for EEG recording, since they are relatively free of both myographic and encephalographic interference [24]. All of the meditation studies referenced in this thesis used linked ears for the reference to the scalp electrodes. Therefore for reproducibility the linked ears reference was also used in the studies reported here.

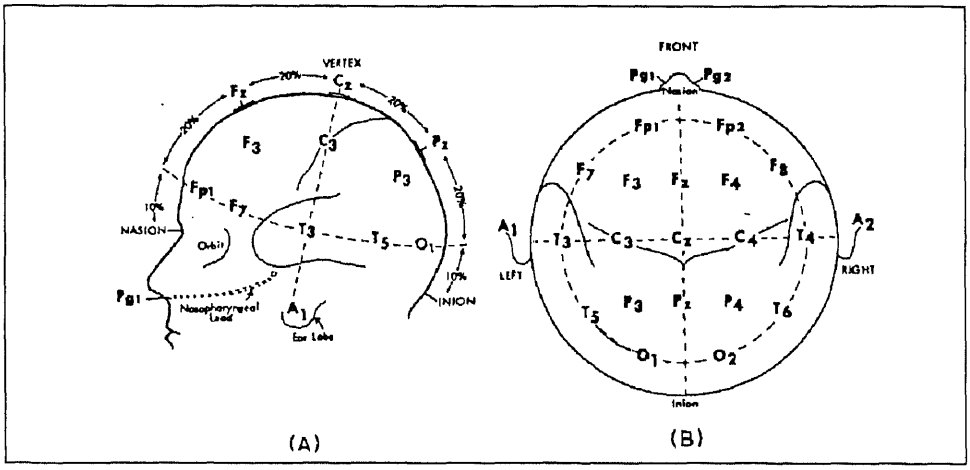

Figure 6.1 The international 10-20 system of electrode placement (from Goff, W. R. *Methods in Physiological Psychology,* 1974.

In order to record a signal from the body, the skin must be cleaned and prepped in order to increase signal transmission from the skin surface to the electrode. For EEG electrodes, OmniPrep (D. O. Weaver & Co., Aurora, CO) was used, applied with a gauze pad. Silver cup electrodes (Jari Electrode Supply, Yucca Valley, CA) were applied using

Elefix EEG electrode paste (Nihon Kohden Corporation, Tokyo, Japan). The F3 and F4 positions were recorded with linked ears (A1 and A2) as a reference. A ground electrode for the amplifier was located at the wrist [2].

The forehead electrodes were connected to the Gould at the (+) position, the linked ears at the (-) position, and the ground at the Gould chassis GND position. The input channels to the A/D board were set at 5 volts. EEG signals generally range from around 50 μV to close to 1 mV. The gain of the amplifier was adjusted so that the output EEG signal from the Gould was around 1-2 Vp-p, which would leave plenty of buffer at the A/D board for relatively high voltage artifacts such as blinking or eye movements. The filters on the amplifier were set for a passband of 1 to 30 Hz, which included the delta (below 4 Hz), theta (4 to 7 Hz), alpha (8 to 12 Hz) and beta (above 12 Hz) EEG bands. EEG waveforms were monitored with a 4-channel digitizing oscilloscope (Gould model DSO 4074, Gould, Inc., Cleveland, OH) connected to the BNC outputs on the rear of the amplifier. Shielded cable connected the 37 pin data output connection, also on the rear of the amplifier, to the data acquisition computer.

6.1.3 Testing Protocols

All data collected from the subjects were divided into three protocols: eyes open, eyes closed and meditation. Before each experiment, subjects were briefed as to the protocol and electrodes were applied as described previously. For each study, subjects were asked to sit quietly for five minutes with their eyes open, then to close their eyes (but not meditate, if the subject happened to be a meditator) for five minutes. The last five minutes

included meditation with their eyes closed. Table 6.2 shows the summary of the experiment I testing protocol.

Table 6.2 Testing protocol of experiment I.

	Channels	Protocol
Individual Meditation	**1 antenna, 2 EEG, 1 ECG**	**Eyes Open, Eyes Closed, Meditation**
Group Meditation (2 subjects)	**2 EEG, 2 EEG**	**Eyes Open, Eyes Closed, Meditation**

6.1.4 Data Acquisition Procedure

Data were acquired and recorded with an IBM compatible microcomputer with a 286 CPU, 8 MHz, 1 MB ram, and a 40 MB hard disk drive. The output of the Gould amplifier was connected via a shielded cable to the DAS-1601 A/D converter board in the computer (Keithley MetraByte/Asyst, Taunton, MA). A diagram of this setup is shown in Figure D.1 (Individual Meditation) and D.2 (Group Meditation) of Appendix D. Once the four inputs were connected to the amplifying equipment, the inputs to the A/D board could be monitored using a display program called Primplot (J. F. Andrews). Any adjustments in gain settings or connection problems could be resolved at this time. When all was in order, data were collected using Streamer v3.25 (Keithley MetraByte/Asyst), a data collection program included with the DAS-1601 board. Once collected, the data files were copied to 1.2 MB floppy diskettes. These files were then transferred onto the hard drive of the 60 MHz Gateway 2000 Pentium (at NJIT) or the 90 MHz Pentium computer (at Kessler) for storage and subsequent analysis. The data on the hard drive of the Pentium computers were periodically backed up onto 125 MB magnetic tape cartridges

using the Colorado tape drive system. For all protocols, data was sampled at 200 samples per second.

6.1.5 Data Analysis

6.1.5.1 Unpacking Data

Data collected on the data acquisition computer by Streamer were saved to the root directory of the hard drive in a packed binary format, using 2 bytes per sample. The software used for data analysis, MATLAB v4.0 (The Math Works, Inc., Natick, MA), cannot read the data in this format, so the data must be converted to an ASCII format which these programs can use. A program called Kunpack2 (a modified version of the unpack utility that Keithley MetraByte/Asyst provided with the DAS-1601 A/D board) was utilized to unpack the data. Kunpack2 converted the raw data files to an ASCII file where each channel of data was represented as a column in a matrix and spaces separated the columns.

The raw data files were moved to the Pentium computers for storage while the ASCII files were copied onto the hard drive of the signal processing workstations for analysis.

6.1.5.2 Coherence Spectral Array (Cospar)

Analysis of the data was performed on a Pentium IBM-compatible 60 or 90 MHz computer. Unpacked data files were imported into MATLAB, a software package that included engineering design and analysis algorithms and permitted the writing of custom MATLAB programs. MATLAB also included a Signal Processing Toolbox, which

included many digital signal processing algorithms such as filters, transforms, and windowing algorithms.

A program called "cospar.m" written by King [2] was used to calculate the cospar using Levine's methods [14]. Two channels of EEG data were given as input arguments to the program. The outputs consisted of mesh and contour plots of coherence above 0.95 vs. time and frequency. A listing of the MATLAB code appears in Appendix B and it worked in the following way [2]. Two channels of EEG signal were lowpass filtered using a 9th order Butterworth filter with cutoff frequency at 45 Hz to remove any residual 60 Hz interference. The signals were then highpass filtered with a 7th order elliptical filter with a cutoff frequency at 1.5 Hz, passband ripple of 0.05 dB, and stopband ripple of 50 dB. The elliptical filter provided the steepest cutoff characteristics, which allowed the low frequency trend to be removed while preserving EEG frequencies above 2 Hz. A zero phase filter algorithm included in MATLAB was employed to eliminate phase distortion.

In order to keep EEG epochs short (thus improving time resolution), Levine specified that a procedure described by Welch be used, where overlapping segments of data are ensembled and averaged [1]. This method was described in section 5.2. Conveniently, MATLAB also contained an algorithm that computed the power spectrum using Welch's method. Five second epochs of EEG were chosen. For each epoch, the two signals were divided into a number of 256 point sections, each of which overlapped by 19 points. Each section was windowed with a Kaiser window algorithm, a 256 point FFT was taken, and then accumulated with a running sum of the previous sections. The cross spectral density of both signals was also calculated in the same way. Specifically, the program calculated the power spectral density as:

$$P_{xx}(e^{j\omega}) = \sum_{i=1}^{k} \left| X_i(e^{j\omega}) \right|^2 \tag{6.1}$$

and the cross spectral density is:

$$P_{xy}(e^{j\omega}) = \sum_{i=1}^{k} Y_i(e^{j\omega}) X_i^*(e^{j\omega}) \tag{6.2}$$

where:

$$k = \frac{n - overlap}{m - overlap} \tag{6.3}$$

Here, n is the sequence length, m is the size of the FFT (256 points), and *overlap* is the number of points the next sequence overlapped the previous one (237 points). (see Figure 6.2)

With the spectral densities evaluated, the coherence for the epoch was calculated as

$$C_{xy} = \frac{\left| P_{xy}(e^{j\omega}) \right|^2}{P_{xx}(e^{j\omega}) P_{yy}(e^{j\omega})} \tag{6.4}$$

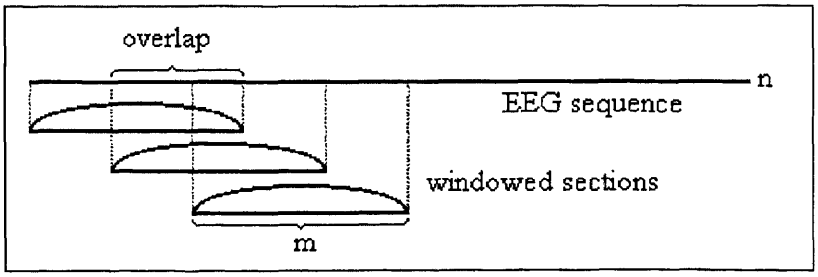

Figure 6.2 Sectioning and Windowing of EEG in MATLAB

For each five second epoch, a vector of coherence versus frequency was produced, with the coherence values ranging between 0 and 1. These vectors were assembled as columns in a matrix, and a threshold of 0.95 was used, so that any coherence value below 0.95 was discarded and set to 0.95. The resulting matrix was graphed as a surface mesh plot and a contour plot of coherence versus time and frequency. An example of a Cospar plot can be seen in Figure 6.3. Figure 6.4 shows a flowchart of this process.

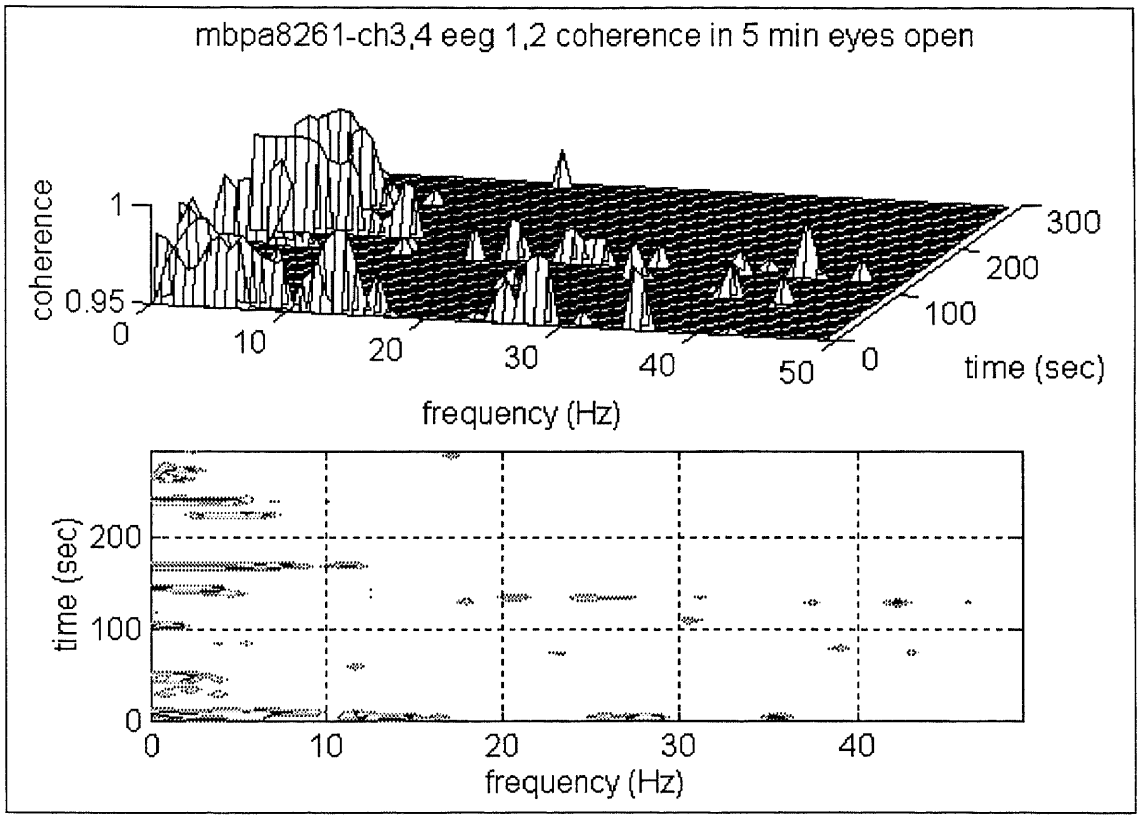

Figure 6.3 An example of a Cospar plot.

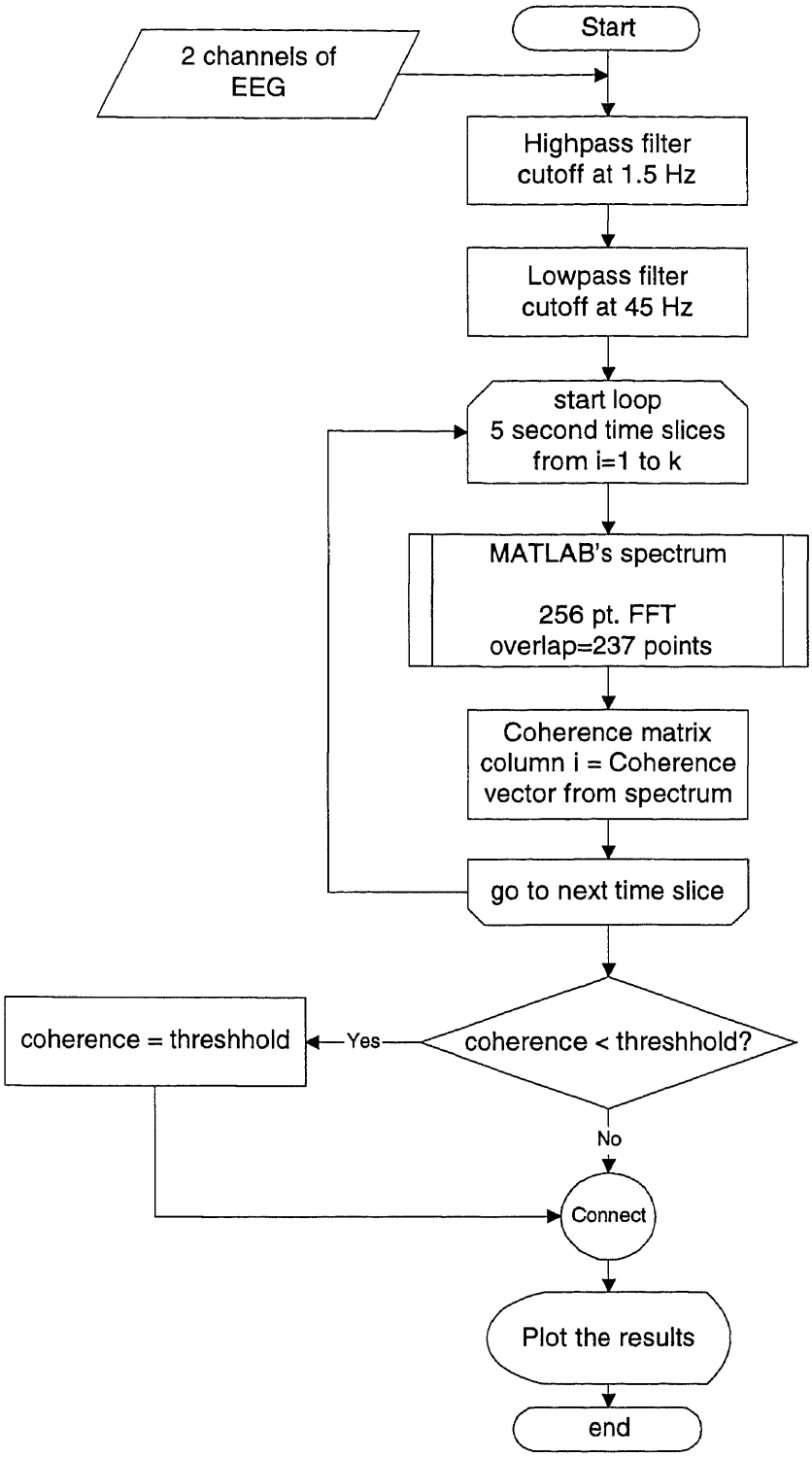

Figure 6.4 Flowchart of Cospar.m

6.2 Experiment II

6.2.1 Setup for Experiment II

This experiment has the following objectives:

1) To determine the suitability of the shielded room in measuring biological signals such as the EEG and ECG that are in the extremely-low-frequencies (ELF) band of the electromagnetic spectrum.
2) To monitor electrical activity in the environment, and to identify man-made and naturally occurring interference, including Schumann resonances.
3) To investigate the possible link between earth-ionosphere waveguide and the alpha coherence of EEG signals in a group meditation.

6.2.2 Antenna Connection

The microstrip patch antenna used in this experiment was made of one square-foot printed circuit board with copper layers on both sides. All antennas used in this experiment were identical. The antenna was connected via a BNC connector. The signal wire of the BNC connector was connected from the antenna signal plane to the Gould amplifier at the (+) position, the ground wire of the BNC connector was connected from the ground plane of the antenna to the (-) position, and the ground at the Gould chassis GND position was connected to the subject's wrist only when the subject was present. This was done to provide short-circuit protection for the subjects and to reduce any artifacts on acquired signal. All other signal adjustments were exactly the same as those of experiment I. The input channels to the A/D board were set at 5 volts. The gain of the amplifier was adjusted so that the output antenna signal from the Gould was around 1-2 Vp-p, which would leave

plenty of buffer at the A/D board for relatively high voltage artifacts such as the switching of the air conditioning systems, and other electrical tools. The filters on the amplifier were set for a passband of 1 to 30 Hz, which covered the same frequency range as the EEG signals. The antenna waveforms were monitored with a 4-channel digitizing oscilloscope (Gould model DSO 4074, Gould, Inc., Cleveland, OH) connected to the BNC outputs on the rear of the amplifier. Shielded cable connected the 37 pin data output connection, also on the rear of the amplifier, to the data acquisition board inside the computer.

6.2.3 Testing Protocols

The study to monitor atmospheric electrical activity in the laboratory was conducted in two parts. The first part, which was called "non-meditation related", included three separate protocols collecting data from antennas. The protocols are listed below:

1) Two antennas were placed at different orientations inside the shielded room. One channel of data was taken for each antenna. Four trials for four different antenna orientations were performed. Data were analyzed to find the best orientation of the antenna in terms of signal clarity. Once the best positions were determined the positions and the orientation of the antennas were kept the same from then on. These positions are explained in chapter 7.

2) One antenna inside the shielded room and one antenna outside in the same orientation as determined in (1). One channel of data was recorded with each antenna. One trial was done for this experiment.

3) Two antennas at NJIT: one inside the shielded room and one outside. The data were collected by the acquisition system at NJIT. Data were also taken from a third

antenna at Kessler (10 miles from NJIT) oriented in same direction and using the same data acquisition equipment as those at NJIT. One trial was performed in this manner.

Antennas were kept connected to measurement apparatus, when meditation experiments were carried out with one subject. This portion of experiment II, which will be referred as "meditation related", involved five protocols. The first protocol required collecting data from two antennas at two different orientations (one vertical antenna pointing North and the other was placed parallel to the ground) for five minutes. This protocol was followed immediately by the next three protocols: eyes open, eyes closed, and meditation of the individual meditation protocol in experiment I. The fifth protocol immediately followed the individual meditation protocol is the same as the first protocol; i.e. only two antennas were being used for data collection within the 5 minutes period. The data from the antenna channel in the individual meditation protocol mentioned in experiment I was used here to analyze the atmospheric signals present in the vicinity of the meditator. Hence, three sets of such data were collected: the eyes open, eyes closed, and meditation protocols of experiment I for each subject. Thus a total of five sets of atmospheric recording could be found per tested subject. The meditation related part of experiment II is summarized in Table 6.3 below.

Table 6.3 Protocols in "meditation related" part of experiment II.

Inside	**In/out ***	**NJIT/Kessler**			
4 trials	1 trial	2 antennas (1 in/1 out) - NJIT 1 antenna - Kessler			
2 antennas	2 antennas				
		Individual Meditation			
	Before	**Eyes Open**	**Eyes Closed**	**Meditation**	After
No. Ant. Channel	2	1	1	1	2

* In/out refers to the location of the antenna, "in" - inside the shielded room, "out" - outside the shielded room.

6.2.4 Data Acquisition Procedure

The data acquisition procedure followed in this phase of the experiment was identical to that in experiment I given in Section 6.1.4. The only difference was that two antenna inputs were used for "before" and "after" protocols.

6.2.5 Data Analysis

6.2.5.1 Unpacking Data

Again the unpacking procedure was the same as described in Section 6.1.5.1. However, the sizes of the data files for "before" and "after" were half as those of experiment I since only two channels were used for these protocols.

6.2.5.2 Spectral Analysis

Spectral analysis is used to describe the frequency content of a signal, random process or system, based on a finite set of data. The estimation of power spectra is useful in identifying man-made components and naturally occurring signals buried in the wide band

noise. In this experiment, the power spectrum of the antenna signals was found from the discrete-time Fourier transform of the windowed collected data. A MATLAB program called "spe_plot" included in Appendix B was used in this phase of the analysis.

The preliminary spectral output clearly identified strong interference due to man-made sources with relatively narrow bandwidths. Then a re-scaling operation that zoomed in on the axes of the spectral plot was performed and new spectral data revealed more details of the lower level signal content. A further re-scaling led to observation of weaker signals, such as Schumann resonances which were observed to be clustered around specific frequencies such as 7.8, 14.1, 20.3, 26.4, 32.5 Hz.

6.2.5.3 Time - Frequency Analysis

In analyzing the data related to atmospheric signals in the entire frequency range from 0 to 50 Hz, the ASCII files that contained the two antenna channels or the four channels (1 antenna, 2 EEG, and one EKG) were loaded into MATLAB. The files were analyzed using the time-frequency technique. The MATLAB program called tf3D.m was written for this analysis. The program output was a 3-D mesh plot of signal power versus time and frequency. For each Schumann resonance, the tf3D.m program was re-run with the interested frequency range entered. The program listing is shown in Appendix B and the analysis procedure is described in Appendix C. An example of the 3-D Time-frequency plot is shown in Figure 6.5. This plot shows the overall picture of the atmospheric signals collected from the antenna. Any man-made or naturally occurring sources can be clearly observed from this plot. The man-made signals in general occurred in a very short time but they have relatively wide spectrum that spread over most or the entire frequency

range. Two man-made signals are displayed in Figure 6.5 near the time 2.3 and 3 minutes. The naturally occurring signals appear at specific frequencies for the entire 5 minutes of data. Two examples are shown in the figure at 20 and 46 Hz. These include the Schumann resonances once the re-scaling operation is performed.

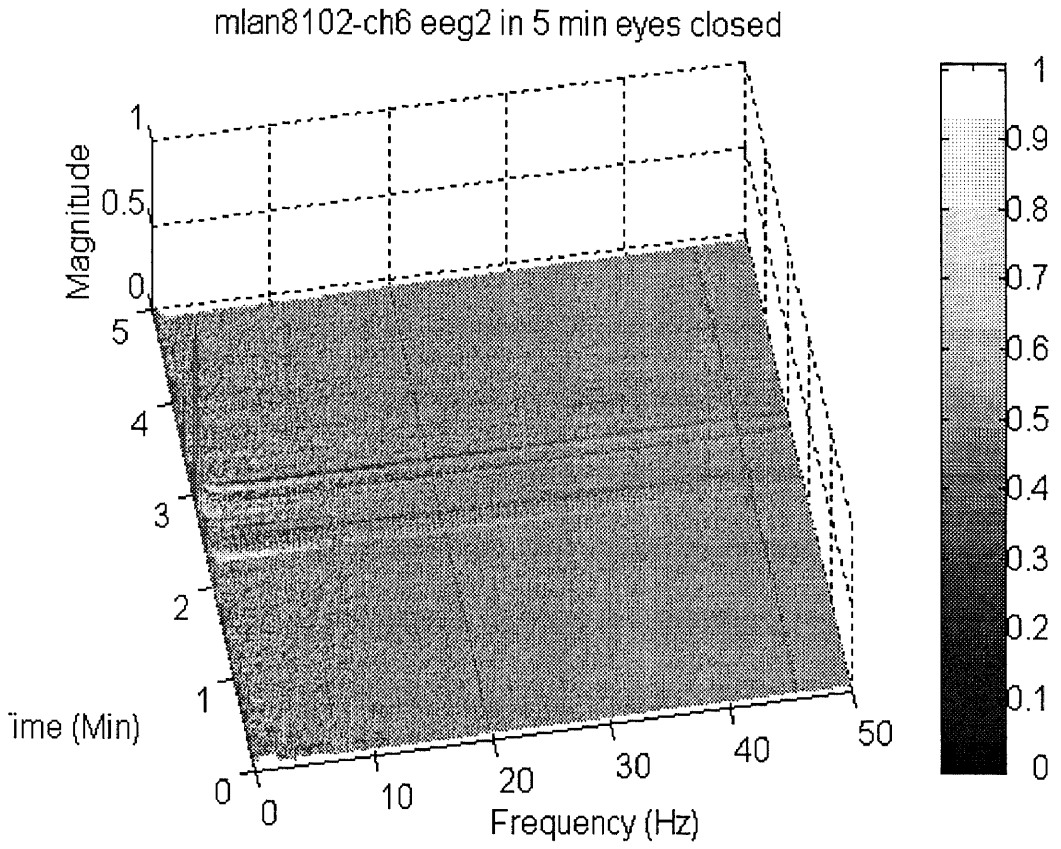

Figure 6.5 An example of 3-D time-frequency plot.

CHAPTER 7

EXPERIMENTAL RESULTS

The experimental study of EEG coherence on human subjects in different conditions (eyes open, eyes closed, and meditation) consisted of recording and analyzing physiological data. Simultaneously, electrical activity of the environment in which subjects were placed was monitored and recorded. Processed data based on external antennas which were attached to monitor atmospheric signals, helped to identify clearly physiological signals in EEG data from the man-made disturbances and naturally occurring events which otherwise would be considered as noise. More careful spectral and time-frequency analysis of this noise component helped to recognize the man-made signals with narrow spectral widths. Much lower level naturally occurring events as Schumann resonances clustered at well-defined frequencies and clearly identifiable in the antenna signal, when embedded within the physiological signals were hardly recognizable. The meditation study has been extended from individual subjects to a group consisting of two subjects. Observations based on experimental data suggested the presence of coupling between subjects and the environment that they are placed in. Detailed analysis of each measurement undertaken including observations made based on analyzed data are presented below.

7.1 Meditation Studies

7.1.1 Individual Meditation Study

Each experimental session began with the subject keeping his/her eyes open for five minutes, then eyes closed for five minutes and then individually meditating for another five minutes. Ten individuals participated in this study as shown in Table 7.1. The last three columns of this table list the coherence values in the individual meditation study that are calculated as the areas under the alpha coherence curve in the frequency range of 8 - 12 Hz at or above the 0.95 level. During the eyes open session, half of the non-meditators (3 out of 6) and all experienced meditators show alpha coherence. During the eyes closed session, all but two subjects (non-meditators subjects 4 and 8) maintain or increase the alpha coherence level. This agrees with the clinical findings in the open literature [26] describing the alpha waves in the EEG of adults with eyes closed. The last column shows the coherence during individual meditation. It is important to note that all subjects show a decrease in alpha coherence in comparison to eyes closed. Typical graphs representing this are shown in Figures 7.1 (b) and 7.2 (a), i.e. less delta and alpha coherence in individual meditation than in the eyes closed session. A possible explanation is that the subject, while meditating, has made less facial movement to decrease the delta band. However, all subjects show a decrease in alpha coherence. This can only be that these subjects are not experienced enough to show strong alpha coherence during an individual meditation session.

Figure 7.1 shows the typical EEG coherence for a subject in an individual meditation session. The figure consists of two parts: (a) eyes open, and (b) eyes closed

and each part contains two graphs. The upper graph is a three-dimensional mesh plot of coherence versus time and frequency whereas the lower graph is a contour plot.

Figure 7.1 (a) shows typically strong coherence both in the delta (0 - 4 Hz) and theta (4 - 7 Hz) bands. This agrees with literature describing the EEG activity while the subject is awake, alert, and eyes open. The coherence that appears in this part is most likely due to facial muscle movement artifact such as head turning, eyes blinks etc.

When the eyes are closed, there are no more visual stimuli to the brain. Less activity forces the subject's mind to feel more relaxed. This state of mind is reflected in Figure 7.1 (b) for a subject with eyes closed. All subjects show the absence of the theta band (4-7 Hz) when their eyes were closed. Very little amount of delta coherence (0-4 Hz) exists. However, this subject shows strong coherence in the alpha band. Strong alpha coherence indicates that there are high-amplitude, well-synchronized sinusoidal waves in the range between 8 and 10 Hz. In short, very little delta, almost no theta and much more alpha coherence are observed. This is in agreement with Orme-Johnson's study in 1980 [15].

Figure 7.2 shows the coherence resulting from individual meditation of two different subjects. The first subject as indicated in Figure 7.2 (a) is a non-meditator. Basic meditation instructions were given to the subject. As a non-meditator following these instructions, the subject was able to achieve the meditative state which is indicated by the presence of alpha coherence. The second subject as shown in Figure 7.2 (b) is considered to be a good TM meditator. The subject has been asked to meditate on three different sessions and has consistently shown strong coherence in the alpha band. In one study, Levine found that most TM meditators showed increased alpha coherence and spread of

coherence to the theta band. However, it was found in this study that only half of the non-meditators showed alpha coherence. All three meditators (TM, Zen and Yoga) showed alpha coherence. It is interesting, however, that the non-meditators who could achieve alpha coherence did better than the subject who practiced the Zen technique.

Reported results in the literature claim that a deep meditation state is associated with a significant broad band coherence [10]. A typical plot of such data obtained in one of the experiments shown in Figure 7.3 (a) depicts that a strong impulse occurred in the EEG recording approximately a minute and a half after the start of the five minute meditation period. After processing, the plot shown in Figure 7.3 (b) confirmed the presence of strong coherence above the threshold of 0.95, covering the lower frequency band up to 20 Hz. A time-frequency plot of the same data in Figure 7.3 (c) validates the presence of a wide band frequency spread which implies that its source must be a short pulse in time domain. Although data presented in Figure 7.3 (a) is due to only one EEG channel, the second channel showed the presence of a short time pulse in the same time interval. Figure 7.3 (b) is obtained using data from both channels. A time-frequency plot of the second EEG channel was very similar to the one in Figure 7.3 (c) and therefore is not included.

Table 7.1 Results for the individual meditation study.
The values are the area under the alpha coherence curve at 0.95 level or above.
* Indicates that there are no alpha coherence above the 0.95 level.

Subject	Technique	Subject ID	Eyes Open	Eyes Closed	Meditation
1	Non-Med	SA	0.0000*	0.2034	0.0285
2	Non-Med	ND	0.0000*	0.0000*	0.0000*
3	Non-Med	RS	0.0000*	0.0000*	0.0843
4	Non-Med	MB	0.0373	0.0298	0.0000*
5	TM	XT	0.0785	0.2661	0.1321
6	ZEN	TN	0.0391	0.0563	0.0189
7	Yoga	RO	0.0478	0.2189	0.1091
8	Non-Med	EN	0.0237	0.0189	0.0000*
9	Non-Med	OZ	0.0418	0.2222	0.0934
10	TM	ML	0.0558	0.2316	0.1112

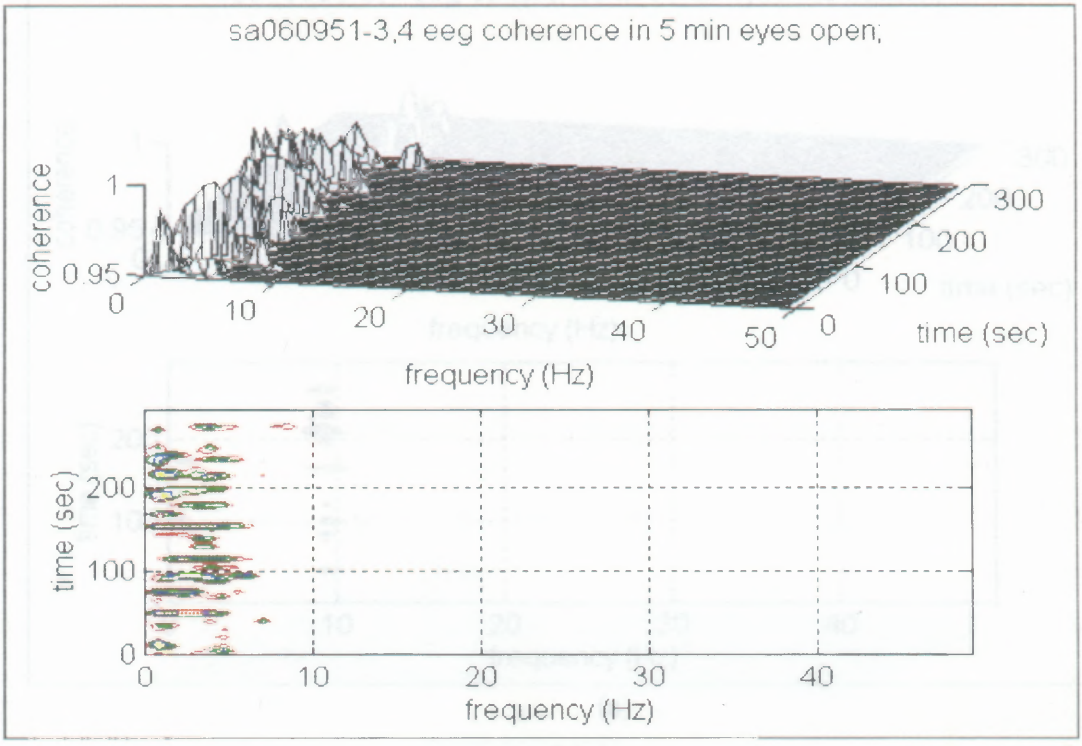

(a)

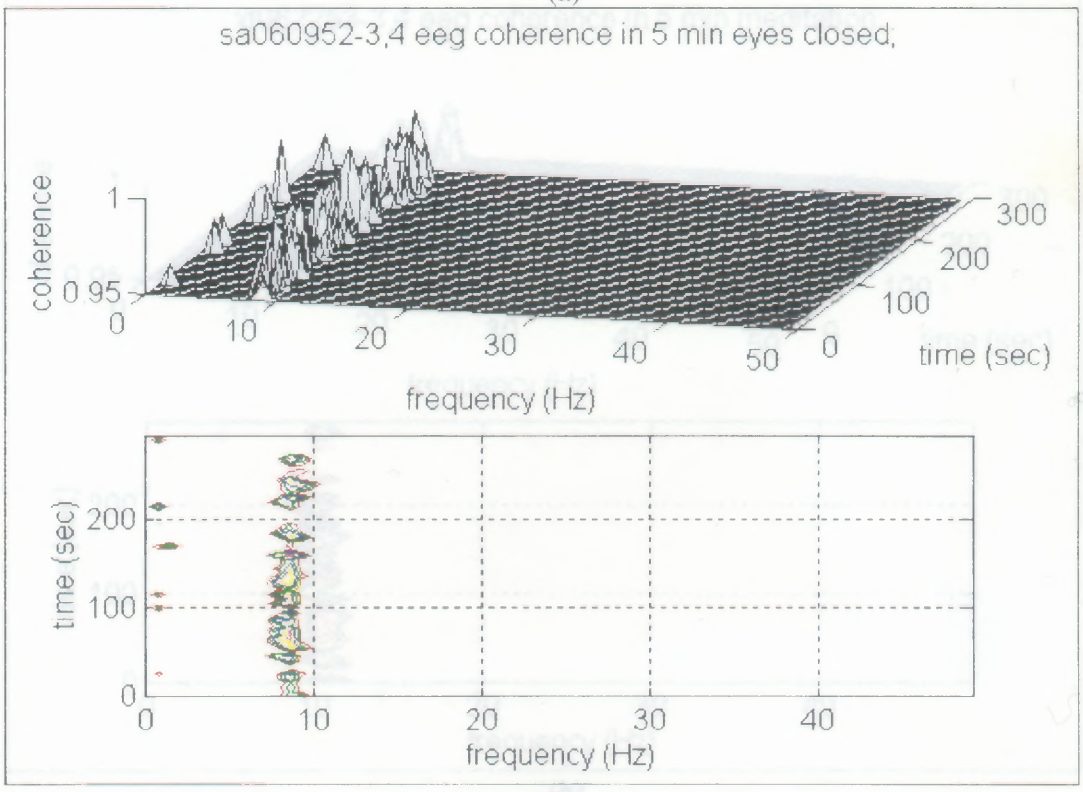

(b)

Figure 7.1 Cospar plots for individual meditation protocol:
(a) Eyes open, and
(b) Eyes closed.

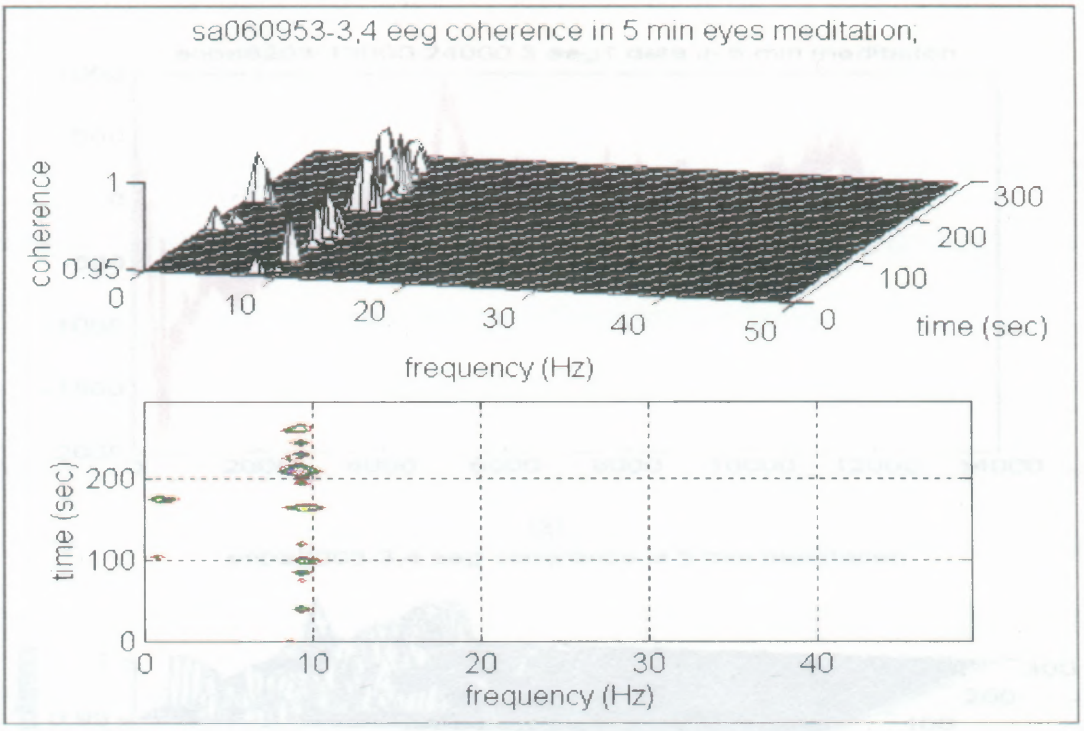

(a)

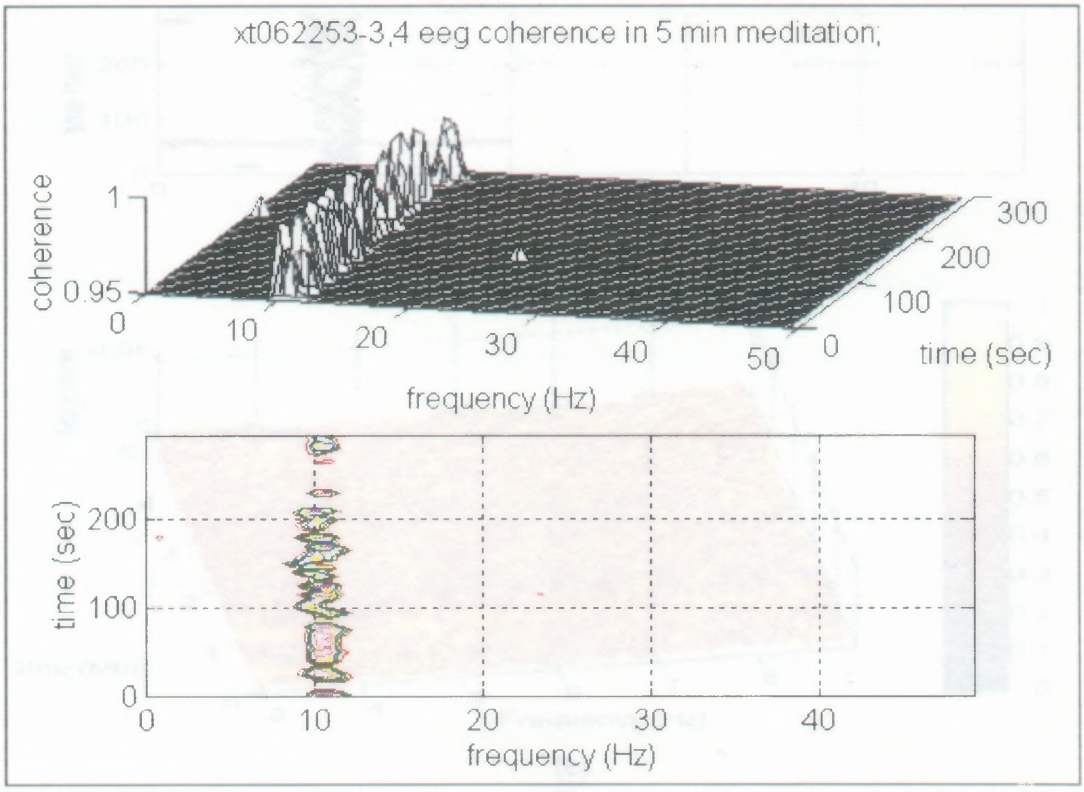

(b)

Figure 7.2 Cospar plots for individual meditation protocol:
(a) Non-meditator, and
(b) Meditator.

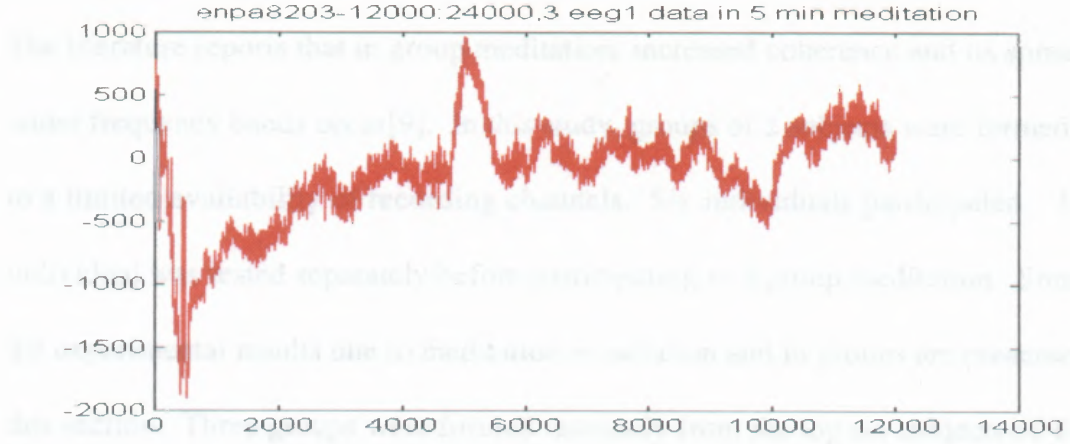

(a)

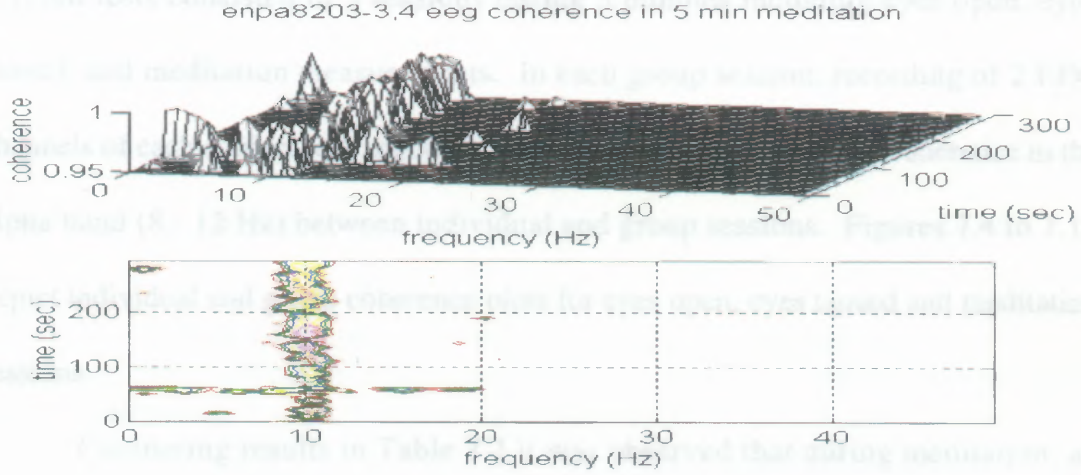

(b)

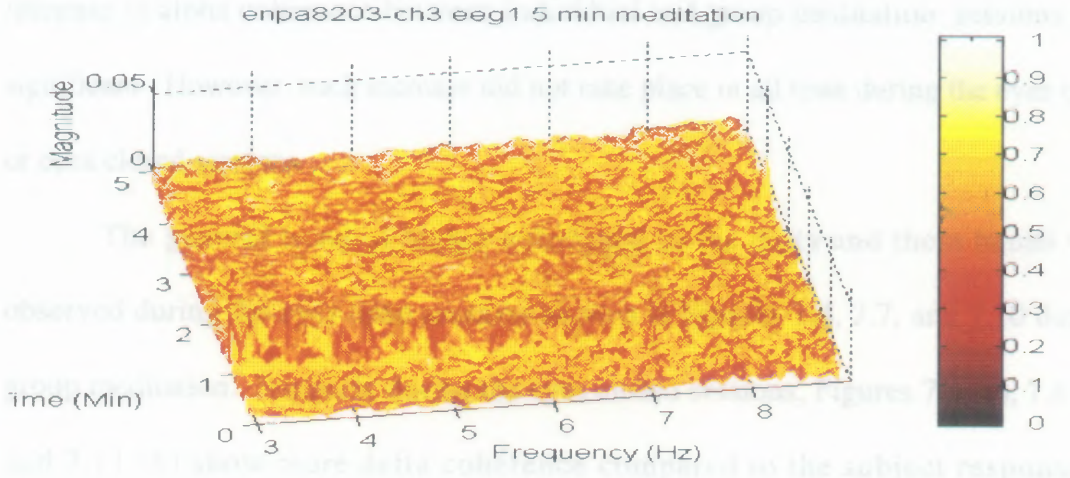

(c)

Figure 7.3 EEG data during meditation. (a) Time domain signal. (b) EEG coherence plot. (c) Time-frequency plot of Figure 7.3 (a).

7.1.2 Group Meditation Study

The literature reports that in group meditation, increased coherence and its spread to wider frequency bands occur[9]. In this study, groups of 2 subjects were formed due to a limited availability of recording channels. Six individuals participated. Each individual was tested separately before participating in a group meditation. Some of the experimental results due to meditation in isolation and in groups are presented in this section. Three groups were formed randomly from the top six subjects of Table 7.1. All tests consisted of 3 sessions lasting 5 minutes including eyes open, eyes closed, and meditation measurements. In each group session, recording of 2 EEG channels of each subject was acquired. Table 7.2 compares results of coherence in the alpha band (8 - 12 Hz) between individual and group sessions. Figures 7.4 to 7.12 depict individual and group coherence plots for eyes open, eyes closed and meditation sessions.

Comparing results in Table 7.2 it was observed that during meditation, an increase in alpha coherence between individual and group meditation sessions was significant. However, such increase did not take place in all tests during the eyes open or eyes closed sessions.

The general trend of higher coherence in the delta and theta bands was observed during the eyes open sessions as seen in Figures 7.4, 7.7, and 7.10 during group meditation. Similarly during the eyes closed sessions, Figures 7.5 (b), 7.8 (b), and 7.11 (b) show more delta coherence compared to the subject response in individual cases. This was also observed by Orme-Johnson in a 1982 study. During the group meditation session, Figure 7.6 shows more alpha coherence with addition to

the theta coherence band (4 - 8 Hz) and less delta (0 - 4 Hz) activity. This shows not only that subjects become more relaxed in a group meditation but that a deeper level of meditation is also achieved, i.e. the cause for the presence of the theta band. Less delta band is shown here because of the deeper state of meditation.

Table 7.2 shows the most important results of the meditation study. For all three pairs of group meditation, the alpha coherence level of each subject is higher than the alpha level in individual meditation. This is true no matter how the subjects are matched together. Significant increase in the alpha coherence may possibly be attributed to the presence of electromagnetic field coupling between two subjects with in phase alpha field components. Similar explanation is valid for the observed increase in the theta band for the group meditation as seen in Figure 7.6.

Table 7.2 Results for individual and group meditation study.
Coherence values are evaluated as areas under the alpha (8 - 12 Hz) coherence above the 0.95 threshold.

		Eyes Open		Eyes Closed		Meditation	
Technique	**Subj. ID**	**Alone**	**Group**	**Alone**	**Group**	**Alone**	**Group**
Non Med.	SA	0.0000	0.0330	0.2034	0.0859	0.0285	0.2950
TM	XT	0.0785	0.0985	0.2661	0.2419	0.1321	0.3671
Non Med.	ND	0.0000	0.3884	0.0000	0.4085	0.0000	0.4331
Non Med.	RS	0.0000	0.0420	0.0000	0.3440	0.0843	0.3708
Non Med.	MB	0.0373	0.3913	0.0298	0.3010	0.0000	0.3113
Zen	TN	0.0391	0.0600	0.0563	0.0713	0.0189	0.0914

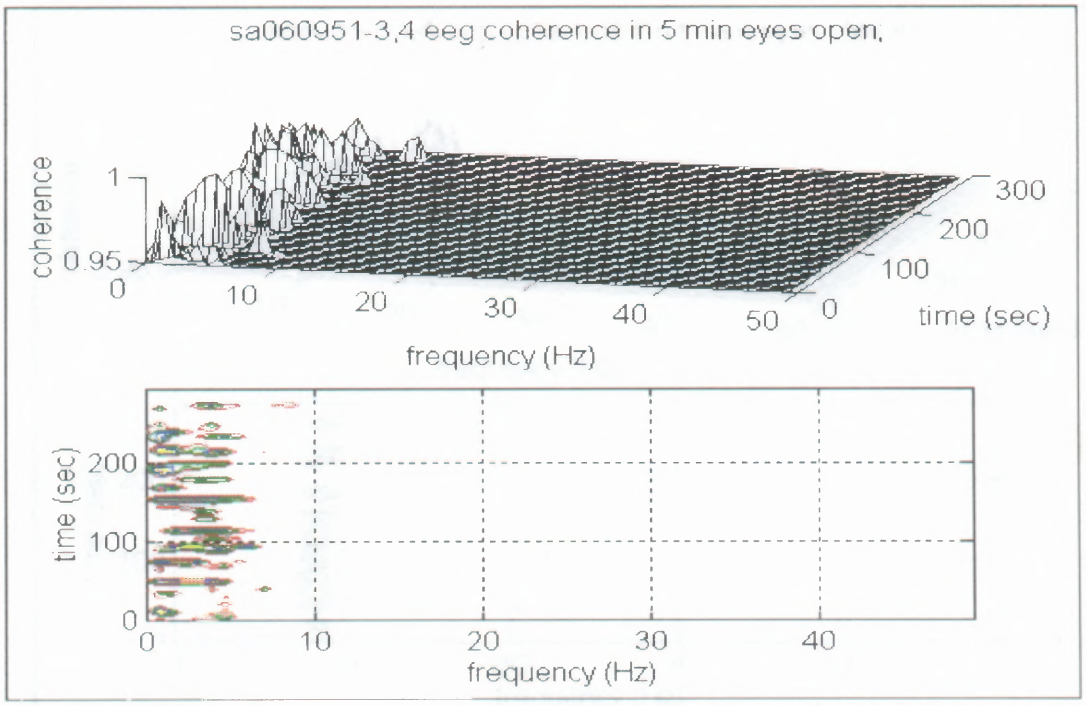

(a)

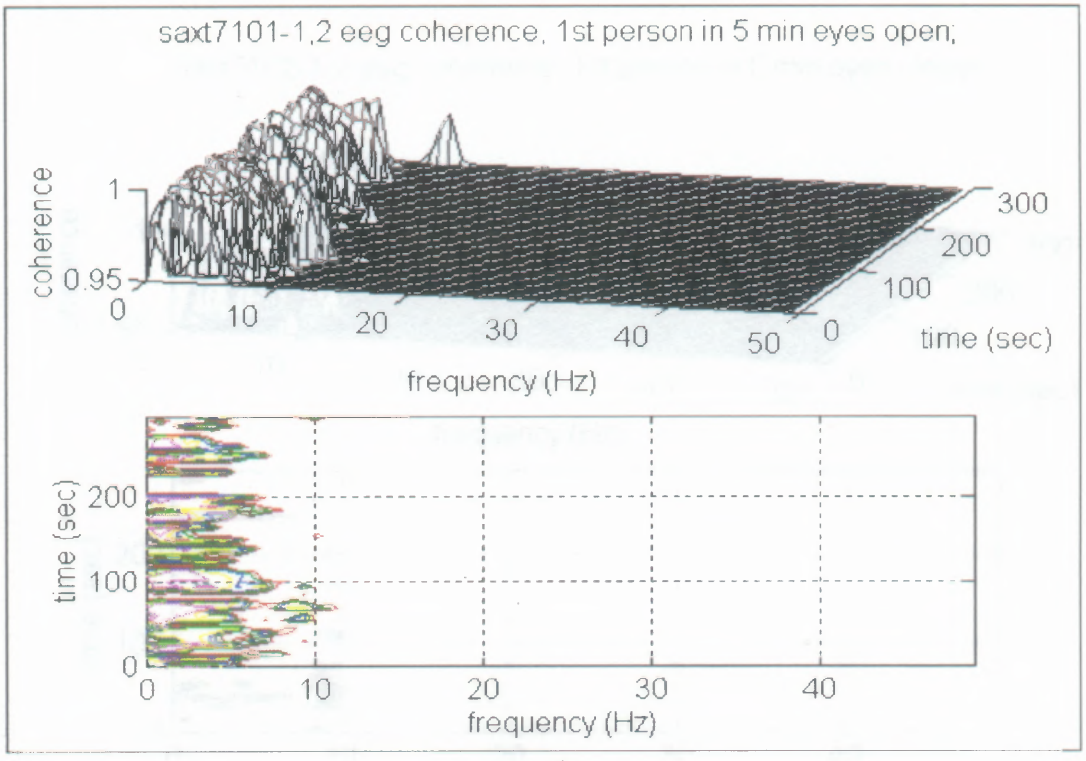

(b)

Figure 7.4 Cospar plots for eyes open:
(a) Individual meditation, and
(b) Group Meditation.

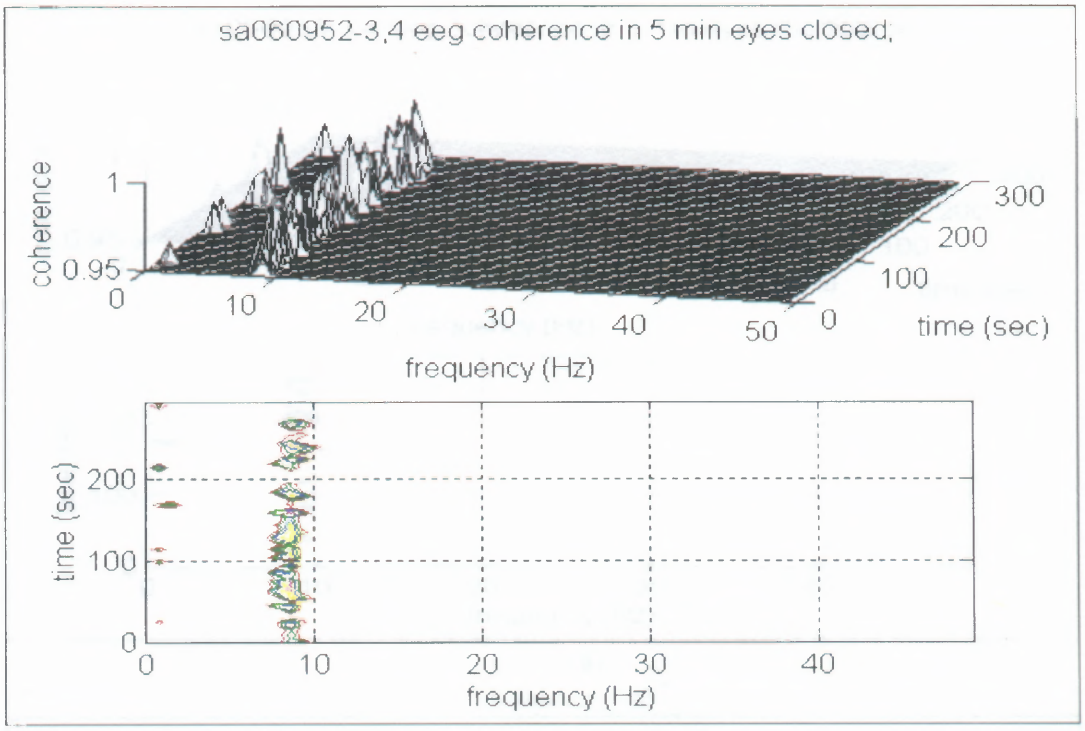

(a)

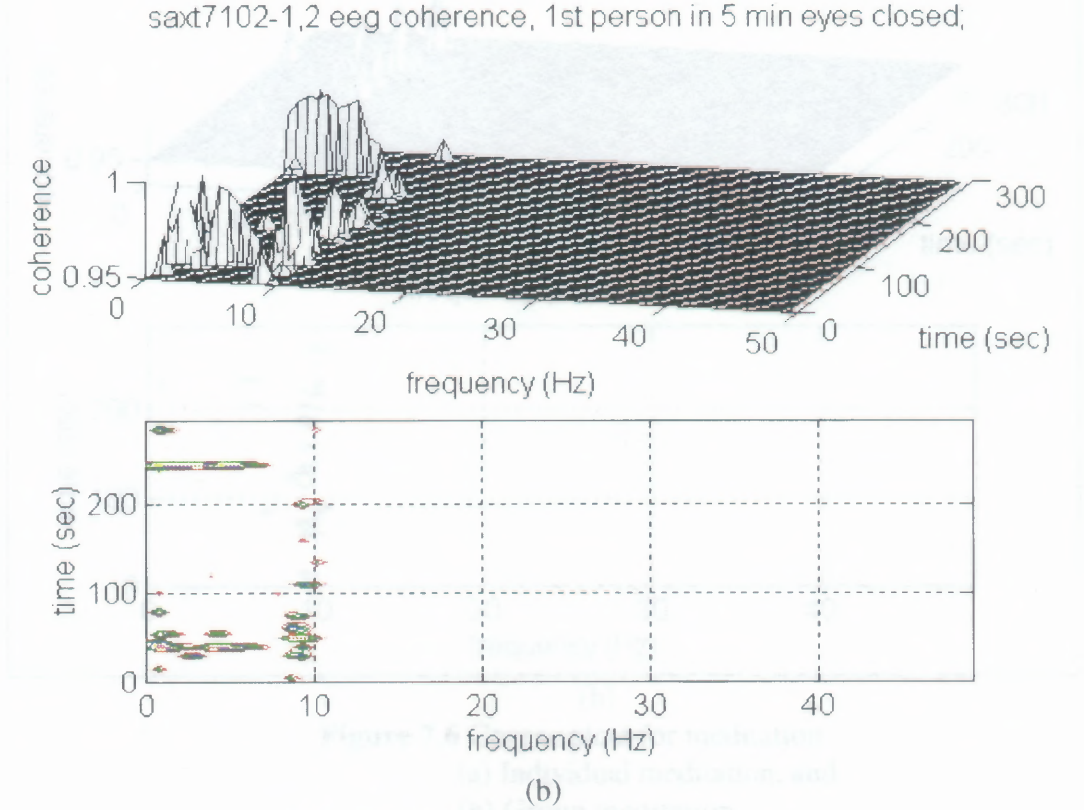

(b)

Figure 7.5 Cospar plots for eyes closed
(a) Individual meditation, and
(b) Group meditation.

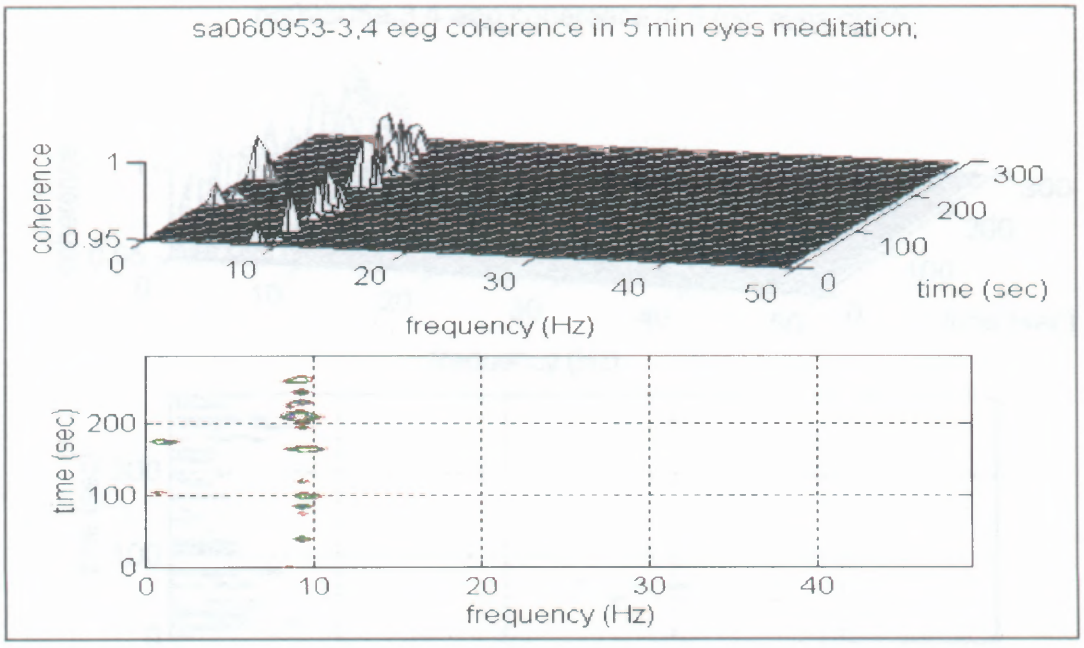

(a)

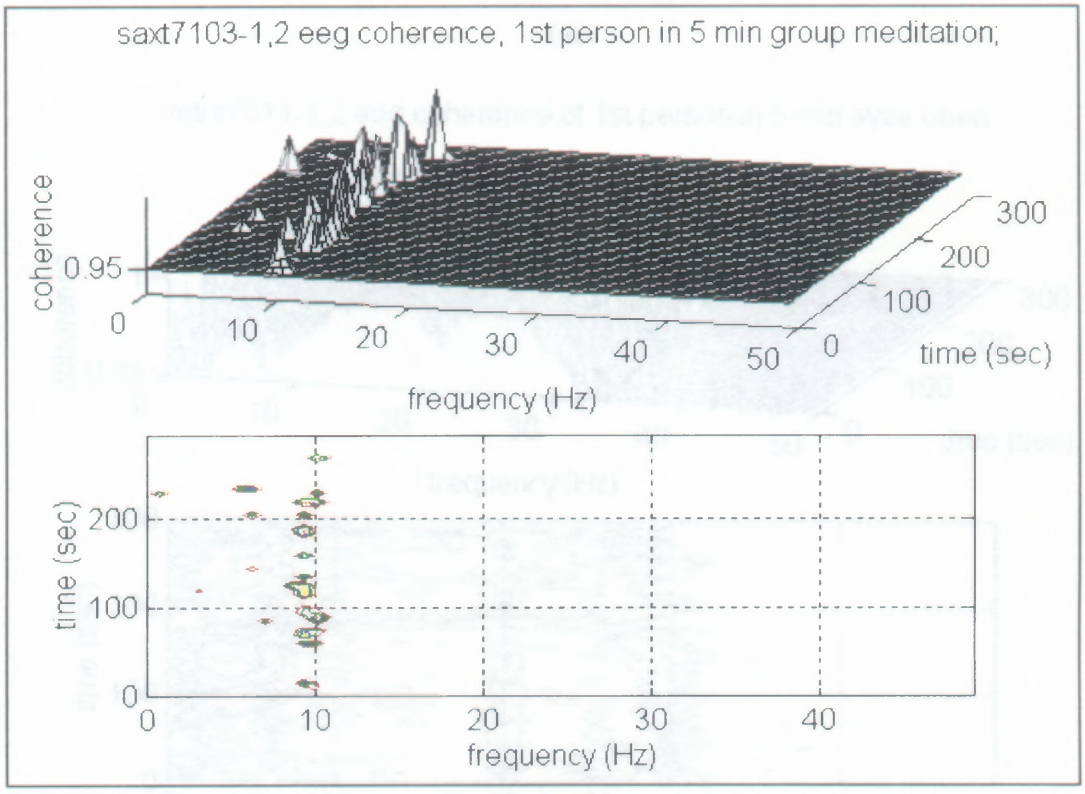

(b)

Figure 7.6 Cospar plots for meditation
(a) Individual meditation, and
(b) Group meditation.

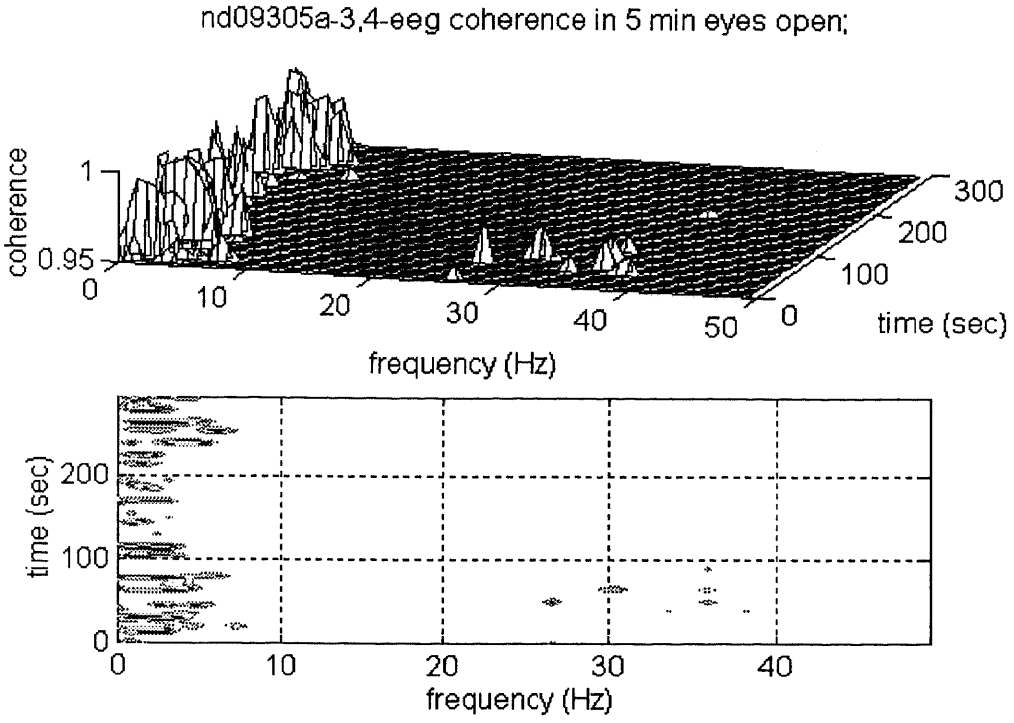

(a)

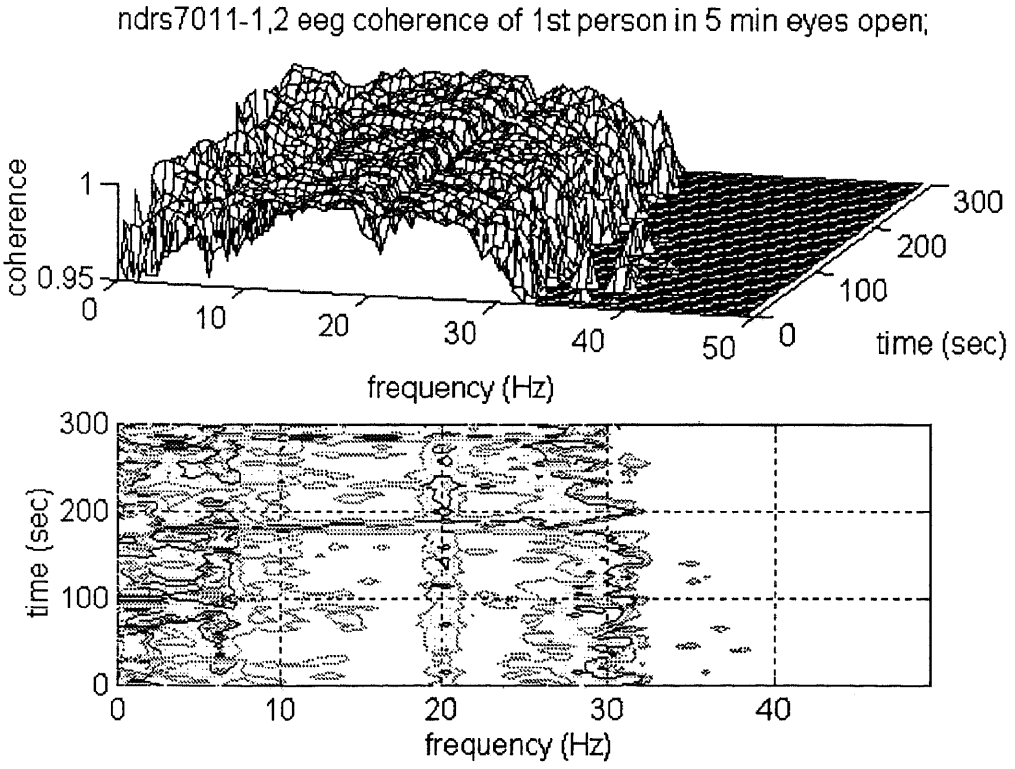

(b)

Figure 7.7 Cospar plots of same subject for eyes open:
(a) individual, and
(b) group.

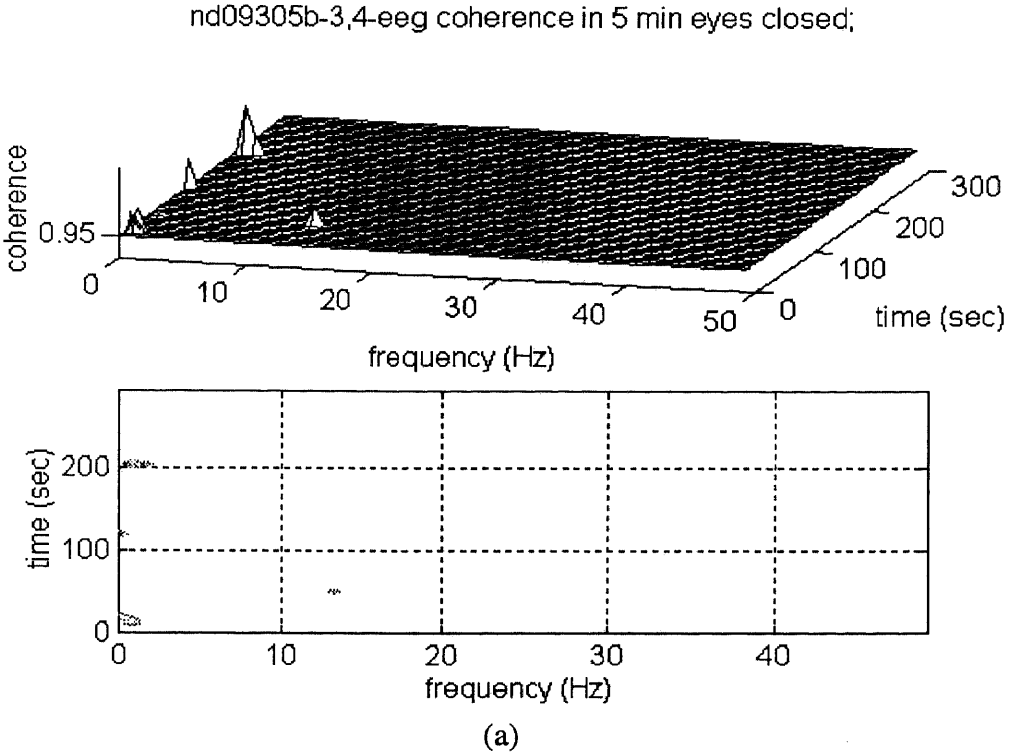

(a)

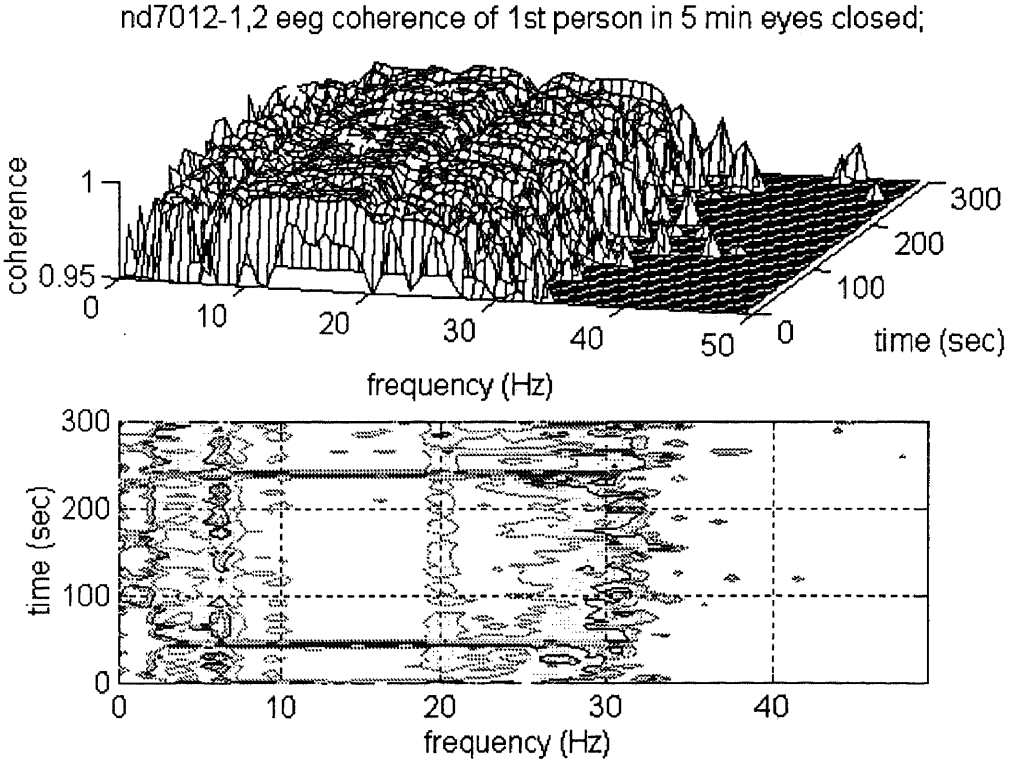

(b)

Figure 7.8 Cospar plots of same subject for eyes closed:
(a) individual, and
(b) group.

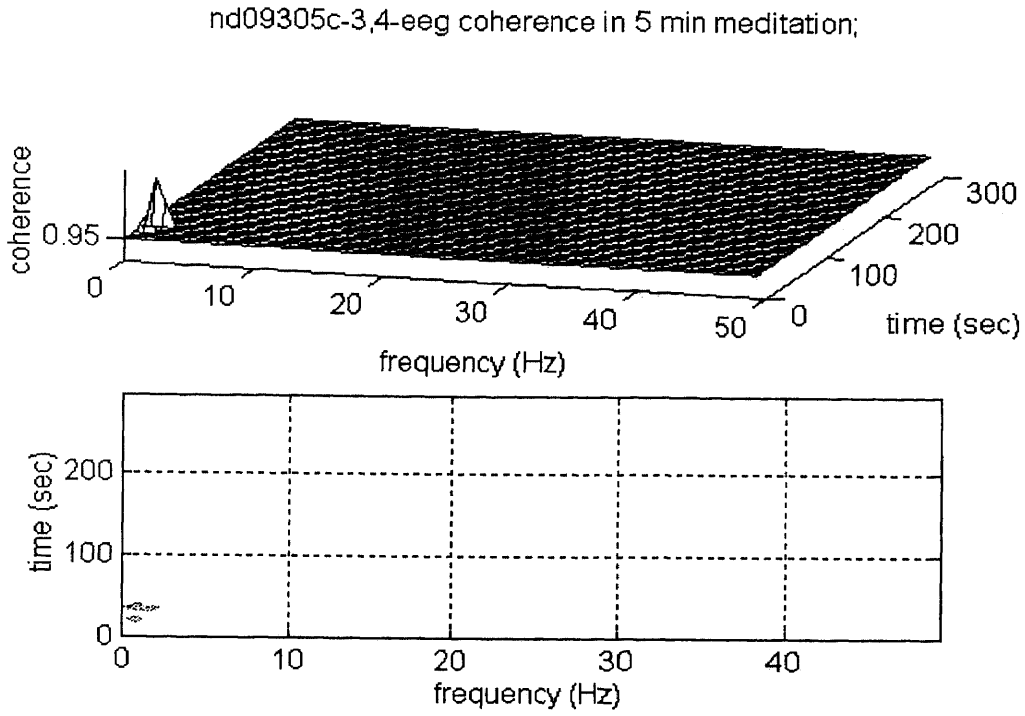

(a)

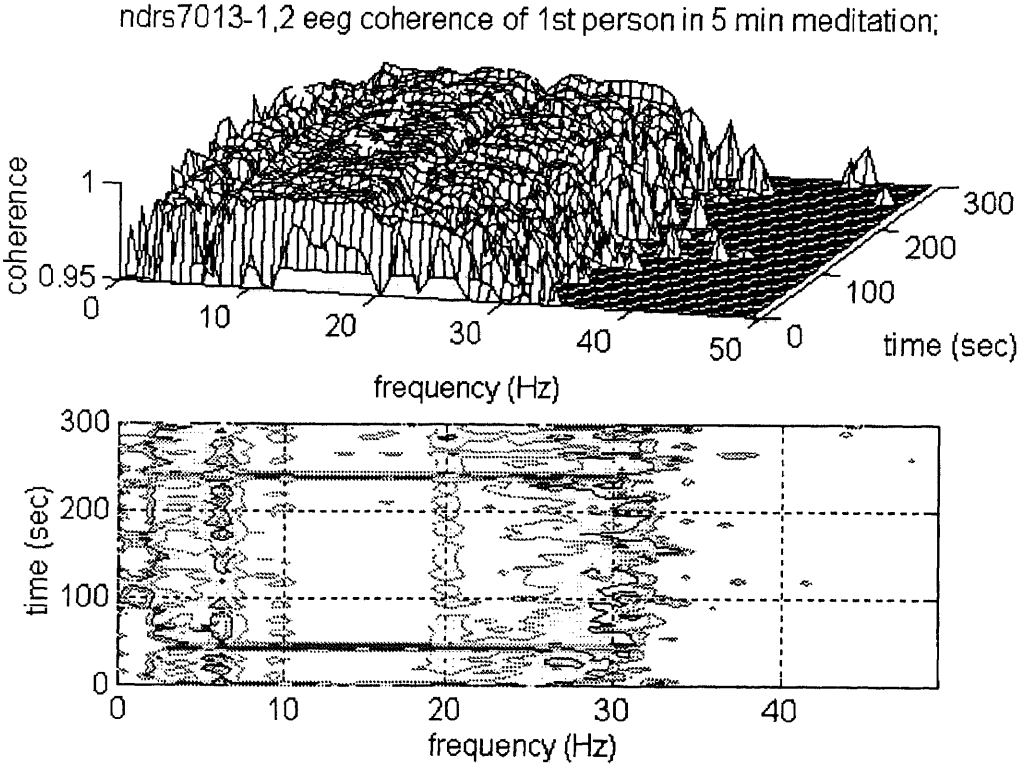

(b)

Figure 7.9 Cospar plots of same subject for meditation:
(a) individual, and
(b) group.

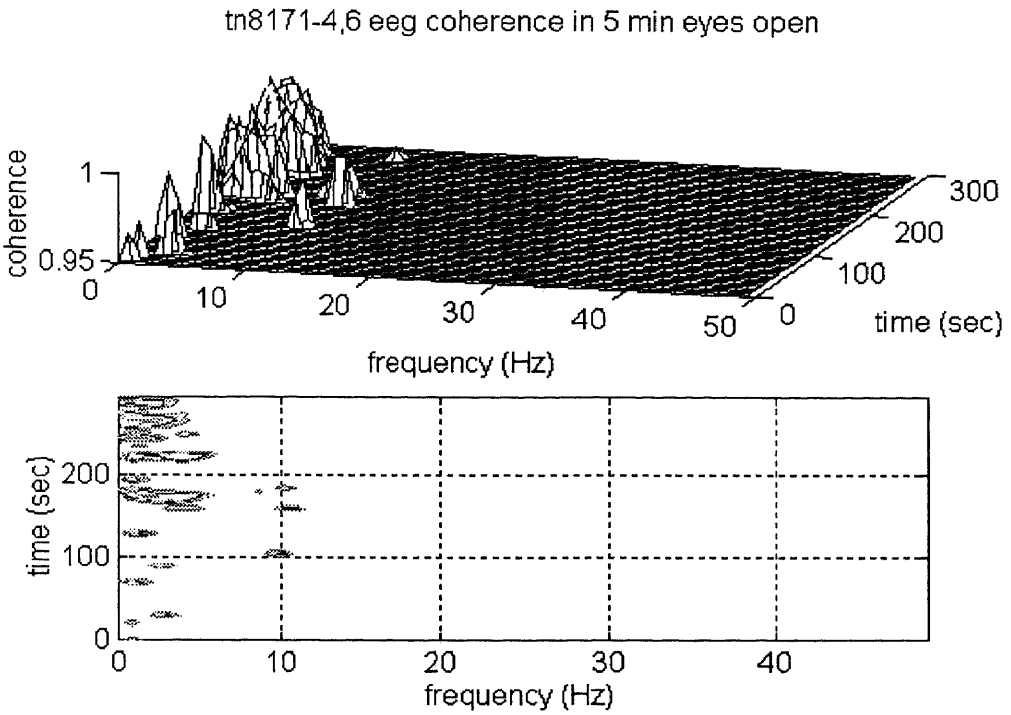

(a)

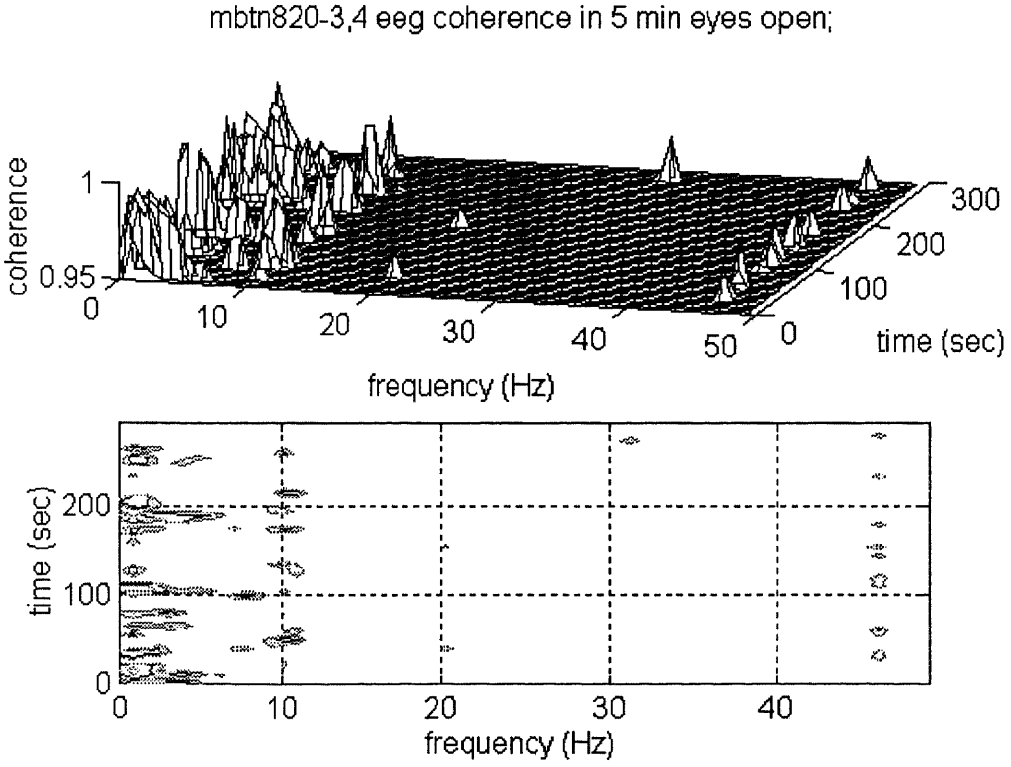

(b)

Figure 7.10 Cospar plots of another subject for eyes open:
(a) individual, and
(b) group.

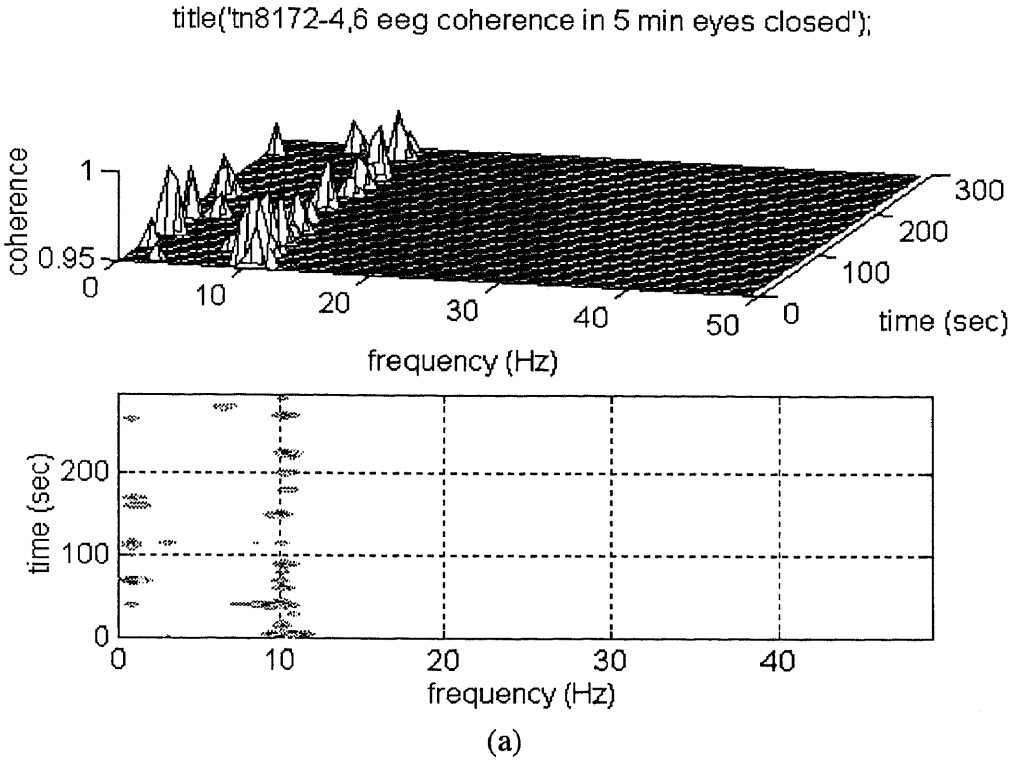

(a)

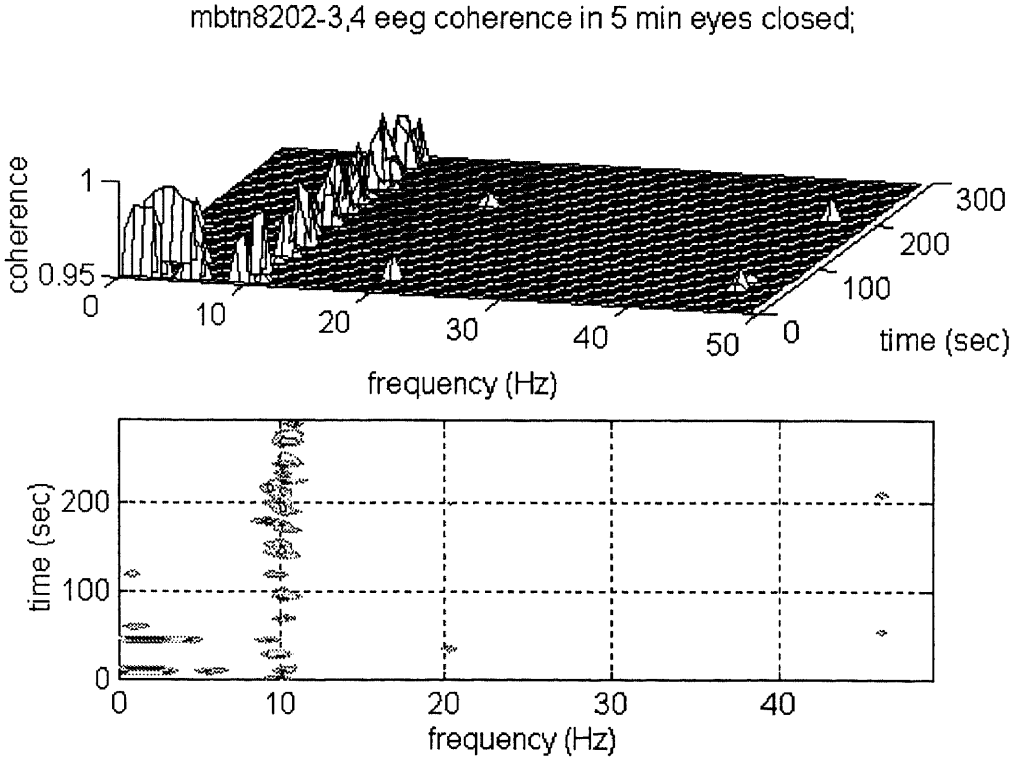

(b)

Figure 7.11 Cospar plots of another subject for eyes closed:
(a) individual, and
(b) group.

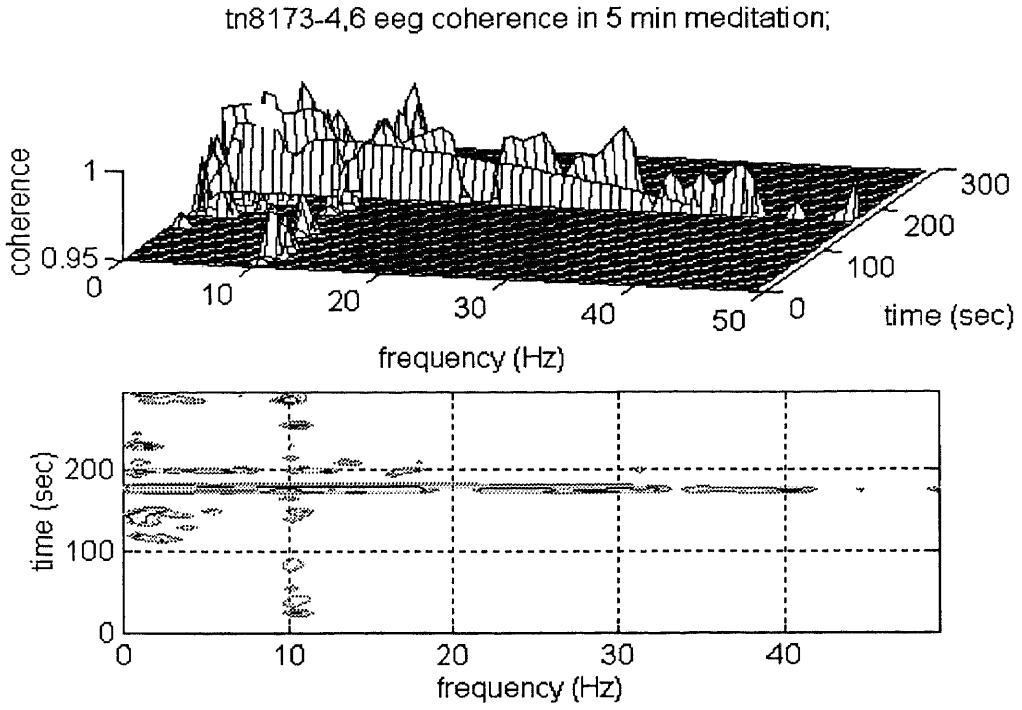

a)

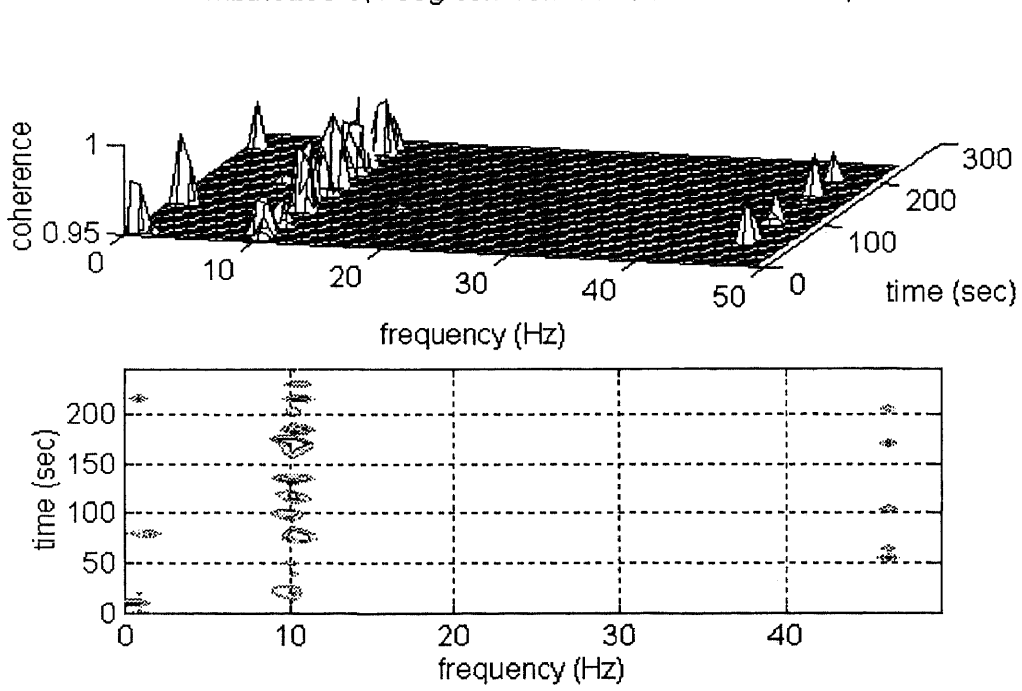

(b)

Figure 7.12 Cospar plots of another subject for meditation
(a) individual, and
(b) group.

7.2 Atmospheric Noise Study

The background on the atmospheric noise is given in chapter 3. Electrical activity in the earth and surrounding atmosphere contains not only man-made signals but additional signals due to various natural events in the form of impulse noise. These signals could be coupled to the earth-ionosphere waveguide and induce Schumann resonances at well defined frequencies determined by atmospheric conditions.

Antennas were connected to EEG and ECG measurement system to monitor such electrical activity in the environment where the meditation study was undertaken. Antenna measurements were carried out in the shielded room at NJIT before, during, and after the meditation study. These recorded signals were processed to identify the nature of various spectral components contained in the analysis.

7.2.1 Non-meditation Related Antenna Measurements:

Orientation of the antenna determines the nature of the polarization of the received signal. Atmospheric noise detected by the antenna in this study is polarization dependent. The orientation of the antenna placed in the shielded room was varied initially, until the signal of significant clarity is observed on the oscilloscope. A clear antenna signal was one that could give distinct frequency components after the spectral analysis and the time-frequency analysis were performed. It is worth to mention that the shielded room mentioned in this study is almost transparent for very low frequency signals below 50 Hz. The shielded room was manufactured by Ray Proof, Norwalk, CT. Series 81 material which is specified having loss of 20 dB at 1 kHz for magnetic fields and 100 dB of electric fields between 200 kHz to 50 MHz was used in its construction. It was observed that the

presence of the shielded room helped to eliminate interference due to 60 Hz power line fields significantly.

Another study was performed by placing one antenna inside and one outside the shielded room. The purpose of this study was to see whether the shielded room is beneficial in studying extremely-low-frequency signals due to atmospheric noise or biological signals such as EEG, ECG, and EMG. It was found that the signal recorded outside the shielded room was especially more noisy with 60 Hz background noise.

The objective of the third study was to observe the spectral content of the signals received by antennas placed apart. The locations chosen were NJIT, Newark, NJ and the Kessler Institute for Rehabilitation which are approximately 10 miles away from each other. Data received by the antennas placed at these locations was processed and their spectral content observed to be very similar. Naturally occurring signal components due to Schumann resonances are shown in Table 7.3. As expected there was no noticeable change in the locations of the frequencies due to Schumann resonances.

Table 7.3 Schumann resonances detected by antennas at various locations

		Resonance Frequencies				
Ant. at	**File**	**n = 1**	**n = 2**	**n = 3**	**n = 4**	**n = 5**
NJIT- inside	aiao7291	7.6	17.1	20	26.5	31.0
NJIT-outside	aiao7292	7.5	17.1	20	26.6	31.0
NJIT-inside	an13730	7.1	14.7	20	26.6	32.5
Kessler	kk13730	7.1	14.9	20	26.9	32.6

7.2.2 Meditation Related Antenna Measurements

Atmospheric signals detected by an antenna exhibited typical characteristics of impulsive noise as seen in Figure 7.13. However, spectral analysis of an antenna signal, as shown in Figure 7.14 reveals that it contains more than just impulse noise. High amplitude narrow spectral width signals as seen in Figure 7.14 could be traced to man-made interferences. After further zooming, spectral clusters as shown in Figure 7.15 could be traced to Schumann resonances of the earth-ionosphere waveguide. Time-frequency plots of antenna signals at these resonances are shown in Figures 7.16 to 7.20. Such observations were made in this meditation study and an outline of approximate results are presented in Table 7.4. As can be seen from these results and their plot in Figure 7.21, the relevant resonances showed little fluctuations with the time of the day and weather conditions in particular.

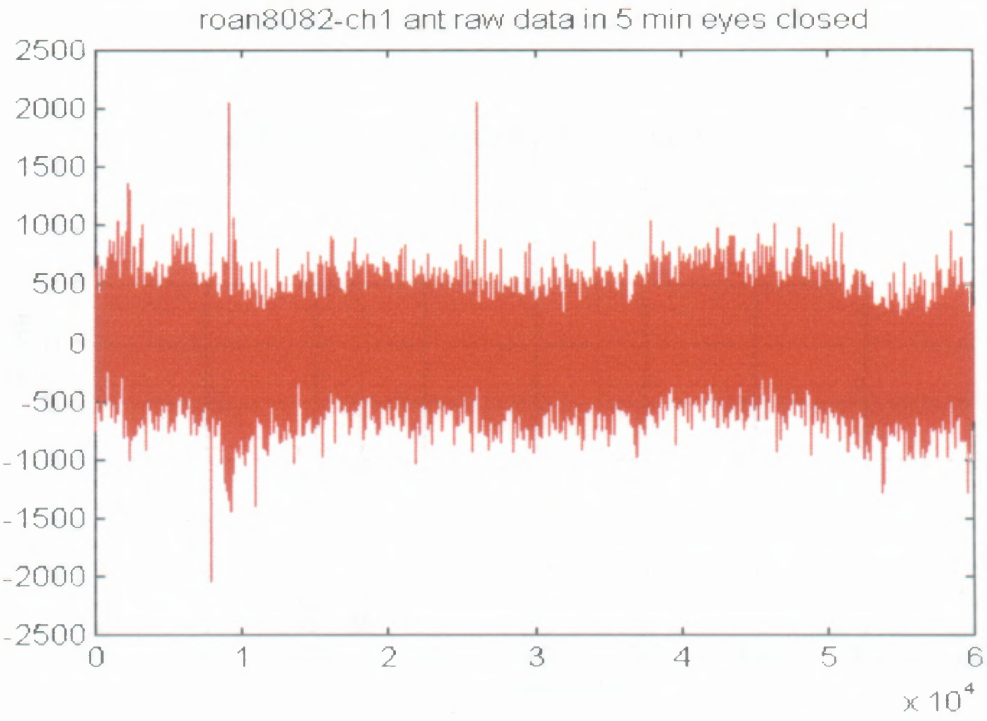

(a)

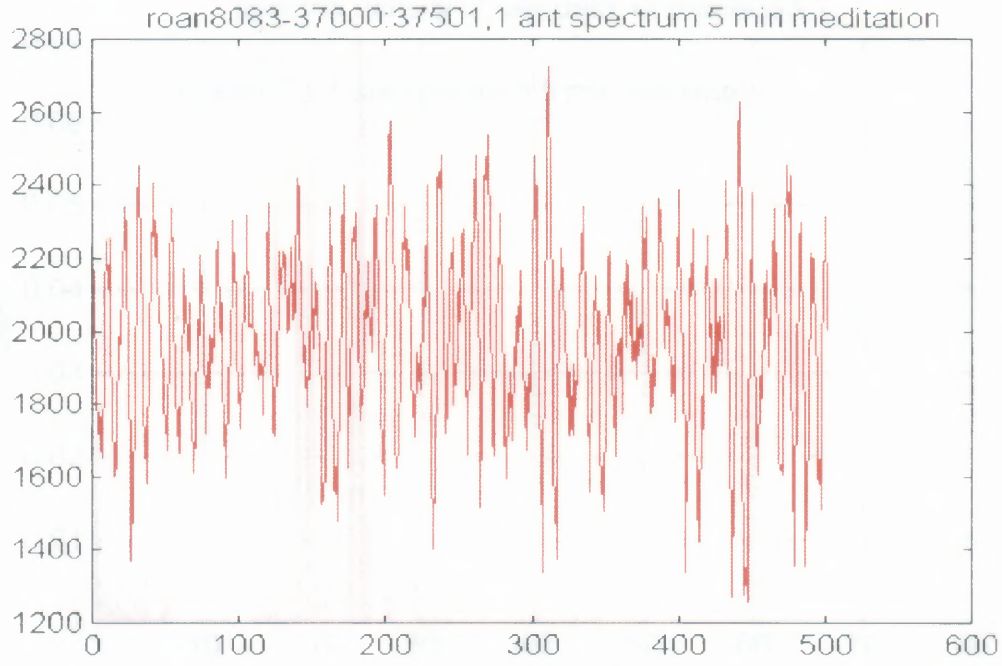

(b)

Figure 7.13 Antenna signal in time domain.
(a) Time interval of 5 minutes.
(b) Expanded version of (a) to time interval of 3 seconds.

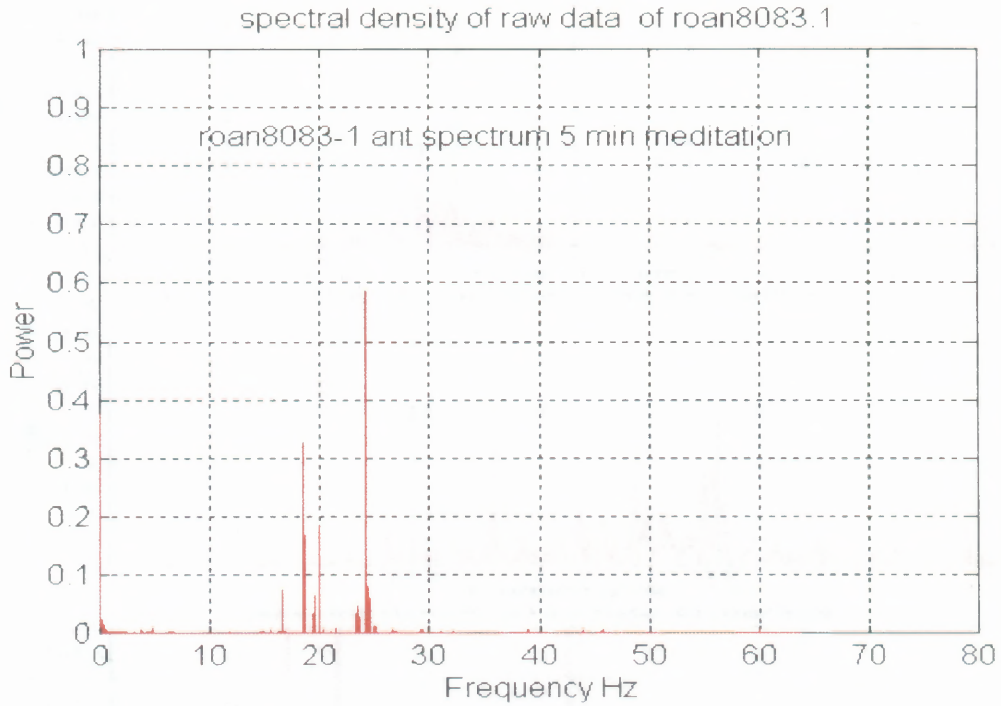

(a)

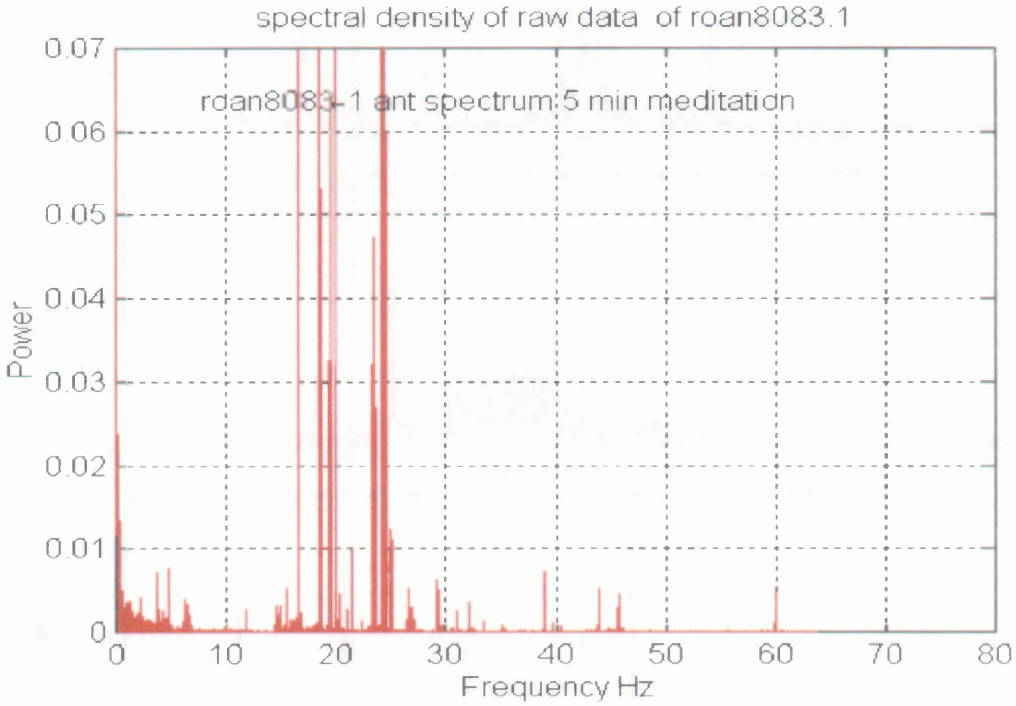

(b)

Figure 7.14 Spectrum of antenna signal during meditation.
(a) Full scale. (b) Expanded scale

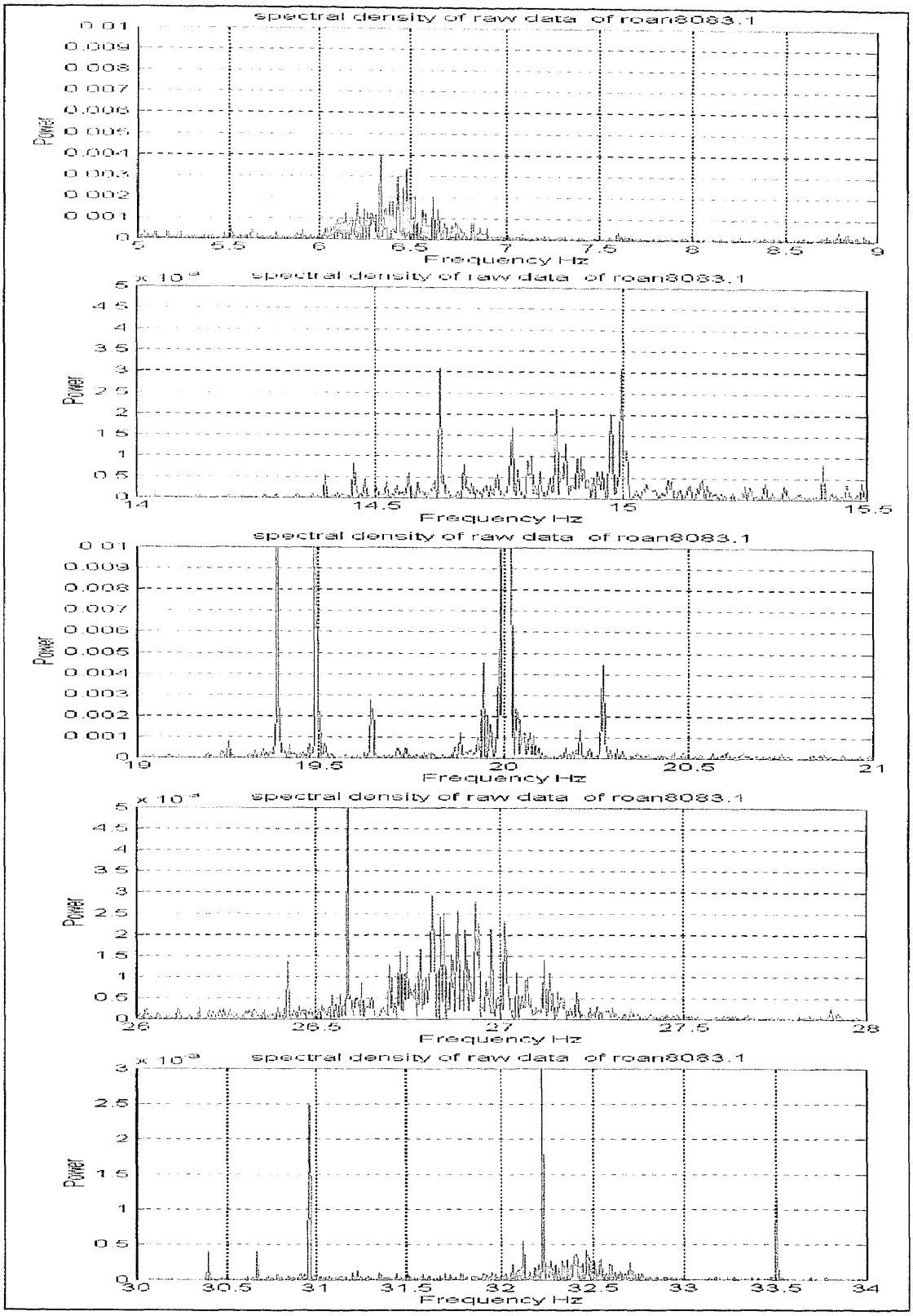

Figure 7.15 The Schumann resonances from antenna in 5 minutes Yoga meditation.

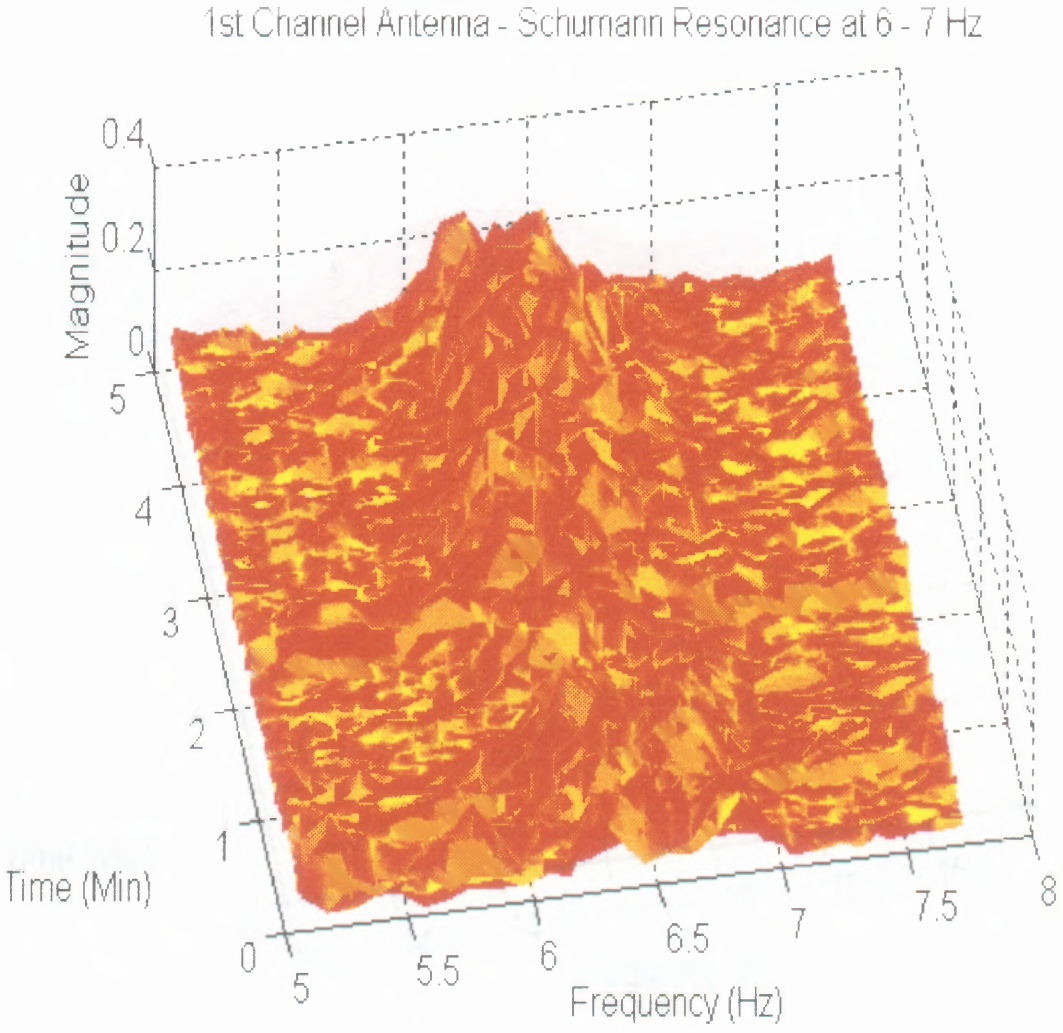

Figure 7.16 Schumann resonance signal at 6 - 7 Hz band.

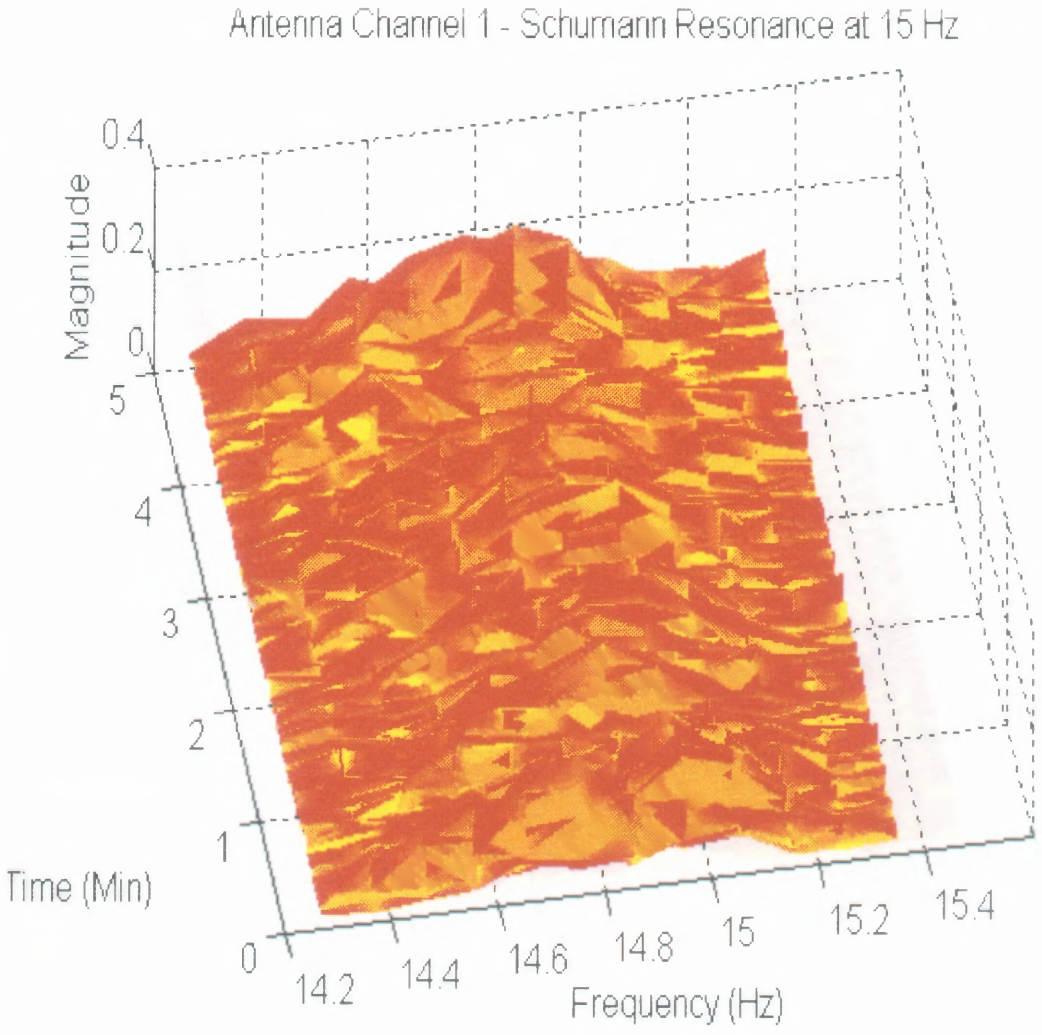

Figure 7.17 Schumann resonance signal at 15 Hz band.

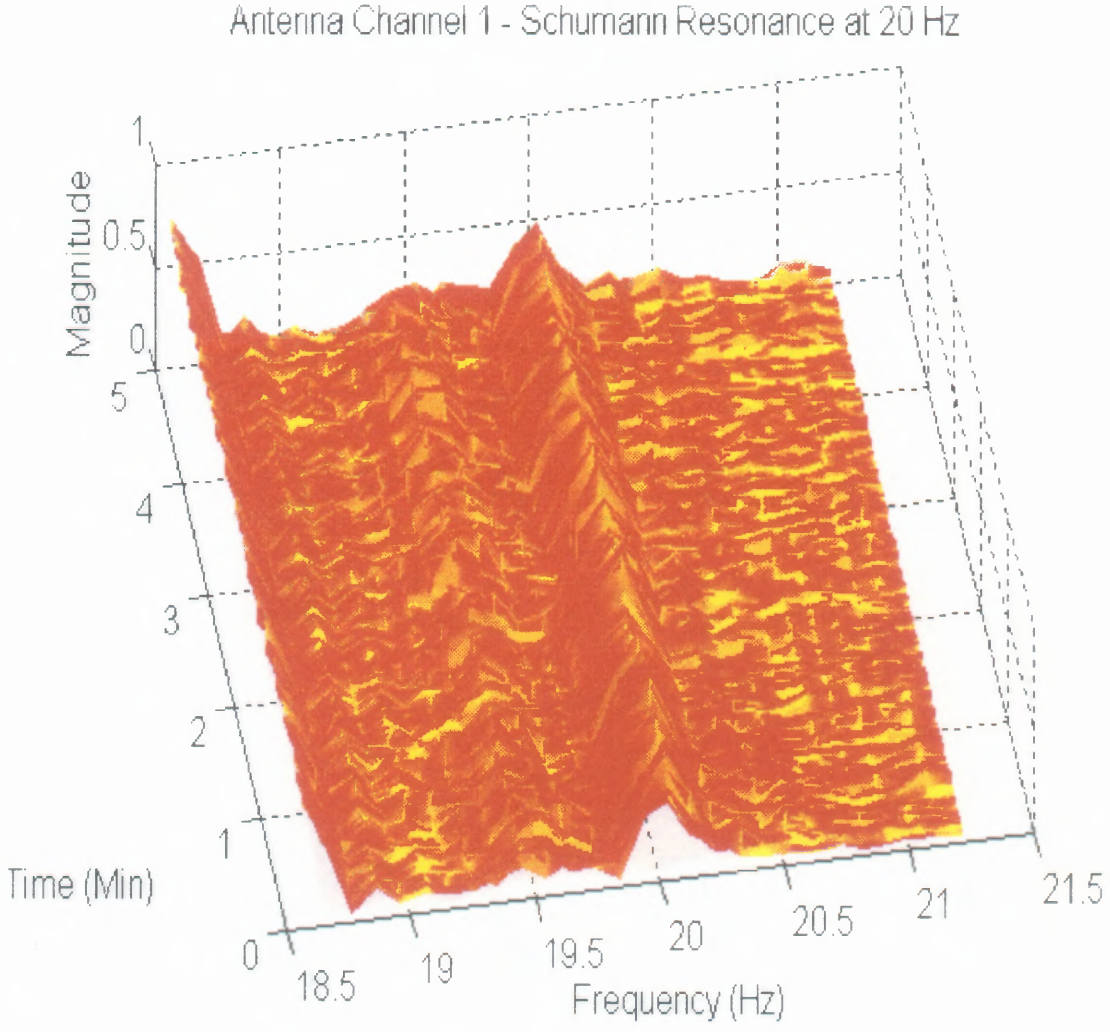

Figure 7.18 Schumann resonance signal at 20 Hz band.

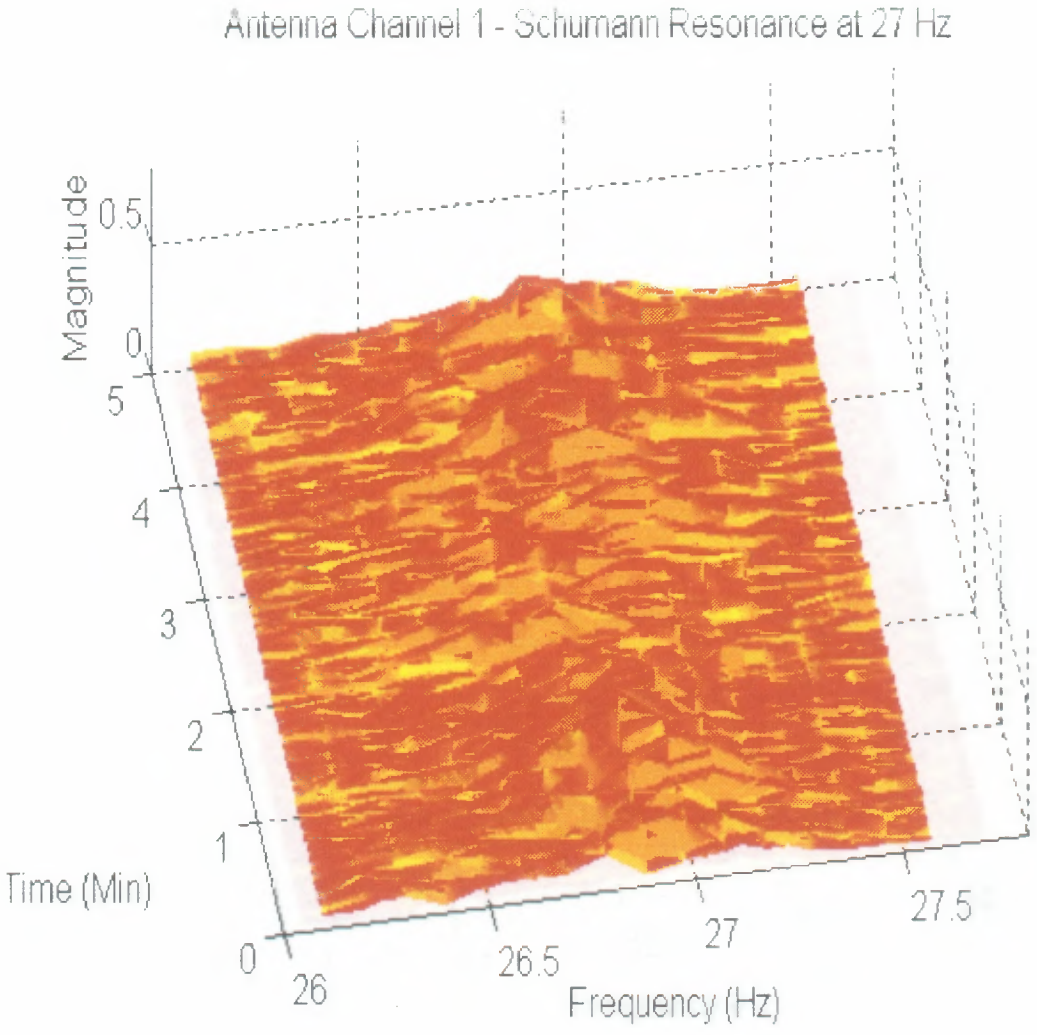

Figure 7.19 Schumann resonance signal at 27 Hz band.

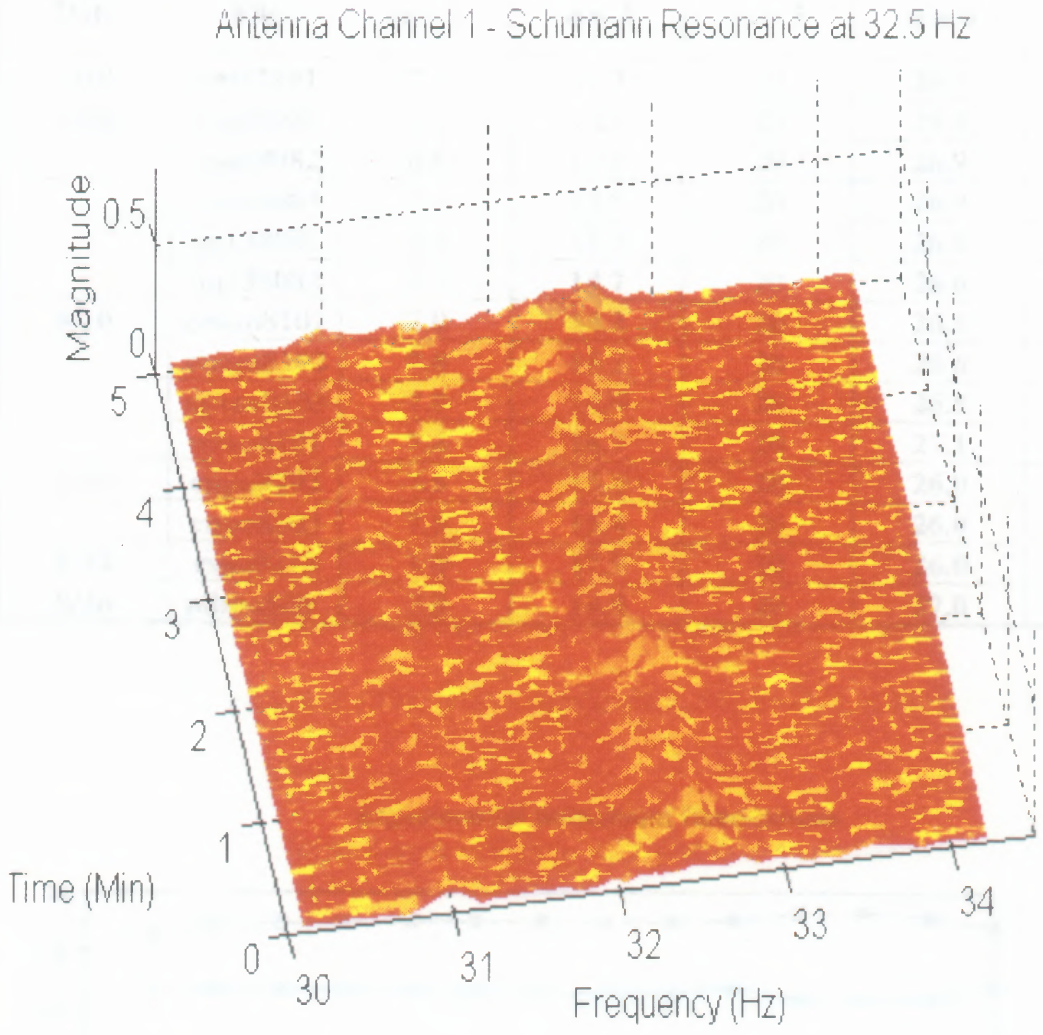

Figure 7.20 Schumann resonance signal at 32.5 Hz band.

Table 7.4 List of Schumann resonances from antenna signals.

		Resonance Frequencies				
Date	File	n = 1	n = 2	n = 3	n = 4	n = 5
7/10	anxt7101	7.3	17.3	20	26.7	31.2
8/08	roan8081	6.4	14.9	20	26.9	32.3
	roan8082	6.5	14.9	20	26.9	32.4
	roan8083	6.5	14.9	20	26.9	32.5
	an138081	6.1	15.0	20	26.6	32.6
	an138083	6.1	14.7	20	26.6	32.5
8/10	oman8101	7.0	14.2	20	26.5	32.5
	oman8102	7.0	14.2	20	26.6	32.5
	oman8103	7.0	14.0	20	26.5	32.6
	mlan8101	7.4	14.7	20	27.1	32.6
8/20	enpa8202	7.5	15.4	20	26.0	37.3
	enpa8203	7.5	15.4	20	26.0	37.3
8/24	rspa8243	7.0	17.9	20	26.0	37.0
8/26	mbpa826	7.0	14.0	20	27.0	32.2

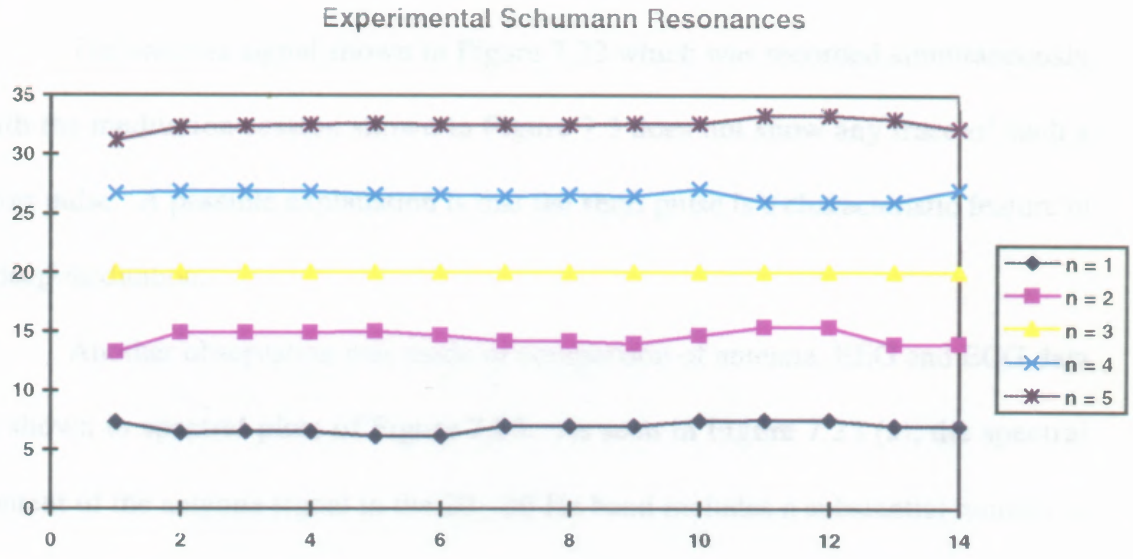

Figure 7.21 Plot of the experimental Schumann resonances.

7.3 Physiological signals and atmospheric noise

EEG and ECG data in this study were acquired using contact electrodes (approximately 0.5 x 0.5 in) which can be considered as electrically small antennas. Any antenna at low frequencies in the 0 -50 Hz range will fall into such classification, i.e. 1 x 1 square ft) antenna, used in atmospheric noise measurements. Here, in this section comparative study of EEG and ECG data obtained simultaneously with antenna signals is made. The purpose of such comparison was to recognize the individual spectral components of the atmospheric interferences and those components of physiological signals generated by the human body. For example, the meditation session shown in Figure 7.3 shows a strong narrow width time pulse occurring in the EEG data. If it was due to atmospheric interference, its presence in the antenna signal would have been expected.

The antenna signal shown in Figure 7.22 which was recorded simultaneously with the meditation session shown in Figure 7.3 does not show any trace of such a short pulse. A possible explanation is that the short pulse is a characteristic feature of a deep meditation.

Another observation was made of comparison of antenna, EEG and ECG data as shown in spectral plots of Figure 7.23. As seen in Figure 7.23 (a), the spectral content of the antenna signal in the 20 - 30 Hz band includes a substantial number of high amplitude narrow width spectral components which can be attributed to man-made sources. Careful analysis leads to observation that many of the high amplitude components are also present in the EEG data of Figure 7.23 (b) and ECG data of Figure 7.23 (c). Though the order of magnitudes in the EEG and ECG data is much

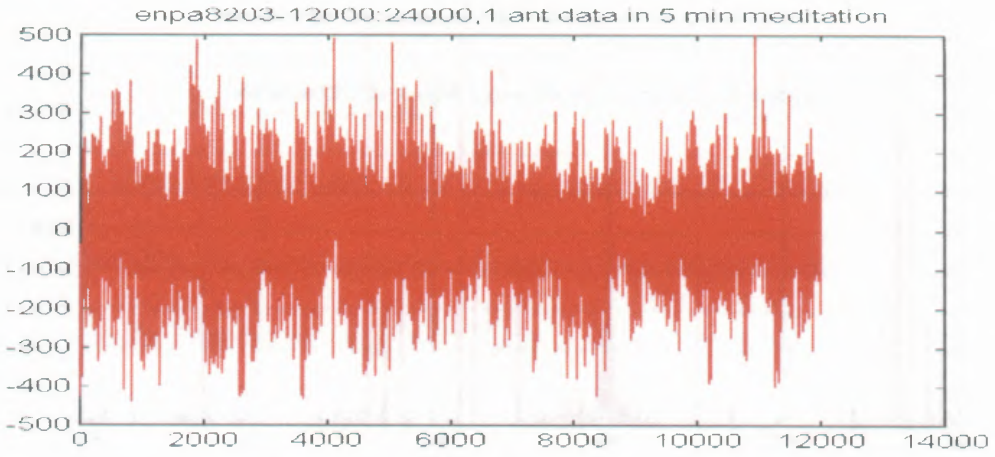

(a)

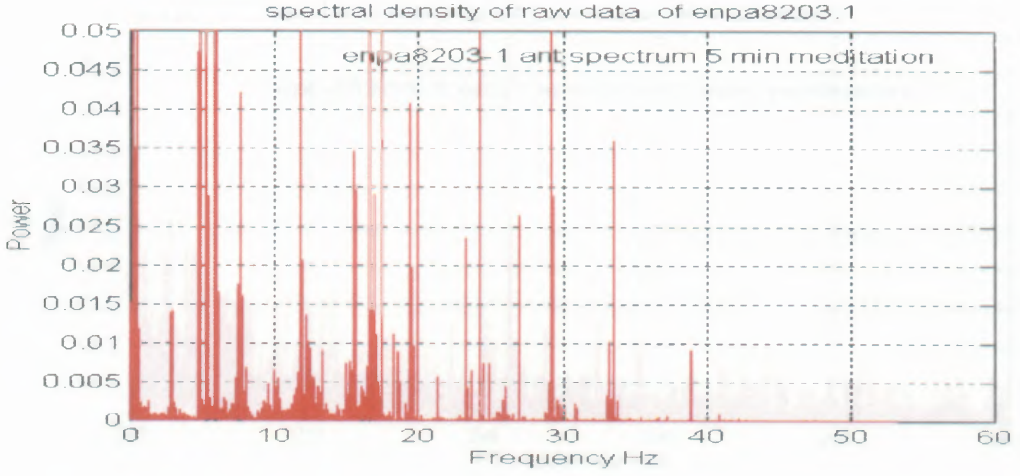

(b)

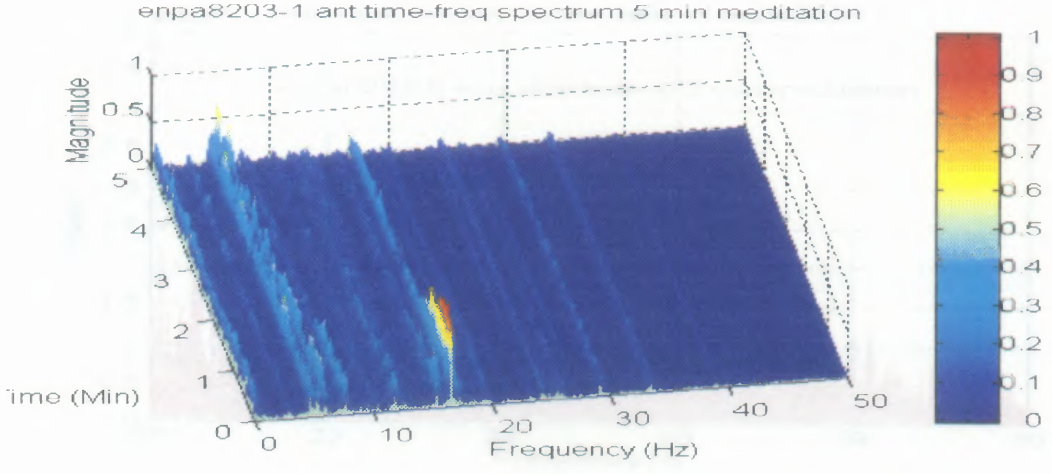

(c)

Figure 7.22 Antenna signal during meditation recorded simultaneously with EEG data of Figure 7.3. (a) Time domain. (b) Spectral representation. (c) Time- frequency plot.

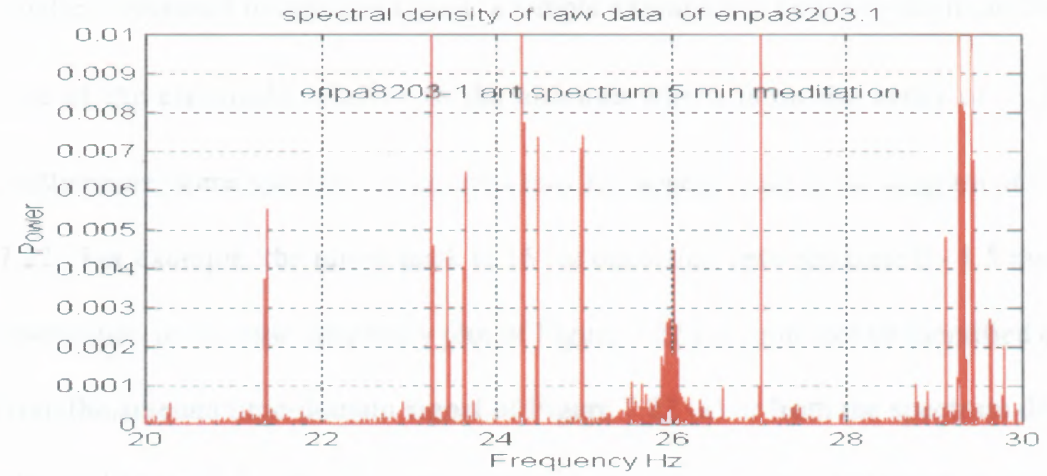

(a)

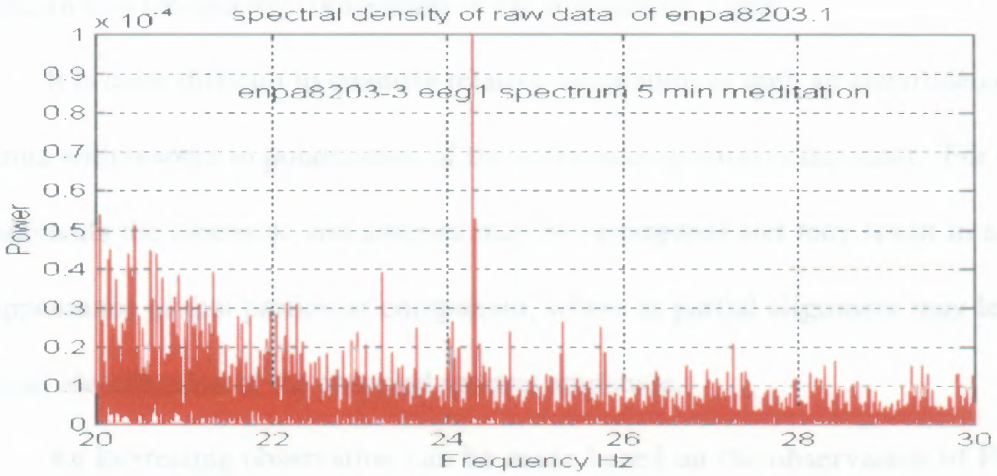

(b)

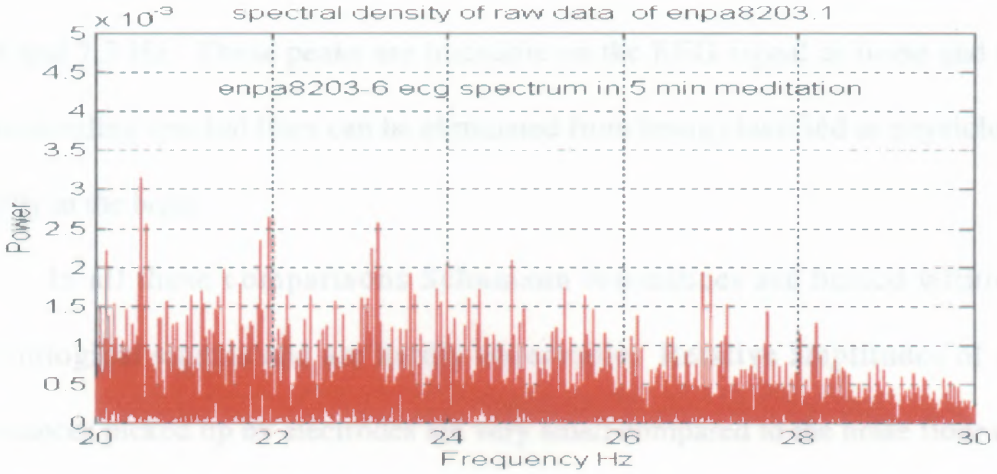

(c)

Figure 7.23 Comparison of power spectra.
(a) Antenna. (b) EEG. (c) ECG.

smaller compared to antenna signal, a simple explanation could be attributed to the size of the electrode relative to the antenna which is on the order of $\approx 1/600$. Furthermore, some spectral components may not appear at all in the diagram of Figure 7.22. For example, the raised peak at 16 Hz occurring between time 0 - 1.5 minutes observable in the time-frequency plot of Figure 7.22 (c) could not be identified either from the antenna time-domain signal of Figure 7.22 (a) or from the spectrum density plot of Figure 7.22 (b). This phenomenon could only be explained in terms of polarization of the spectral components in the atmospheric signal.

It is quite difficult to quantify relative orientation of both an electrode and an antenna with respect to polarization of the individual spectral component. For some components the electrode and antenna may be orthogonal and may result in a total disappearance of that particular component, where as partial alignment may lead to difficult identification of the observed spectral amplitude.

An interesting observation can be made based on the observation of Figure 7.24. As can be seen from Figure 7.24 (a) the antenna spectrum has distinct peaks at 5.25 and 7.3 Hz. These peaks are traceable on the EEG signal as noise and these corresponding spectral lines can be eliminated from being classified as physiological activity in the brain.

In all these comparisons Schumann resonances are buried within the physiological signals and are hardly observable. Relative amplitudes of these resonances picked up by electrodes are very small compared to the noise floor of the physiological signals.

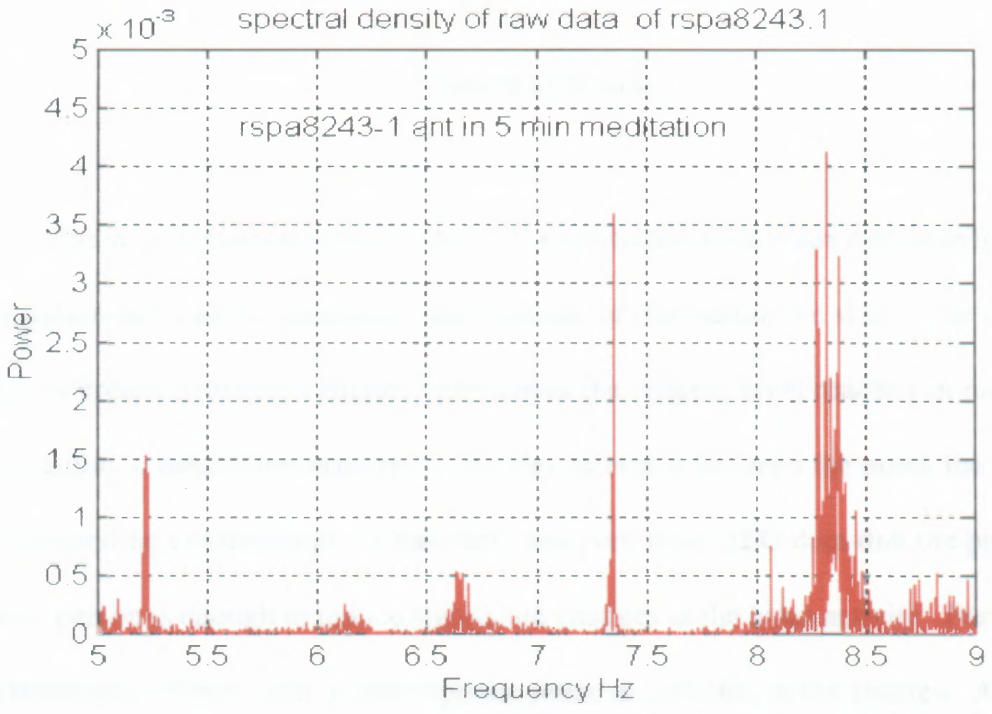

(a)

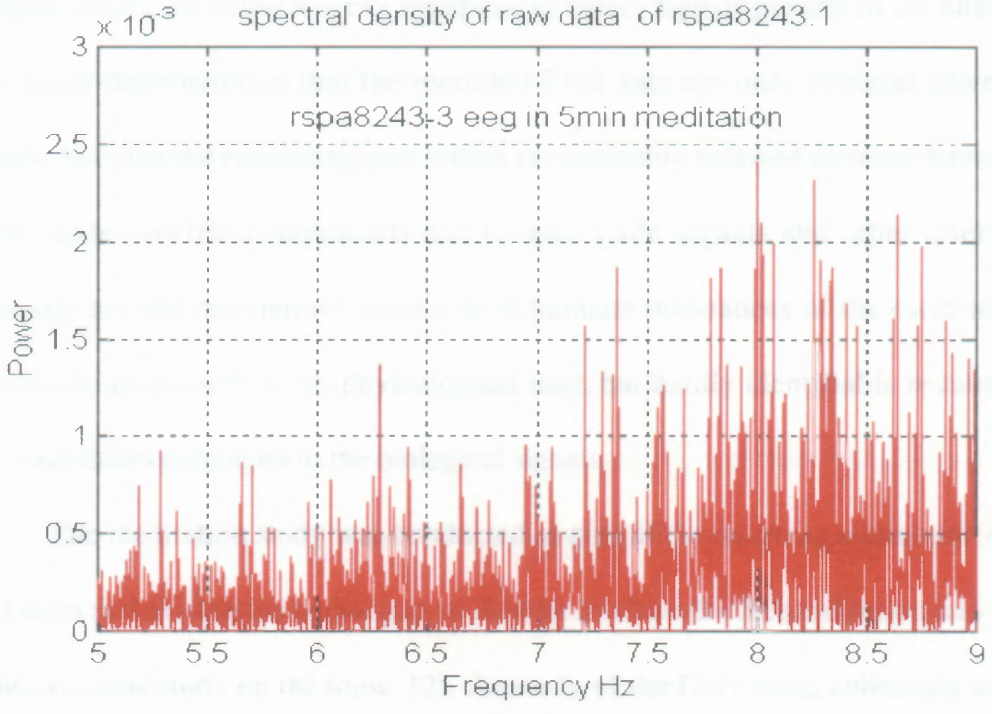

(b)

Figure 7.24 Spectral plots during meditation in the frequency band of 5 - 9 Hz. (a) Antenna spectrum. (b) EEG spectrum.

CHAPTER 8

CONCLUSIONS

The non-invasive measurement of meditation responses can provide useful information and lead to qualitative observations of the meditative state. The amount of alpha coherence provides valuable clues about the relative level reached in meditation. The reaction to meditation involves a complex interplay between the mind, the body and the surrounding environment. It has been observed from EEG data that the presence of another person is enough to induce significant changes in the brain activity. Furthermore, environmental effects such as atmospheric noise is included in the studies. Additional antennas were connected to EEG apparatus to detect signals present in the environment. This study demonstrated that the recorded EEG data not only contains physiological signals, but also the remaining part which is commonly referred as noise having clearly identifiable spectral components due to man made signals and other interferences. Naturally excited oscillations known as Schumann resonances of the earth-ionosphere waveguide are present in the physiological data, but hardly identifiable because of their low magnitudes compared to the biological signals.

The meditation study was conducted as part of the on-going autonomic studies on relaxation and meditation techniques at Kessler Institute for Rehabilitation and NJIT. As in the previous study on the topic, [2], the study of the EEG using coherence and related measures such as time-frequency spectral analysis have revealed a wealth of details about the electrical activity within the brain at different frequencies during the major states of

consciousness - eyes open, eyes closed, and meditation. The experimental data of this study supports the observations of Orme-Johnson that there is an increase in alpha coherence in group meditation. In general the existence of high alpha band coherence is not unique to the meditators. However, the patterns of increased alpha coherence and its spread to other frequencies appeared to be a characteristic "signature" of the meditative state.

In group meditation, there are obvious changes in alpha and delta coherence even though there is no direct contact or verbal communication between subjects. With no physical contact, it is hypothesized that the effect could have propagated not on direct level of interaction, but via a "field". Data obtained during the group meditation, suggests that there is a coupling effect between the subjects. Since, subjects were placed in the vicinity of each other, electromagnetic coupling could be a plausible cause. Further studies have to be made to include the Schumann resonances which may lead to clarify coupling over long distances due to possible increased coherence resulting from a massive group meditation.

8.1 Future Research

It has been shown in this study, that the presence of another person in a group meditation could cause significant changes in the response of the meditator. Some might say that the field effect was the cause of these changes. Others might blame it on the anticipation effect. To make these studies more objective, future sessions should emphasize to avoid anticipation effects where each subject should not be given information regarding the presence or the activity of the other. The act of knowing or not

knowing about the state of consciousness of the other person while meditating in a group can be randomly initiated in order to reduce any statistical errors that are due to chance alone. The order of individual and group meditation should also be randomly intermixed to avoid the result of less physiological arousal in the testing situation during the second session. Differences in frontal coherence may be affected by the effects of repeated measurements.

There are many other directions that this study could be extended in both the individual and group meditation areas. The areas under the curves of the power spectrum of the EEG signals can be quantified, recorded and classified to represent the state of health or a state of mind for patients in clinical settings.

Future study should focus on more experienced meditators who could produce wide band spectral coherence. Simultaneous measurements of atmospheric signals should include at least three orthogonal antenna elements. The sampling rate has to be increased from the current 200 samples per second to provide finer resolution in the spectral data so that easier comparison could be made in the future. Antennas with better performance at ELF band will significantly improve the quality of the acquired data.

APPENDIX A

DERIVATION OF THE SCHUMANN RESONANCE EQUATION

A.1 Theory of Earth-Ionosphere Resonator

The resonances and natural oscillations of the earth-ionosphere region could be determined [9] from solutions of source free Maxwell's equations:

$$\nabla \times \overline{\mathrm{E}}(\bar{r},t) = -\mu_0 \frac{\delta}{\delta t} \overline{\mathrm{H}}(\bar{r},t) \tag{A.1}$$

$$\nabla \times \overline{\mathrm{H}}(\bar{r},t) = \frac{\delta}{\delta t} \overline{D}(\bar{r},t) \tag{A.2}$$

$$\nabla \cdot \overline{D}(\bar{r},t) = 0 \tag{A.3}$$

$$\nabla \cdot \overline{H}(\bar{r},t) = 0 \tag{A.4}$$

subject to the boundary conditions. Here, $\overline{E}(\bar{r},t)$ and $\overline{H}(\bar{r},t)$ are time domain electric and magnetic field intensities, respectively. The medium can be assumed to have magnetic properties similar to the free space. i.e. permeability $\mu_0 = 4\pi \times 10^{-7}[H/m]$ and electrically anisotropic and inhomogeneous, i.e.

$$\overline{D}(\bar{r},\omega) = \varepsilon_0 \overline{\overline{\varepsilon}}_r(\omega,r)\overline{E} \tag{A.5}$$

where time dependence is assumed to have the form of $e^{j\omega t}$. The plasma medium is characterized by the electrical permittivity tensor $\bar{\bar{\varepsilon}} = \bar{\bar{\varepsilon}}(\omega, \bar{r})$ which is a function of angular frequency ω and position $\bar{r}$.

Considering the simplest model in terms of a homogeneous troposphere and ionosphere having relative dielectric permittivity:

$$\varepsilon_r(r) = \begin{matrix} 1 & a \le r < b & troposphere \\ \varepsilon_r & r \ge b & ionosphere \end{matrix} \qquad \text{(A.6)}$$

with "a" being the earth's radius and "b" being the radial boundary between troposphere and ionosphere as shown in Figure A.1.

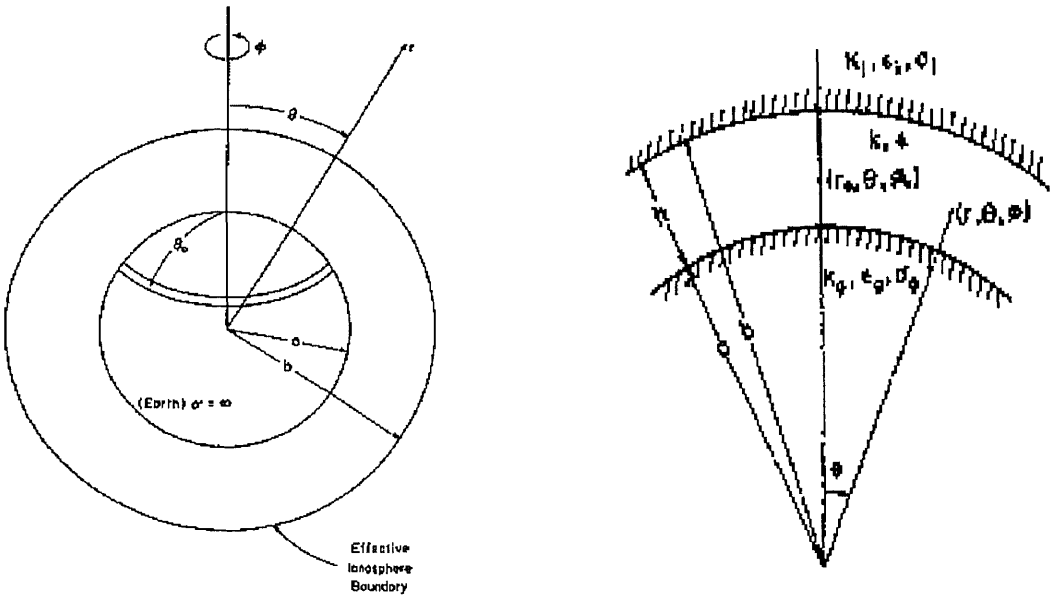

Figure A.1. A simple earth-ionosphere cavity model.

Using spherical coordinates (r,θ,φ) with the origin at the earth's center, Maxwell's equation in scalar form become:

$$\frac{1}{r\sin\theta}\left[\frac{\delta}{\delta\theta}(\sin\theta \cdot E_\varphi) - \frac{\delta}{\delta\varphi}(E_\theta)\right] = -j\omega\mu_0 \cdot H_r \qquad \text{(A.7a)}$$

$$-\frac{1}{r\sin\theta}\left(\frac{\delta}{\delta r}r\sin\theta\cdot E_{\varphi}-\frac{\delta E_r}{\delta\varphi}\right)=j\omega\mu_0\cdot H_{\theta} \tag{A.7b}$$

$$\frac{1}{r}\left[\frac{\delta}{\delta r}(r\cdot E_{\theta})-\frac{\delta}{\delta\theta}(E_r)\right]=-j\omega\mu_0\cdot H_{\varphi} \tag{A.7c}$$

$$\frac{1}{r\cdot\sin\theta}\left[\frac{\delta}{\delta\theta}(\sin\theta\cdot H_{\varphi})-\frac{\delta}{\delta\varphi}(H_{\theta})\right]=j\omega\varepsilon_0\varepsilon_r E_r \tag{A.8a}$$

$$-\frac{1}{r\sin\theta}\left(\frac{\delta}{\delta r}r\sin\theta\cdot H_{\varphi}-\frac{\delta H_r}{\delta\varphi}\right)=-j\omega\varepsilon_0\varepsilon_r E_{\theta} \tag{A.8b}$$

$$\frac{1}{r}\left[\frac{\delta}{\delta r}(r\cdot H_{\theta})-\frac{\delta}{\delta\theta}(H_r)\right]=j\omega\varepsilon_0\varepsilon_r E_{\varphi} \tag{A.8c}$$

Introducing scalar potentials U and V defined as:

$$E_r=\left(\frac{\delta^2}{\delta r^2}+\frac{\varepsilon_r\omega^2}{c^2}\right)\cdot\frac{r}{\sqrt{\varepsilon_r}}U \tag{A.9a}$$

and

$$H_r=\left(\frac{\delta^2}{\delta r^2}+\frac{\varepsilon_r\omega^2}{c^2}\right)\cdot rV \tag{A.9b}$$

where $c=\frac{1}{\sqrt{\varepsilon_0\mu_0}}\cong 3\times10^8[m/s]$ is the speed of light in vacuum. Then tangential components of electric and magnetic fields can be expressed in terms of scalar potentials as:

$$E_\theta = \frac{1}{r\sqrt{\varepsilon_r}} \cdot \frac{\delta^2}{\delta r \delta\theta}(rU) - \frac{j\omega\mu_0}{\sin\theta}\frac{\delta}{\delta\varphi}(V) \tag{A.10a}$$

$$H_\varphi = -j\varepsilon_0\omega\sqrt{\varepsilon_r}\frac{\delta}{\delta\theta}(U) + \frac{1}{r\sin\theta}\frac{\delta^2}{\delta r\delta\varphi}(rV) \tag{A.10b}$$

$$E_\phi = j\omega\mu_0\frac{\delta}{\delta\theta}V + \frac{1}{r\sqrt{\varepsilon_r}\sin\theta}\frac{\delta^2}{\delta r\delta\varphi}(rU) \tag{A.10c}$$

$$H_\theta = \frac{1}{r}\frac{\delta^2}{\delta r\delta\theta}(rV) + \frac{j\omega\varepsilon_0\sqrt{\varepsilon_r}}{\sin\theta}\cdot\frac{\delta}{\delta\varphi}(U) \tag{A.10d}$$

Substitution of (A.10) into (A.7a) and (A.8a) yields wave equation for U and V as:

$$\{\frac{1}{r^2}[\frac{1}{\sin\theta}\frac{\delta}{\delta\theta}(\sin\theta\frac{\delta}{\delta\theta}) + \frac{1}{\sin^2\theta}\frac{\delta^2}{\delta\varphi^2}] + \frac{\delta^2}{\delta r^2} + \frac{\varepsilon_r\omega^2}{c^2}\}rF = 0 \tag{A.11}$$

where F is either U or V. The solution can be obtained by the method of separation of variables in which function $F = F(r,\theta,\varphi)$ can be shown to be in the region $a \le r \le b$ ($\varepsilon_r = 1$) as:

$$F = \sum_{n=0}^{\infty}\sum_{m=-n}^{+n}[A_{nm}h_n^{(1)}(kr) + B_{nm}h_n^{(2)}(kr)]\cdot Y_{nm}(\theta,\varphi) \tag{A.12}$$

where $h_n^{(1,2)}(kr)$ are spherical Bessel functions of 1st and 2nd kind that represent superposition of incoming and outgoing waves, and $Y_{nm}(\theta,\varphi)$ are spherical harmonics defined as:

$$Y_{nm}(\theta,\varphi) = [\frac{2n+1}{4\pi}\frac{(n-m)!}{(n+m)!}]^{1/2}\cdot P_n^m(\cos\theta)e^{im\varphi} \tag{A.13}$$

and $P_n^m(\cos\theta)$ is the Associated Legendre function. Similar solution can be obtained in the ionospheric region $r > b$ as:

$$F^i = \sum_{n=0}^{\infty} \sum_{m=-n}^{+n} C_{nm} h_n^{(2)}(kr) \cdot Y_{nm}(\theta,\varphi) \tag{A.14}$$

where superscript "i" stands for ionosphere and radial function represents an outgoing wave satisfying the radiation boundary condition as $r \to \infty$.

The boundary conditions at $r = a$ and $r = b$ must be satisfied to obtain a unique solution and determine the unknown expansion coefficients A_{nm}, B_{nm}, and C_{nm}.

Assuming that the earth's surface is a perfect conductor, the tangential component of the electric field vanishes at $r = a$.

$$E_\theta\big|_{r=a} = E_\varphi\big|_{r=a} = 0 \tag{A.15}$$

requires that:

$$\frac{\delta}{\delta r}(rU)\Big|_{r=a} = 0 \tag{A.16a}$$

and:

$$V\big|_{r=a} = 0 \tag{A.16b}$$

as can be verified by equation (A.10).

The boundary conditions at $r = b$ require that the tangential components of electric and magnetic fields $\overline{E}$ and $\overline{H}$ must be continuous. Then, from (A.10) it follows:

$$U\big|_{r=b} = \sqrt{\varepsilon_r}\,U^i\big|_{r=b} \tag{A.17a}$$

$$\frac{\delta}{\delta r}(rU)\big|_{r=b} = \frac{1}{\sqrt{\varepsilon_r}}\frac{\delta}{\delta r}(rU^i)\big|_{r=b} \tag{A.17b}$$

$$V\big|_{r=b} = V^i\big|_{r=b} \tag{A.17c}$$

$$\frac{\delta}{\delta r}(rV)\big|_{r=b} = \frac{\delta}{\delta r}(rV^i)\big|_{r=b} \tag{A.17d}$$

Hence, using (A.16) and (A.17) the unknown expansion coefficients can be determined. These solutions contain two independent sets which can be classified as oscillatory modes:

a) Electric or Transverse Magnetic (TM) modes $(U \neq 0, V = 0)$; E-modes

b) Magnetic or Transverse Electric (TE) modes $(U = 0, V \neq 0)$; H-modes

Now, considering TM modes $(U \neq 0, V = 0)$, the solution can be simplified as the potentials:

$$U = \sum_{n,m}[A_{nm}h_n^{(1)}(kr) + B_{nm}h_n^{(2)}(kr)]\cdot Y_{nm}(\theta,\varphi) \tag{A.18a}$$

$$U^i = \sum_{n,m} C_{nm}h_n^{(2)}(kr)\cdot Y_{nm}(\theta,\varphi) \tag{A.18b}$$

and boundary conditions,

$$\frac{\delta}{\delta r}(rU)\big|_{r=a} = 0 \tag{A.19a}$$

$$U\big|_{r=b} = \sqrt{\varepsilon_r} U^i\big|_{r=b} \tag{A.19b}$$

$$\frac{\delta}{\delta r}(rU)\big|_{r=b} = \frac{1}{\sqrt{\varepsilon_r}} \frac{\delta}{\delta r}(rU^i)\big|_{r=b} \tag{A.19c}$$

The field components are reduced into:

$$E_r = (\frac{\delta^2}{\delta r^2} + \varepsilon_r \frac{\omega^2}{c^2}) \cdot \frac{r}{\sqrt{\varepsilon_r}} U \tag{A.20a}$$

$$E_\theta = \frac{1}{r\sqrt{\varepsilon_r}} \frac{\delta^2}{\delta r \delta \varphi}(rU) \tag{A.20b}$$

$$E_\varphi = \frac{1}{r\sqrt{\varepsilon_r}\sin\theta} \frac{\delta^2}{\delta r \delta \varphi}(rU) \tag{A.20c}$$

$$H_r = 0 \tag{A.20d}$$

$$H_\theta = \frac{j\omega\varepsilon_0\sqrt{\varepsilon_r}}{\sin\theta} \frac{\delta}{\delta\theta} U \tag{A.20e}$$

$$H_\varphi = -j\omega\varepsilon_0\sqrt{\varepsilon_r} \frac{\delta}{\delta\theta} U \tag{A.20f}$$

Similarly, TE modes can be summarized as below for the potential functions:

$$V = \sum_{n,m} [D_{nm} h_n^{(1)}(kr) + G_{nm} h_n^{(2)}(kr)] \cdot Y_{nm}(\theta, \varphi) \tag{A.21a}$$

$$V^i = \sum_{n,m} F_{nm} h_n^{(2)}(kr) \cdot Y_{nm}(\theta, \varphi) \tag{A.21b}$$

The boundary conditions reduce into:

$$V\big|_{r=a} = 0 \tag{A.22a}$$

$$V\big|_{r=b} = V^i\big|_{r=b} \tag{A.22b}$$

$$\frac{\delta}{\delta r}(rV)\big|_{r=b} = \frac{\delta}{\delta r}(rV^i)\big|_{r=b} \tag{A.22c}$$

and the individual field components can be expressed as:

$$H_r = \frac{\delta^2}{\delta r^2} + \varepsilon_r k^2 \cdot rV \tag{A.23a}$$

$$H_\theta = \frac{1}{r}\frac{\delta^2}{\delta r \delta\theta}(rV) \tag{A.23b}$$

$$H_\varphi = \frac{1}{r\sin\theta}\frac{\delta^2}{\delta r \delta\varphi}(rV) \tag{A.23c}$$

$$E_r = 0 \tag{A.23d}$$

$$E_\theta = -\frac{j\omega\mu_0}{\sin\theta}\frac{\delta}{\delta\varphi}V \tag{A.23e}$$

$$E_\varphi = j\omega\mu_0\frac{\delta}{\delta\theta}V \tag{A.23f}$$

Since the Transverse Electric (TE) modes cut-off is at roughly 1.5 kHz. for current purposes in the range $f < 60$ Hz, only Transverse Magnetic (TM) modes will be considered. Substituting (A.18) into (A.19) and equating coefficients of $Y_{nm}(\theta,\varphi)$, the following set of equations are obtained:

$$A_{nm}U_n^1(ka) + B_{nm}V_n^1(ka) = 0 \tag{A.24a}$$

$$A_{nm}U_n(kb) + B_{nm}V_n(kb) = \sqrt{\varepsilon_r}V_n(\sqrt{\varepsilon_r}kb)\cdot C_{nm} \tag{A.24b}$$

$$A_{nm}U_n^1(kb) + B_{nm}V_n^1(kb) = V_n^1(\sqrt{\varepsilon_r}kb)\cdot C_{nm} \tag{A.24c}$$

where $U_n(x) = x\cdot h_n^{(1)}(x)$ and $V_n(x) = x\cdot h_n^{(2)}(x)$.

The condition for a non-zero solution of (A.24) is that the determinant of (A.24) must be equal to zero which leads to the eigenvalue equation:

$$[U_n^1(kb)\cdot V_n^1(ka) - U_n^1(ka)\cdot V_n^1(kb)]\cdot V_n(\sqrt{\varepsilon_r}kb) = \frac{1}{\sqrt{\varepsilon_r}}[U_n(kb)\cdot V_n^1(ka) - V_n(kb)\cdot U_n^1(ka)]\cdot V_n^1(\sqrt{\varepsilon_r}kb) \tag{A.25}$$

Solutions of the equation (25) for $k_n a \cong 1$ correspond to ELF band. The permittivity of the homogeneous isotropic ionosphere is:

$$\varepsilon_r = 1 - \frac{\omega_0^2}{\omega(\omega - jV_{eff})} \tag{A.26}$$

where $\omega_0 = (\frac{Ne^2}{m\varepsilon_0})^{1/2}$ is the electron plasma frequency, N is the electron density, e and m are the charge and mass of the electron, respectively. V_{eff} is the effective collision

frequency between electrons. Since in lower ionosphere V_{eff} is largely determined by collisions between neutral particles, ω_0, $V_{eff} >> \omega$, equation (26) reduces into:

$$\varepsilon_r \approx \frac{\omega_0^2}{i\omega V_{eff}} \tag{A.27}$$

at altitudes $h = 60km$, $\omega_0 \approx 5\times 10^5 / s$, $V_{eff} \approx 3\times 10^7 / \sec$, $\omega \approx 100 / \sec$ and $\varepsilon_r \approx -100i$.

Using the asymptotic properties of spherical Bessel functions for large arguments (A.25) simplifies into:

$$[V_n^1(k_n a)\cdot U_n^1(k_n b) - U_n^1(k_n a)\cdot V_n^1(k_n b)] = -\frac{i}{\sqrt{\varepsilon_r}}[U_n(k_n b)\cdot V_n^1(k_n a) - U_n^1(k_n a)\cdot V_n(k_n b)] \tag{A.28}$$

Following further simplification of radial functions based the small parameter as:

$$F_n(k_n b) \approx F_n(k_n a)[1+\frac{\mu_n^2}{2}(\frac{n(n+1)}{k_n^2 a^2}-1)] + \mu_n F_n^1(k_n a) \tag{A.29}$$

where

$$F_n^1(k_n b) \approx F_n(k_n a)[1+\frac{\mu_n^2}{2}(\frac{n(n+1)}{k_n^2 a^2}-1)] + \mu_n[\frac{n(n+1)}{k_n^2 a^2} - 1 - \frac{n(n+1)}{k_n^3 a^3}]F_n^1(k_n a)$$

and $F_n = U_n$ or V_n.

Substitution of (A.29) into (A.28) simplifies the eigenvalue equation drastically leading to:

$$\frac{n(n+1)}{k_n a}\frac{(b-a)}{a}(1-\frac{(b-a)}{a}) = k_n(b-a) - iZ - \frac{iZ}{2}k_n^2(b-a)^2[\frac{n(n+1)}{k_n^2 a^2} - 1] \tag{A.30}$$

where $Z = \frac{1}{\sqrt{\varepsilon_r}}$ and $\frac{b-a}{a}$ are small quantities.

Omission of the last term on the right-hand-side of equation (A.30) leads to:

$$k_n a \approx \{n(n+1)[1-\frac{b-a}{a}]-\frac{Z^2}{4}\frac{a^2}{(b-a)^2}\}^{1/2}+\frac{iZ}{2}\frac{a}{b-a} \tag{A.31}$$

Considering the perfectly conducting walls, i.e. $Z = 0$ yields:

$$\omega_n = \frac{c}{a}\sqrt{n(n+1)[1-\frac{b-a}{a}]} \tag{A.32}$$

Neglecting the small term $\frac{b-a}{a} \cong 0.01$, the well known Schumann's formula for the spherical resonator with perfectly conducting walls becomes:

$$f_n = \frac{\omega_n}{2\pi} \approx \frac{c}{2\pi a}\sqrt{n(n+1)} = 10.6\sqrt{\frac{n(n+1)}{2}} \tag{A.33}$$

Which is the same as equation 3.1 of Section 3.2.

APPENDIX B

COMPUTER PROGRAMS

COSPAR is a MATLAB program to calculate the Coherence Spectral Array.

```
function cospar(x,y,Fs)
% COSPAR(x,y,Fs) Coherence Spectral Array. This routine calculates
% coherence for two signals and creates a cospar matrix
% using the methods of Levine (1976). The matrix is displayed
% in a mesh and contour plot with COHMESH.

x=x(:);
y=y(:); %column vectors
n=max(size(x));
%Fs=200;

% parameters for SPECTRUM
% 256 point windows shifted by 19 points
m=256;
noverlap=237;
threshhold=0.95;  % Coherence threshhold

% filter data to remove low frequency components
[b,a]=ellip(7,0.05,50,1.5/(Fs/2),'high');
x=filtfilt(b,a,x);
y=filtfilt(b,a,y);

% filter 60 Hz interference from the signal
[b,a]=butter(9,45/(Fs/2));
x=filtfilt(b,a,x);
y=filtfilt(b,a,y);

% calculate coherence for 5 second intervals and compile in a matrix
k=fix(n/(5*Fs));
index=1:(5*Fs);
Coh=zeros(m/2,k);

for i=1:k
 P=spectr2(x(index),y(index),m,noverlap);
 Coh(:,i)=P(:,5);
```

```
 index=index+(5*Fs);
 disp(k-i)
end

% leave only coherence peaks above threshhold
for j=1:m/2;
for l=1:k;
   if Coh(j,l)<threshhold
     Coh(j,l)=threshhold;
   end
 end
end

% plot the results
cohmesh(Coh,Fs);
Title=input('enter graph title: ','s');
subplot(211),title(Title);
```

COHMESH creates the output plots for COSPAR

```
function cohmesh(C,Fs)
%  COHMESH Graph results of COSPAR.
%  COHMESH(C,Fs) generates a mesh plot and a contour plot of the
%  coherence spectral array calculated by COSPAR.

[m,n]=size(C);
t=((5*n)*(0:n-1)/n)/60;
f=(0:m-1)/m*Fs/2;
Co=C(1:m/2,:);

% mesh plot
subplot(211),mesh(f(1:m/2),t,Co');
view([15,55]);
ylabel('time (min)');
xlabel('frequency (Hz)');
zlabel('coherence');
colormap('gray');
brighten(-1);

%contour plot
subplot(212),contour(f(1:m/2),t,Co',5);
ylabel('time (min)');
xlabel('frequency (Hz)');
```

```
grid
end
```

SPECTR2 is a modified form of the SPECTRUM program included in MATLAB's Signal Processing Toolbox.

```
function P = spectr2(x,y,m,noverlap)
%SPECTR2 Slightly modified SPECTRUM for use with COSPAR
%
%SPECTRUM Power spectrum estimate of one or two data sequences.
%       P = SPECTRUM(X,Y,M) performs FFT analysis of the two sequences
%       X and Y using the Welch method of power spectrum estimation.
%       The X and Y sequences of N points are divided into K sections of
%       M points each (M must be a power of two). Using an M-point FFT,
%       successive sections are Hanning windowed, FFT'd and accumulated.
%       SPECTRUM returns the M/2 by 8 array
%         P = [Pxx Pyy Pxy Txy Cxy Pxxc Pyyc Pxyc]
%       where
%         Pxx  = X-vector power spectral density
%         Pyy  = Y-vector power spectral density
%         Pxy  = Cross spectral density
%         Txy  = Complex transfer function from X to Y
%              (Use ABS and ANGLE for magnitude and phase)
%         Cxy  = Coherence function between X and Y
%         Pxxc,Pyyc,Pxyc = Confidence range (95 percent).
%
%       See SPECPLOT to plot these results.
%       P = SPECTRUM(X,Y,M,NOVERLAP) specifies that the M-point sections
%       should overlap NOVERLAP points.
%       Pxx = SPECTRUM(X,M) and SPECTRUM(X,M,NOVERLAP) return the single
%       sequence power spectrum and confidence range.
%
%       See also ETFE, SPA, and ARX in the Identification Toolbox.

%       J.N. Little 7-9-86
%       Revised 4-25-88 CRD, 12-20-88 LS, 8-31-89 JNL, 8-11-92 LS
%       Copyright (c) 1986-92 by the MathWorks, Inc.

%       The units on the power spectra Pxx and Pyy are such that, using
%       Parseval's theorem:
%
%          SUM(Pxx)/LENGTH(Pxx) = SUM(X.^2)/LENGTH(X) = COV(X)
%
%       The RMS value of the signal is the square root of this.
```

```
%       If the input signal is in Volts as a function of time, then
%       the units on Pxx are Volts^2*seconds = Volt^2/Hz.
%       To normalize Pxx so that a unit sine wave corresponds to
%       one unit of Pxx, use Pn = 2*SQRT(Pxx/LENGTH(Pxx))
%
%       Here are the covariance, RMS, and spectral amplitude values of
%       some common functions:
%       Function  Cov=SUM(Pxx)/LENGTH(Pxx)  RMS      Pxx
%       a*sin(w*t)      a^2/2          a/sqrt(2)  a^2*LENGTH(Pxx)/4
%Normal: a*rand(t)       a^2            a          a^2
%Uniform: a*rand(t)      a^2/12         a/sqrt(12) a^2/12
%
%       For example, a pure sine wave with amplitude A has an RMS value
%       of A/sqrt(2), so A = SQRT(2*SUM(Pxx)/LENGTH(Pxx)).
%
%       See Page 556, A.V. Oppenheim and R.W. Schafer, Digital Signal
%       Processing, Prentice-Hall, 1975.

if (nargin == 2), m = y; noverlap = 0; end
if (nargin == 3)
        if (max(size(y)) == 1)
                noverlap = m;
                m = y;
                nargin = 2;
        else
                noverlap = 0;
        end
end

x = x(:);               % Make sure x and y are column vectors
y = y(:);
n = max(size(x));       % Number of data points
k = fix((n-noverlap)/(m-noverlap));   % Number of windows
                                      % (k = fix(n/m) for noverlap=0)
index = 1:m;
w = kaiser(m,9);        % Window specification; change this if you want:
                        % (Try HAMMING, BLACKMAN, BARTLETT, or your own)
                        %
                        % Kaiser was chosen here based on Harris (1978)
                        % for discriminating closely spaced frequency
                        % components.  -CK
                        %
KMU = k*norm(w)^2;          % Normalizing scale factor
```

```
if (nargin == 2)          % Single sequence case.
        Pxx = zeros(m,1); Pxx2 = zeros(m,1);
        for i=1:k
                xw = w.*detrend(x(index));
                index = index + (m - noverlap);
                Xx = abs(fft(xw)).^2;
                Pxx = Pxx + Xx;
                Pxx2 = Pxx2 + abs(Xx).^2;
        end
        % Select first half
        select = [1:m/2];
        Pxx = Pxx(select);
        Pxx2 = Pxx2(select);
        cPxx = zeros(m/2,1);
        if k > 1
                c = (k.*Pxx2-abs(Pxx).^2)./(k-1);
                c = max(c,zeros(m/2,1));
                cPxx = sqrt(c);
        end
        pp = 0.95; % 95 percent confidence.
        f = sqrt(2)*erfinv(pp);  % Equal-tails.
        P = [Pxx f.*cPxx]/KMU;
        return
end

Pxx = zeros(m,1); % Dual sequence case.
Pyy = Pxx; Pxy = Pxx; Pxx2 = Pxx; Pyy2 = Pxx; Pxy2 = Pxx;

for i=1:k
        xw = w.*detrend(x(index));
        yw = w.*detrend(y(index));
        index = index + (m - noverlap);
        Xx = fft(xw);
        Yy = fft(yw);
        Yy2 = abs(Yy).^2;
        Xx2 = abs(Xx).^2;
        Xy  = Yy .* conj(Xx);
        Pxx = Pxx + Xx2;
        Pyy = Pyy + Yy2;
        Pxy = Pxy + Xy;
        Pxx2 = Pxx2 + abs(Xx2).^2;
        Pyy2 = Pyy2 + abs(Yy2).^2;
        Pxy2 = Pxy2 + Xy .* conj(Xy);
end
```

```
% Select first half
select = [1:m/2];

Pxx = Pxx(select);
Pyy = Pyy(select);
Pxy = Pxy(select);
Pxx2 = Pxx2(select);
Pyy2 = Pyy2(select);
Pxy2 = Pxy2(select);

cPxx = zeros(m/2,1);
cPyy = cPxx;
cPxy = cPxx;
if k > 1
  c = max((k.*Pxx2-abs(Pxx).^2)./(k-1),zeros(m/2,1));
  cPxx = sqrt(c);
  c = max((k.*Pyy2-abs(Pyy).^2)./(k-1),zeros(m/2,1));
  cPyy = sqrt(c);
  c = max((k.*Pxy2-abs(Pxy).^2)./(k-1),zeros(m/2,1));
  cPxy = sqrt(c);
end

Txy = Pxy./Pxx;
Cxy = (abs(Pxy).^2)./(Pxx.*Pyy);

pp = 0.95; % 95 percent confidence.
f = sqrt(2)*erfinv(pp);  % Equal-tails.

P = [ [Pxx Pyy Pxy]./KMU ...
    Txy Cxy ...
    f.*[cPxx cPyy cPxy]./KMU ];
```

SPE_PLOT is used to calculate then plot the power spectrum of an input signal

```
[p,f]=rspec(file(:,3),200) ;
        %plot(f(400:800),p(400:800)/max(p),'r');
        plot(f(10:14000),p(10:14000)/max(p),'r');
        xlabel('Frequency Hz')
        ylabel('Power')
        title(sprintf('spectral density of raw data  of %s',f_str));
```

RSPEC is a short program to calculate the FFT using the given sampling frequency

```
function [Pyy,f]=rspec(x,Fs)
        fftsize=length(x);

        %put alternative fft method here
                x=x-mean(x);
                fftx=fft(x,fftsize);
                Pyy=fftx.*conj(fftx)/fftsize;
                f=Fs*(0:(fftsize/2-1))/fftsize;
                clear fftx
```

TF3D is the program to calculate and plot the 3-D time-frequency mes
plots

```
function []=tf3D(ch,WL,SL,LF,HF);

     [fout,tindx,findx]=tf(ch,WL,SL) ;
%      L1=round(LF/(60/512));L2=round(HF/(60/512));
     L1=round(LF/(50/512));L2=round(HF/(50/512));
        figure(1);
        surfl(findx(L1:L2),tindx,fout(:,L1:L2));
%       meshz(findx(L1:L2),tindx,fout(:,L1:L2));
%       plot(f(10:16000),p(10:16000)/max(p),'r');
%       axis([5 10 0 5 0 0.3])
        view(-10,70)
        grid on
        colormap('bone')
        colorbar('vert')
        brighten(0.5)
        shading interp
        xlabel('Frequency (Hz)')
        ylabel('Time (Min)')
        zlabel('Magnitude')
%       title(sprintf('Time Frequency Plot of %s',f_str));
```

TF is the short program called by TF3D to calculate the FFT

```
% THIS PROGRAM IS FOR TIME-FREQUENCY ANALYSIS OF SIG
DURING MEDITATION.
```

```
%
% The methodology is as the following:
% (1) A time-window is chosen for analysis [175-256].
% (2) The time-window is slided through the EEG signal to get new short-time
% signal. The procedures [2] are repeated until the end of the signal file.
% (3) The resulting signal is displayed in the Time-Frequency Plane
%
% PROGRAM BY      : MEHMET V. TAZEBAY
% PROGRAM DATE    : 08/16/1995
% LAST MODIFICATION : 08/18/1995 by Douglas A. Newandee
%
% _____GENERAL USAGE_____
% [D_OUT,t_indx,F_OUT,f_indx,FILT] = tf_analysis(data,WL,SWL);
% D_OUT   : Short-time Normalized Data (MxN matrix).
% F_OUT   : Frequency Responses the corresponding Filtered D_OUT(MXK matrix).
% DNor_OUT : Short-time Data (MxN matrix).
% FNor_OUT : Frequency Responses the corresponding Filtered D_OUT(MXK matrix).
% t_indx  : Time index.
% f_indx  : Frequency index.
% data    : Input data vector
% WL      : Data Window Length
% SWL     : Sliding Window Length.
%
function [FOUT,tindx,findx]=tf(data,WL,SWL);

% INITIAL PARAMETERS
% DATA LOADING
 KK  = 512;
 N   = WL; % Data Window Length
 K   = SWL; % Sliding Window Length
 C   = floor(length(data)/N);  % Counter
 L   = 1;
 i   = 1;

% MAIN LOOP
  while ((L+N)<=min([length(data)]))

% MEAN EXTRACTION
      [o]=data(L:L+N-1)' - mean(data(L:L+N-1)');

% OUTPUT DATA MATRIX
      D_OUT(i,:) = o;

% NORMALIZED DATA
      o_n = o/sqrt(o*o');
```

```
    DNOUT(i,:) = o_n;

% OUTPUT DATA FREQUENCY RESPONSE
    FO=fresp(o);
    FOUT(i,:) = FO(1:KK);

% LOOP VARIABLES
    tindx(i)=(L-1)+N/2;
    L = L + K;
    i = i+1;
  end

  fi = [0:pi/1023:pi];
  findx = (fi(1:KK)*100)/pi;
  tindx = tindx/(200*60);
  FOUT=FOUT/max(max(FOUT));
```

APPENDIX C

DATA ANALYSIS PROCEDURES

C.1 EEG Coherence Analysis

1. From any network computer, select File manager, open 2 windows for drive c: and drive s: directories. From the Window icon, select Tile Vertically to display the directories side by side.

2. Copy data files from drive s: to drive c:. Now use the data file dn07145a.dat as an example. Drag the files (hold down the left mouse button) from s:\users\doug to c:\users\doug.

3. The dn07145a.dat (...b.dat, ...c.dat) data file is in binary format. They must be converted into ascii format before they can be analyzed by MATLAB. Unpack the .dat files to ...a.1, ...b.1, and ...c.1 files using eeg_unpk.bat batch file. Go to MSDOS and type:

```
cd c:\users\doug
eeg_unpk dn07145
dir
```

Check to see if all 3 unpacked ascii files are about the same size.

4. Use alt tab keys to go to Program Manager. Double click to select MATLAB for Windows. Double click MATLAB again to run the program.

5. Check to see the background of the graphs to white. Type:

```
figure
```

MATLAB will display a blank graph. Make sure the background is white. If background is black. Click on File, Close, and type:

```
whitebg
```

Once the background is white. Click on File, Close.

6. Make sure the following files are present in the directory. Type:

cd c:\users\doug
dir

The directory must have the following files:

cospar.m
comesh.m
inp.m
powspec.m
powspec2.m
rspec.m
spe_plot.m
spectr2.m
tf.m
tf3d.m

7. Load the ...a.1 data file into MATLAB, type:

load dn07145a.1;

8. The computer will load the ascii file into its RAM memory. Now you can check the status of the file just loaded by typing:

whos

The computer will display the relevant information about the loaded file such as: file name, number of samples, file size etc. In our example, the dn07145a.1 file contains data for 6 channels. You can see these six channels by typing:

type dn07145a.1;

The computer will display the six columns of data from start to end. To stop the display, hit ctrl x, ctrl c.

9. Now you can plot the data of a particular channel, type:

plot(dn07145a(1:2000,1));

The format is:

plot(filename(start:end,channel));

where: filename=same as before.
channel=number of channel to be seen.
start=starting sample point. Must be equal or greater than 1.

end=ending sample point. In the example above 1:2000 means the first 10 seconds of data (10 sec x 200 samples/sec=2000).

To see all the sample points, type:

```
plot(dn07145a(:,1));
```

The computer will display the plot of the data of the channel you request. You can give it a title by typing:

```
title('enter the title you want between the quotes');
```

If you only want to print the graph, click on **W**indows, select the graph you want, select **F**ile, **P**rint..., **O**K to print the graph.

10. To find the frequency spectrum plot, use alt Tab to switch to **Program Manager**. Double clicks on **Accessories**, **Notepad**. Click on File, **O**pen, c:\users\doug\eeg. Select All Files(*.*). Move down arrow to select spe_plot.m then click **O**K. The computer will display the spe_plot.m file. Now look at the first line of the program:

```
[p,f]=rspec(file(:,1),200);
```

where: file=name of ascii data file loaded in MATLAB memory.
: =range of sample points of interest.
1 =channel number of interest.
200=sampling rate

In this case, (file(:,1),200) means the power spectrum of **all** sample points of channel 1 at a rate of 200 samples per second. This sampling rate must agree with the data rate at the time of acquisition. Change the parameters for other channels and sample points accordingly. When finish, click on **F**ile, **s**ave, **F**ile, E**x**it, then return to MATLAB work area.

To find the spectrum, type:

```
close all;
clear all
inp
```

The computer will ask you to enter the data filename. Enter the filenam extension:

```
Please enter the name of file to be loaded --> dn07145a
```

The computer will load the content of the ascii file into its memory. Now you can get the frequency spectrum plots by typing:

spe_plot

The computer will display the plot of the data of the channel you request. You can give it a title by typing:

title('enter the title you want between the quotes');

If you only want to print the graph, click on **W**indows, select the graph you want, select **F**ile, **P**rint..., **O**K to print the graph.

11. To find the coherence spectrum between two channels, type:

cospar(dn07145a(:,3),dn07145a(:,4));

The computer will analyze the data and display the coherence graphs of channel 3 and channel 4 of the data file dn07145a. The computer will ask you to enter the title of the graphs. Type in the title you want. For example:

Please enter the graph title: dn07145a-eeg coherence ch3 and 4- 5 min eyes open.

Again to print the graph, click on **W**indows, select the graph you want, select **F**ile, **P**rint..., **O**K to print the graph.

12. To find the time-frequency 3D plot, type:

tf3d(ch,wl,sl,lf,hf);

where: ch=channel of the file of interest.
wl=FFT window length in power of 2 (best to use 1024).
sl =sliding windoe length in power of 2 (best to use 256)
lf =low frequency limit (0.01 to 50, cannot be 0 or greater than high frequency range - hf).
hf=high frequency limit (0.01 to 50, cannot be 0 or less than low frequency range - hf).

An example is:

tf3d(dn07154a(:,1),1024,256,0.1,50);

The computer will display the plot of the data of the channel you request. You can give it a title by typing:

title('enter the title you want between the quotes');

If you only want to print the graph, click on Windows, select the graph you want, select File, Print..., OK to print the graph.

13. To quit the analysis when done, type:

exit

C.2 Time-Frequency Analysis of Schumann Resonances

This program is a MATLAB m-file. Upon starting MATLAB, type `whitebg` for a white graph background.

1. Load the ...a.1 data file into MATLAB, type:

load dn07145a.1;

2. The computer will load the ascii file into its RAM memory. Now you can check the status of the file just loaded by typing:

whos

The computer will display the relevant information about the loaded file such as: file name, number of samples, file size etc. In our example, the dn07145a.1 file contains data for 6 channels. You can see these six channels by typing:

type dn07145a.1;

The computer will display the six columns of data from start to end. To stop the display, hit ctrl x, ctrl c.

3. Now you can plot the data of a particular channel, type:

plot(dn07145a(1:2000,1));

The format is:

plot(filename(start:end,channel));

where: filename=same as before.
channel=number of channel to be seen.
start=starting sample point. Must be equal or greater than 1.

end=ending sample point. In the example above 1:2000 means the first 10 seconds of data (10 sec x 200 samples/sec=2000).

To see all the sample points, type:

```
plot(dn07145a(:,1));
```

The computer will display the plot of the data of the channel you request. You can give it a title by typing:

```
title('enter the title you want between the quotes');
```

If you only want to print the graph, click on **W**indows, select the graph you want, select **F**ile, **P**rint..., **O**K to print the graph.

4. To find the frequency spectrum plot, use alt Tab to switch to **Program Manager**. Double clicks on **Accessories**, **Notepad**. Click on File, **O**pen, c:\users\doug\eeg. Select All Files(*.*). Move down arrow to select spe_plot.m then click **O**K. The computer will display the spe_plot.m file. Now look at the first line of the program:

```
[p,f]=rspec(file(:,1),200);
```

where: file=name of ascii data file loaded in MATLAB memory.
: =range of sample points of interest.
1 =channel number of interest.
200=sampling rate

In this case, (file(:,1),200) means the power spectrum of **all** sample points of channel 1 at a rate of 200 samples per second. This sampling rate must agree with the data rate at the time of acquisition. Change the parameters for other channels and sample points accordingly. When finish, click on **F**ile, **s**ave, **F**ile, E**x**it, then return to MATLAB work area.

To find the spectrum, type:

```
close all;
clear all
inp
```

The computer will ask you to enter the data filename. Enter the filename without the extension:

```
Please enter the name of file to be loaded --> dn07145a
```

The computer will load the content of the ascii file into its memory. Now you can get the frequency spectrum plots by typing:

spe_plot

The computer will display the plot of the data of the channel you request. You can give it a title by typing:

title('enter the title you want between the quotes');

If you only want to print the graph, click on **W**indows, select the graph you want, select **F**ile, **P**rint..., **O**K to print the graph.

5. To find the time-frequency 3D plot, type:

tf3d(ch,wl,sl,lf,hf);

where: ch=channel of the file of interest.
wl=FFT window length in power of 2 (best to use 1024).
sl =sliding windoe length in power of 2 (best to use 256)
lf =low frequency limit (0.01 to 50, cannot be 0 or greater than hig frequency range - hf).
hf=high frequency limit (0.01 to 50, cannot be 0 or less than low frequency range - hf).

An example is:

tf3d(dn07154a(:,1),1024,256,0.1,50);

The computer will display the plot of the data of the channel you request. You can give it a title by typing:

title('enter the title you want between the quotes');

If you only want to print the graph, click on **W**indows, select the graph you want, select **F**ile, **P**rint..., **O**K to print the graph.

6. To quit the analysis when done, type:

exit

APPENDIX D

EQUIPMENT SETUP

The diagram below shows the laboratory setup for both the meditation and the Schumann resonance experiments. Both the subject(s) and the antennas are placed inside the EM shielded room. All other equipment and the experimenter are outside. All electrodes and antenna connections are brought outside through the honey comb opening near the entrance door.

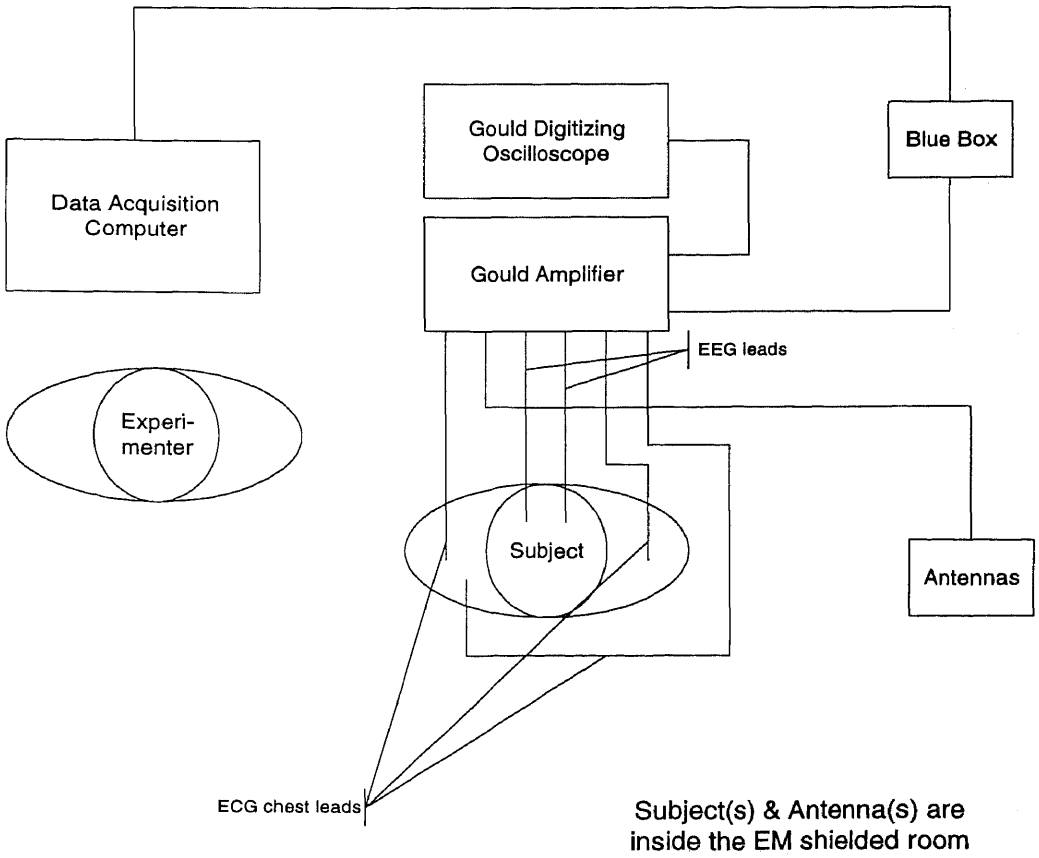

Figure D.1 Setup for individual meditation

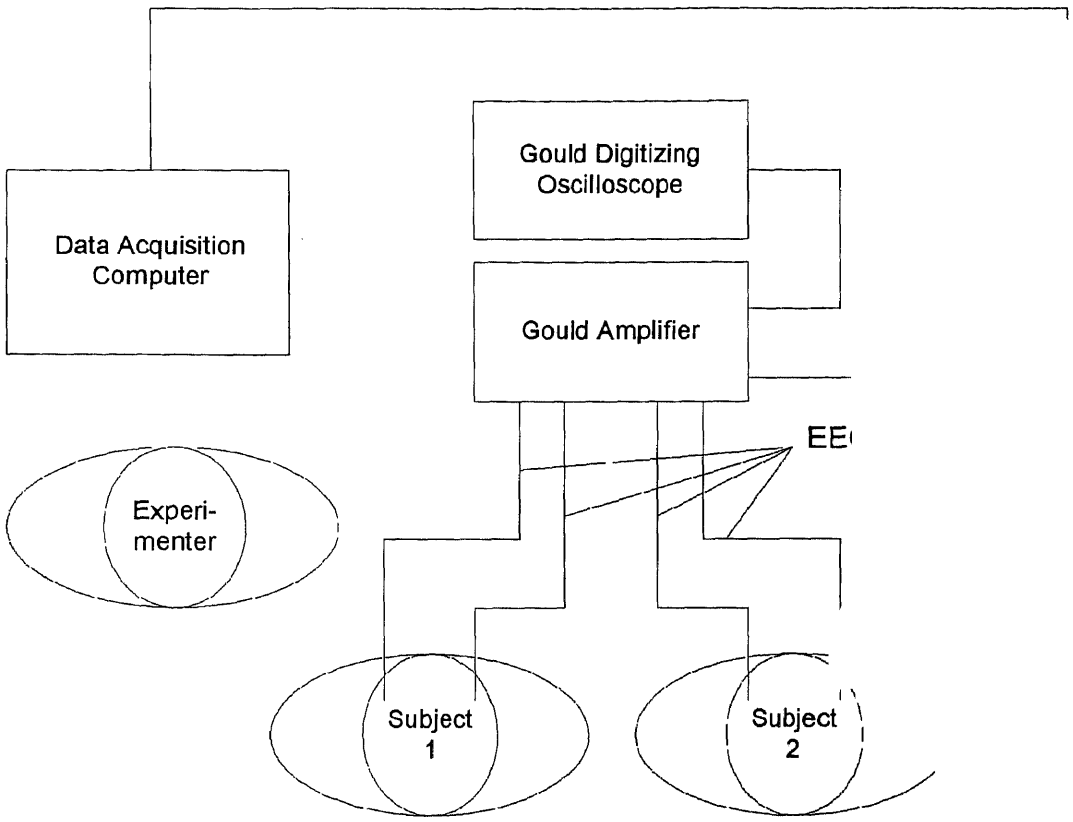

Figure D.2 Setup for group meditation.

REFERENCES

[1] R. Jevning, R. K. Wallace, and M. Beidebach, "The physiology of Meditation: A Review. A Wakeful Hypometabolic Integrated Response," *Neuroscience and Behavioral Reviews*, vol. 16, pp. 415-24, 1992.

[2] C. B. King, "Measurement of the Reaction to Stress and Meditation Using Brain Wave Coherence and Heart Rate Variability," Masters Thesis, New Jersey Institute of Technology, Newark, NJ., 1994.

[3] H. H. Bloomfield, M. P. Cain, and D. T. Jaffe, *TM: Discovering Inner Energy and Overcoming Stress*, New York, Delacorte Press, 1975.

[4] R. R. Baker, *The evolutionary ecology of animal migration*, Hodder and Stoughton, London, 1978.

[5] K. Schmidt-Koenig, and W. R. Keeton (Eds.), *Animal migration, navigation and homing.* Heidelberg: Springer, 1978.

[6] W. R. Adey, and S. M. Bawin, "Brain Interactions with electric and magnetic fields," *Neurosciences Research Program Bulletin*, vol. 15, pp. 1-129, 1974.

[7] L. H. Domash, "The Transcendental Meditation technique and quantum physics: Is pure consciousness a macroscopic quantum state in the brain?," *Scientific Research on the Transcendental Meditation Program: Collected Papers*, Vol. 1, West Germany: MERU Press, 1976.

[8] C. I. J. M. Stuart, Y. Takahashi, and H. Umezawa, "Mixed system brain dynamics: Neural memory as a macroscopic ordered state," *Foundation of Physics*, vol. 9, pp. 310-318, 1979.

[9] D. Orme-Johnson, M. C. Dillbeck, and R. Wallace, "Intersubject EEG Coherence: Is Consciousness A Field?," *Intern. J. Neuroscience.*, vol. 16, pp. 203-09, 1982

[10] D. Orme-Johnson, C. T. Haynes, "EEG Coherence, Pure Consciousness, Creativity, and TM-Sidhi Experiences," *Neuroscience*, vol. 13, pp. 211-17, 1981.

[11] Maharishi Mahesh Yogi, *Enlightenment and invincibility*, West Germany, MERU Press, pp. 26-37, 43-50,258-262, 406-410, 419-449, 1978.

[12] L. Cohen, "Time-Frequency Distributions - A Review," *Proceedings of the IEEE,* vol. 77, no. 7, pp. 941-81, July 1989.

[13] M. C. Dillbeck, and D. W. Orme-Johnson, "Physiological Differences Between Meditation and Rest," *American Psychologist,* pp. 879-81, Sept. 1987.

[14] P. Levine, "The Coherence Spectral Array (COSPAR) and its Application to the Study of Spatial Ordering in the EEG," *Proceedings of the San Diego Biomedical Symposium.* San Francisco, Academic Press, vol. 15, pp. 237-47, 1976.

[15] D. W. Orme-Johnson, and C. T. Haynes, "EEG Phase Coherence, Pure Consciousness, Creativity, and TM-Sidhi Experiences," *Neuroscience,* vol. 13, pp. 211-217, 1981.

[16] W. O. Schumann, "Uber die Strahlungslosen Eigenschwingungan einer leitenden Kügel die von Liftschicht und einer Ionosphärenhülle umbegen ist," Z. *Naturforsch. Teil,* A7, pp. 149-154, 1952.

[17] J. R. Wait, D. B. Large, "Resonances of the Thin-Shell Model of the Earth-Ionosphere Cavity With a Dipolar Magnetic Field," *Radio Science,* vol. 2, no. 7, pp. 695-702, July 1967.

[18] J. Galejs, "Schumann resonances," *J. Res. NBS. Radio Sci.*, vol. 69D, pp. 1043-1055, 1965.

[19] P. V. Bliokh, V. N. Bormotov, and V. M. Kontorovich, *et al.*, "Removal of degeneracy from the spherical earth-ionosphere resonator," Preprint No. 10, Scientific Research Institute of Radiophysics and Electronics, Academy of Science of the Ukrainian SSR, Kharkov, 1971.

[20] M. Balser, and C. A. Wagner, "Observation of earth-ionosphere cavity resonances," *Nature,* 188, pp. 638-641, 1960.

[21] F. W. Chapman, and D. LI. Jones, "Observation of earth-ionosphere cavity resonances and their interpretation in terms of a two layer ionosphere model," *J. Res. NBS. Radio Sci.*, vol. 68D, pp. 1177-1185, 1964.

[22] M. J. Rycroft, "Resonances of the earth-ionosphere cavity observed at Cambridge, England," *J. Res. NBS. Radio Sci.*, vol. 69D, pp. 1071-1081, 1965.

[23] A. Egeland, and T. R. Larsen, "Measurements of the earth-ionosphere cavity resonances frequencies at high latitude," *Phys. Norveg.*, vol. 2, pp. 85-97, 1967.

[24] W. R. Goff, "Human Averaged Evoked Potentials: Procedures for Stimulating and Recording," *Methods in Physiological Psychology*; Vol. I: Bioelectric Recording Techniques; Part B: Electroencephalography and Human Brain Potentials, New York, Academic Press, 1974.

[25] J. W. Clark, "The Origin of Biopotentials" in *Medical Instrumentation: Application and Design*, J. G. Webster, ed. Boston, Houghton Mifflin Company, 1992.

[26] A. C. Guyton, *Textbook of Medical Physiology*, Eighth Edition, Philadelphia, Harcourt Brace Jovanovich, 1991.

[27] M. A. West, "Meditation and the EEG," *Psychological Medicine*, vol. 10, pp. 369-375, 1980.

[28] R. G. Brown, *Introduction to Random Signal Analysis and Kalman Filtering*, New York, John Wiley & Sons, 1983.

[29] R. W. Harris, and T. J. Ledwidge, *Introduction to Noise Analysis*, London, Pion Limited, 1974.

[30] P. D. Welch, "The Use of Fast Fourier Transform for the Estimation of Power Spectra: A Method Based on Time Averaging Over Short, Modified Periodograms," *IEEE Transactions on Audio and Electroacoustics*, vol. AU-15, no. 2, pp. 70-3, 1967.

[31] S. Fernando, and S. Reisman, "Biomedical Applications of Time-Frequency Analysis," *Proceedings of the IEEE-SP International Symposium on Time-Frequency and Time-Scale Analysis*, pp. 576-9, 1994.

[32] M. C. Dillbeck, and E. C. Bronson, "Short-term Longitudinal Effects of The Transcendental Meditation Technique on EEG Power and Coherence," *Intern. J. Neuroscience,* vol. 14, pp. 147-51, 1981.

[33] M. C. Dillbeck, D. W. Orme-Johnson, and R. K. Wallace, "Frontal EEG Coherence, H-Reflex Recovery, Concept Learning, and the TM-Sidhi Program," *Intern. J. Neuroscience*, vol. 15, pp. 151-57, 1981.